NASA TECHNICAL NOTE

NASA TN D-8416

NASA TN D-8416

IMPLICATIONS OF OUTER-ZONE RADIATIONS ON OPERATIONS IN THE GEOSTATIONARY REGION UTILIZING THE AE4 ENVIRONMENTAL MODEL

John W. Wilson and Fred M. Denn

Langley Research Center
Hampton, Va. 23665

NATIONAL AERONAUTICS AND SPACE ADMINISTRATION · WASHINGTON, D. C. · MAY 1977

1 Report No	2. Government Accession No	3 Recipient's Catalog No
NASA TN D-8416		

4 Title and Subtitle	5 Report Date
IMPLICATIONS OF OUTER-ZONE RADIATIONS ON OPERATIONS IN THE GEOSTATIONARY REGION UTILIZING THE AE4 ENVIRONMENTAL MODEL	May 1977
	6 Performing Organization Code

7 Author(s)	8 Performing Organization Report No
John W. Wilson and Fred M. Denn	L-11280
	10 Work Unit No 506-25-33-01
9 Performing Organization Name and Address NASA Langley Research Center Hampton, VA 23665	11 Contract or Grant No
	13 Type of Report and Period Covered Technical Note
12 Sponsoring Agency Name and Address National Aeronautics and Space Administration Washington, DC 20546	14 Sponsoring Agency Code

15 Supplementary Notes

John W. Wilson: Langley Research Center, Hampton, Virginia.
Fred M. Denn: Old Dominion University, Norfolk, Virginia.

16 Abstract

The radiation exposure in the region of geostationary orbits is examined in detail in search for means of optimizing human performance. It is found that the use of slightly inclined circular orbits is one means by which exposure and space-suit thickness requirements can be reduced. Another effective technique is to limit the extravehicular activity to those days when the short-term fluctuations result in low exposure. Space-suit shielding approaching 1/2 g/cm^2 or less may be possible by utilizing work stoppages and inclined orbits. If aluminum and other low-atomic-number materials are used to construct the habitat, then excessive wall thicknesses are required. If special bremsstrahlung shielding is used, then the habitat shield may be reduced to as low as 2 g/cm^2. Numerous tables and graphs are presented for future analysis of dose in the geostationary region.

17 Key Words (Suggested by Author(s))	18 Distribution Statement
Geostationary operations Radiation protection Space power Trapped electrons	Unclassified - Unlimited Subject Category 93

19 Security Classif. (of this report)	20. Security Classif (of this page)	21 No of Pages	22 Price*
Unclassified	Unclassified	69	$4.50

* For sale by the National Technical Information Service, Springfield, Virginia 22161

IMPLICATIONS OF OUTER-ZONE RADIATIONS ON OPERATIONS IN THE GEOSTATIONARY REGION UTILIZING THE AE4 ENVIRONMENTAL MODEL

John W. Wilson and Fred M. Denn*
Langley Research Center

SUMMARY

The radiation exposure in the region of geostationary orbits is examined in detail in search for means of optimizing human performance. It is found that the use of slightly inclined circular orbits is one means by which exposure and space-suit thickness requirements can be reduced. Another effective technique is to limit the extravehicular activity to those days when the short-term fluctuations result in low exposure. Space-suit shielding approaching 1/2 g/cm^2 or less may be possible by utilizing work stoppages and inclined orbits. If aluminum and other low-atomic-number materials are used to construct the habitat, then excessive wall thicknesses are required. If special bremsstrahlung shielding is used, then the habitat shield may be reduced to as low as 2 g/cm^2. Numerous tables and graphs are presented for future analysis of dose in the geostationary region.

INTRODUCTION

Space systems operating in geostationary orbits (circular equatorial orbits with a 24-hr period) are particularly important for commercial communication and power applications. The need to develop means by which man can perform useful work in the geostationary region is required for the timely advancement of industrialization in this region of space. A preliminary analysis of radiation protection requirements has indicated that the outer-zone electron environment is the main limiting factor on manned operations for periods less than a year (ref. 1). Although solar cosmic rays have complete access to this region of space, they pose no operational problems as long as adequate monitoring and easily accessible radiation shelters are provided during the brief periods of these transient solar particle increases. The fact that solar cosmic rays are not an operational problem does not imply that solar cosmic radiation is not a serious protection problem, but only that the impact on work activity is small if adequate protection is provided to keep the health risk within acceptable levels (ref. 1). As noted in reference 1, the galactic cosmic rays produce a low level of radiation with high linear energy transfer (high LET) and may be the ultimate limiting factor for extensive space operations (that is, long staying periods). The protection requirements against galactic radiation are uncertain since the shielding parameters and radiobiological factors are currently unknown.

---

*Old Dominion University, Norfolk, Virginia.

The purpose of the present paper is to analyze the protection requirements for operations in the geostationary region using the most recent environmental model entitled AE4 (ref. 2). Several methods for reducing the exposure to the trapped radiations will be considered. These include shielding determinations for the habitat and the space-suit requirements during extravehicular activity (EVA). The potential use of local time variations to reduce exposure will be further examined along with the use of slightly inclined geosynchronous circular orbits (referred to hereinafter as the geostationary region). The effects of the geomagnetic axis tilt relative to the geographic axis will also be examined. Numerous graphs and tables are presented for estimation of shield requirements during manned operations in the geostationary region.

SYMBOLS

$b_Z(X,L)$	local time coefficient of average dose rate, dimensionless
B	magnetic field intensity on magnetic L-shell, gauss
$B_0(L)$	equatorial magnetic field intensity on magnetic L-shell, gauss
C(E,Z)	local time coefficient of average flux, dimensionless
$C_T(E,L)$	local time coefficient of average flux during epoch denoted by T, dimensionless
$D(X,L,\leqq P)$	restricted average dose rate, rad/day
$\bar{D}(X,L)$	average dose rate, rad/day
$D_Z(X,L,\phi,P)$	interval limit dose rate associated with probability level P, rad/day
$\bar{D}_Z(X,L,\phi)$	average dose rate as a function of local time, rad/day
E	electron energy, MeV
G(B,L)	latitudinal variation of radiation environment, dimensionless
i	orbit inclination, deg
$J(E,B,L,\phi,t)$	instantaneous electron flux, electrons/cm^2-sec
L	magnetic L coordinate, Earth radii
m(L)	power-law parameter on magnetic L-shell, dimensionless
N(E,L,t)	equatorial instantaneous electron flux, electrons/cm^2-sec
P	probability level, dimensionless

r	distance from Earth's center, Earth radii
$\vec{r}_e$	vector in Earth coordinates, Earth radii
$\vec{r}_i$	vector in inertial coordinates, Earth radii
$\vec{r}_o$	vector in coordinates of orbital plane, Earth radii
t	universal time, sec
T	time of solar epoch, year
X	shield thickness, g/cm^2 of aluminum
Z	sunspot number
$\delta(E,L,t)$	log flux deviation, dimensionless
η	angle between line of nodes and x_i-axis, deg
θ_o	orbital starting phase, deg
$[\theta]_x, [\theta]_y, [\theta]_z$	rotation matrix for rotating through an angle θ about x-, y-, and z-axis, respectively
λ_g	geographic latitude, deg
λ_m	geomagnetic latitude, deg
$\mu(E,L)$	mean log flux, log (electrons/cm^2-sec)
$\mu_T(E,L)$	mean log flux at epoch T, log (electrons/cm^2-sec)
$\sigma(E,L)$	log flux standard deviation, dimensionless
$\sigma_T(E,L)$	log flux standard deviation at epoch T, dimensionless
τ	time averaging period, hr
ϕ	satellite local time, hr
ϕ_g	geographic longitude, deg
ϕ_o	Greenwich local time, hr
$\Phi(E,L,\phi,t)$	instantaneous local time variation, dimensionless
$\Phi_T(E,L,\phi)$	average local time variation during epoch T, dimensionless
ω	Earth rotational period, deg/hr
Ω_o	angle between anti-Sun-Earth line and x_i-axis, deg

Dose used in this report is expressed in units of rad corresponding to 100 ergs/g in soft tissue.

PARAMETRIC REPRESENTATION OF AE4 MODEL IN THE GEOSTATIONARY REGION

The outer-zone radiations consist mostly of electrons and protons. The protons are of low energy (less than 2 MeV) and are stopped by even the lightest weight space suit, while the electrons are very energetic (up to several MeV) and appreciable numbers will penetrate more than 1 centimeter of tissue. These outer-zone radiations undergo large temporal variations as related to long-term-average solar activity (ref. 2), 27-day solar rotation (ref. 3), geomagnetic storms due to solar-flare events (refs. 3 to 5), geomagnetic substorms (refs. 3 to 5), and distortions produced in the geomagnetic field by the solar wind which causes radiation-intensity modulations in local time (ref. 6). These variations are represented by the following functions:

$$J(E,B,L,\phi,t) = N(E,L,t)\ \Phi(E,L,\phi,t)\ G(B,L) \tag{1}$$

where $J(E,B,L,\phi,t)$ represents the instantaneous electron flux as a function of electron energy E at locations given by the corresponding B and L coordinates (for the main dipole field) at local time ϕ and universal time t. The L coordinate for the main dipole field is a surface composed of all field lines which have a fixed intensity at the magnetic equator and B is the field intensity on each L surface (see fig. 1). The effect of geomagnetic distortions from dipole values is embodied in the local time dependence. In equation (1), $N(E,L,t)$ is the instantaneous electron flux averaged over local time (that is, longitude) at the magnetic equator, $\Phi(E,L,\phi,t)$ is the instantaneous local time dependence with normalization (that is, the average value over 24 hr) given by

$$\frac{1}{24}\int_0^{24} \Phi(E,L,\phi,t)\ d\phi = 1 \tag{2}$$

and $G(B,L)$ describes the geomagnetic latitudinal variation with normalization (that is, the value on the geomagnetic equator) given by

$$G\left[B_0(L),L\right] = 1 \tag{3}$$

where $B_0(L)$ is the equatorial field strength of the magnetic L-shell.

This factorized form for the environment is a considerable simplification introduced here in close analogy to environmental model functions derived by Vette and coworkers (ref. 7) but may not be appropriate for the electron environment. For example, it is quite reasonable to expect that local time (longitude) and latitude are coupled (that is, $G(B,L)$ should depend on ϕ). Furthermore, one might expect the latitude variation to be different for different times due to changes in the solar plasma output (that is, $G(B,L)$ should depend on t). The only virtue of equation (1) is that appropriate averages of it result in the functional relations assumed for the AE4 environmental model (ref. 2). Note, however, that equation (1) is not unique in that respect. The relation of equation (1) to the AE4 environmental model will now be considered.

The main features of the AE4 model are the statistical treatment of short-term fluctuations in the equatorial flux averaged over local time and the extraction of only the average local time dependence (ref. 2). The main features not given by the AE4 model are the short-term correlations and the local time dependence as a function of geomagnetic disturbance (ref. 6). A better knowledge of these short-term correlations and the frequency of large-scale fluctuations are required to evaluate the effects on work performance (ref. 1). Clearly, if a period of low radiation exposure lasts no more than an hour or two, it cannot be effectively utilized. The data of Paulikas and Blake (ref. 4) indicate correlations are on the order of several hours to several days.

The equatorial flux can be written as

$$N(E,L,t) = 10^{\mu_T(E,L)+\delta(E,L,t)} \tag{4}$$

where the mean-log flux

$$\mu_T(E,L) = \frac{1}{2\tau}\int_{-\tau}^{\tau} \log\left[N(E,L,T+\tau')\right]\, d\tau' \tag{5}$$

with τ chosen sufficiently large to average over short-term fluctuations (that is, $\tau \approx 4$ months). The mean-log flux near geosynchronous altitude shows a weak dependence on the phase of the solar cycle below 100 keV (ref. 2), which is of little consequence from the point of view of radiation protection and will be ignored. A parametric representation valid for electrons of energy from a few hundred keV to several MeV of the cycle independent mean-log flux in the geosynchronous region is found to be

$$\mu(E,L) = \mu_0(L) + \mu_1(L)E + \mu_2(L)E^2 + \mu_3(L)E^3 \tag{6}$$

where values of the $\mu_i(L)$ coefficients are given in table I. Coefficients for intermediate L values are found by linear interpolation. The log flux deviation about the mean (that is, $\delta(E,L,t)$), if observed at random times, is found to have a normal distribution with standard deviation given by

$$\sigma_T(E,L) = \left[\frac{1}{2\tau}\int_{-\tau}^{\tau} \delta^2(E,L,T+\tau')\, d\tau'\right]^{1/2} \tag{7}$$

It is found by Singley and Vette (ref. 2) that $\sigma_T(E,L)$ is nearly independent of the phase of the solar cycle, and a parametric representation for energies above 400 keV but less than several MeV near geosynchronous altitudes is found as

$$\sigma(E,L) = \sigma_0(L) + \sigma_1(L)E + \sigma_2(L)E^2 + \sigma_3(L)E^3 \tag{8}$$

where values of the $\sigma_j(L)$ coefficients are given in table II. Coefficients for intermediate L values are formed by numerical interpolation. The paramet-

ric representation given by equations (6) and (8) will be used for the estimation of the instantaneous equatorial flux averaged over local time and the equatorial flux averaged over short-term fluctuations.

The local time dependence is a function of the degree of geomagnetic disturbance. During quiet periods the local time variations are at a minimum in amplitude. The amplitude of local time variation increases in the geosynchronous region during disturbed periods. The amplitude increases appear due to movement of the magnetospheric boundary and most greatly affect high-energy electrons due to their large radius of curvature about the geomagnetic-field lines (ref. 4). Although low-energy electrons which are injected through the tail region also contribute to local time variations, they are of no consequence to radiation protection. The AE4 model gives only the local time variation averaged over short-term fluctuations (ref. 2). It is found by Singley and Vette (ref. 2) that the local time variation coefficient can be taken as

$$C_T(E,L)\cos\frac{\pi}{12}(\phi - 11) = \frac{1}{2\tau}\int_{-\tau}^{\tau} \log\left[\Phi(E,L,\phi,T+\tau')\right] d\tau' \tag{9}$$

and local time variations in the AE4 model are found to be

$$\Phi_T(E,L,\phi) = \frac{1}{F\left[C_T(E,L)\right]}\, 10^{C_T(E,L)\cos\frac{\pi}{12}(\phi-11)} \tag{10}$$

where

$$F(C) = \frac{1}{12}\int_0^{12} 10^{C\cos\frac{\pi}{12}\phi}\, d\phi \tag{11}$$

is the appropriate normalization factor. The coefficient $C_T(E,L)$ shows strong dependence on the phase of the solar cycle (refs. 2 and 8). The values given for solar minimum conditions in AE4, however, do not seem to agree with the observations. The observed values of the local time variation coefficient at geosynchronous altitude (L = 6.6) are shown in figure 2 along with the (time-shifted) smoothed sunspot number corresponding to the time of observations (values are taken from figs. 12 and 60 of ref. 8). Note that solar epoch T is represented in figure 2 by time-shifted smoothed sunspot numbers Z. If $C_T(E,L = 6.6)$ is represented by $C\left[E,Z(T)\right]$ then

$$C(E,Z) = 0.035 + 0.14 \log E + 0.04 \log^2 E + \frac{0.75 + 0.04(0.089788Z^{1.4})}{1 + 0.089788Z^{1.4}} \tag{12}$$

is seen to represent the local time variation coefficient accurately at the geosynchronous altitude by comparing the curves generated by equation (12) with the corresponding experimental data in figure 2. The normalization function F(C) is approximated by

$$F(C) = 0.9881 + 0.2559C + 0.3002C^2 + 1.2974C^3 \tag{13}$$

The L dependence of $C(E,Z)$ is ignored since the average local time variation has only a limited meaning in terms of manned-space operations, and the variations at $L = 6.6$ are conservative from the point of view of radiation protection (since the degree of variation generally increases with increasing L). Generally, it is anticipated that larger time fluctuations occur than are given by equation (12) even at $L = 6.6$, as is indicated by comparing the local time variation of the average flux with the variation of the median flux, as shown in figure 3 near solar maximum (ref. 4).

The effects of geomagnetic latitude variations are given by

$$G(B,L) = \left[B/B_0(L)\right]^{-m(L)} \qquad (B \ll B_c) \tag{14}$$

where B_c is the cutoff intensity and is large compared to field intensities in the region of geostationary orbits (ref. 2). The ratio in the brackets in equation (14) is a function of magnetic latitude only

$$\frac{B}{B_0(L)} = \frac{1}{\cos^6 \lambda_m}(1 + 3 \sin^2 \lambda_m)^{1/2} \tag{15}$$

The exponent in equation (14) is given by the AE4 model and has the value

$$m(L) = 0.6 \qquad (4 \leqq L \leqq 8.5) \tag{16}$$

The experimental uncertainty in $m(L)$ in the geostationary region appears to yield

$$m(L) = 0.6 \pm 0.6 \tag{17}$$

in the region of interest here as can be seen from figures 61 to 64 of reference 8.

RELATION OF SPATIAL TO MAGNETIC COORDINATES

The orbits of interest are restricted to circular orbits for which the period is 24 hr and the inclination of the orbit plane relative to the Earth's equator is small. The orientation of the orbit plane is taken as constant relative to the fixed stars and is defined by a line of nodes in the equatorial plane and an inclination angle. Due to the Earth's orbital motion about the Sun, the anti-Sun-Earth line rotates relative to the line of nodes and such a rotational cycle is completed in 1 solar year. The description of such orbits is now derived, and the relations to geographic coordinates are determined.

Define a frame located at the center of the Earth and with orientation fixed relative to the distant stars. The x_i-axis is taken along the projection of the anti-Sun-Earth line at the beginning of the solar year (that is, at $\Omega_0 = 0^\circ$ in fig. 4). Note that Ω_0 increases to 360° at the end of the solar year. A coordinate system is defined in the satellite orbit plane as

$$\vec{r}_o = [i]_x[\eta]_z\vec{r}_i \tag{18}$$

where η is the angle between the x_i-axis and the line of nodes and i is the orbit inclination angle relative to the Earth's equator. The orbital equations can then be written in the orbital plane as

$$\vec{r}_o = \begin{bmatrix} r\cos(\omega\phi_o - \Omega_o - \theta_o) \\ r\sin(\omega\phi_o - \Omega_o - \theta_o) \\ 0 \end{bmatrix} \tag{19}$$

where ϕ_o is taken as Greenwich local time, Ω_o is the phase between the anti-Sun-Earth line and the x_i-axis, and θ_o gives the orbital starting phase at the beginning of the first Greenwich day ($\phi_o = 0$) at the beginning of the solar year ($\Omega_o = 0^o$). The orbital motion will now be transformed to geographic coordinates.

A coordinate system is defined at the center of the Earth with z_e-axis coincident with the north pole and x_e-axis at zero longitude. This system rotates with respect to the distant stars at the rate $\omega = 15^o/hr$. The phase is chosen so that

$$\vec{r}_e = [\omega\phi_o - \Omega_o]_z\vec{r}_i \tag{20}$$

Motion in the orbit plane is then related to geographic coordinates as

$$\vec{r}_e = [\omega\phi_o - \Omega_o - \eta]_z[-i]_x\vec{r}_o \tag{21}$$

The equations of motion for circular geosynchronous orbit in terms of geographic coordinates (λ_g is geographic latitude, and ϕ_g is geographic longitude) are then

$$\sin\lambda_g = \sin i \sin(\omega\phi_o - \Omega_o - \theta_o) \tag{22}$$

$$\tan\phi_g = \frac{\cos(\omega\phi_o - \Omega_o - \eta)\sin(\omega\phi_o - \Omega_o - \theta_o)\cos i - \sin(\omega\phi_o - \Omega_o - \eta)\cos(\omega\phi_o - \Omega_o - \theta_o)}{\sin(\omega\phi_o - \Omega_o - \eta)\sin(\omega\phi_o - \Omega_o - \theta_o)\cos i + \cos(\omega\phi_o - \Omega_o - \eta)\cos(\omega\phi_o - \Omega_o - \theta_o)} \tag{23}$$

and, in the limit as $i \to 0$,

$$\lambda_g = 0 \tag{24}$$

$$\phi_g = \eta - \theta_o \tag{25}$$

For small inclinations a simple pattern of motion in geographic coordinates is traced out as indicated in figure 5. Even for rather large inclinations, the longitudinal variations are small and the approximations

$$\lambda_g \approx i \sin(\omega\phi_o - \Omega_o - \theta_o) \tag{26}$$

$$\phi_g \approx \eta - \theta_o \tag{27}$$

appear appropriate for $0 \leqq i \leqq 30^{\circ}$. This motion may then be expressed in terms of satellite local time ϕ by noting that

$$\phi = \phi_o + \frac{\phi_g}{\omega} \tag{28}$$

for which

$$\lambda_g \approx i \sin (\omega\phi - \eta - \Omega_o) \tag{29}$$

In order to assess the effects of inclined orbital motion on the radiation exposure, the relation of geographic to geomagnetic coordinates is required.

The environmental models are ordered according to magnetic coordinates B and L. At large distances the geomagnetic field may be approximated by the dipole contribution for which

$$L = \frac{r}{\cos^2 \lambda_m} \tag{30}$$

$$B = \frac{B_0}{\cos^6 \lambda_m}(1 + 3 \sin^2 \lambda_m)^{1/2} \tag{31}$$

where λ_m is the geomagnetic latitude (ref. 9). The magnetic north pole is approximately located at 11° colatitude and 290° longitude (latitudinal and longitudinal drifts are at the rate of 0.2° to 0.3° per year). The appropriate relation between magnetic latitude and geographic coordinates is then

$$\sin \lambda_m = \sin \lambda_g \cos 11^{\circ} + \cos \lambda_g \sin 11^{\circ} \cos (\phi_g - 290^{\circ}) \tag{32}$$

The maximum excursions in magnetic latitude will occur at $\phi_g = 110^{\circ}$ and 290° while the minimum excursions will occur at $\phi_g = 20^{\circ}$ and 200°. Since the exposure decreases with increasing L, the minimum exposures are expected at $\phi_g = 110^{\circ}$ and 290°, at least for the lowest inclinations. The latter location is placed over the Atlantic seaboard. For $\phi_g = 290^{\circ}$,

$$\sin \lambda_m = \sin (\lambda_g + 11^{\circ}) \tag{33}$$

for which significant variations in magnetic latitude are seen to be produced by the use of inclined orbits.

A preliminary assessment of the advantage of slightly inclined circular orbits may now be made. The effects of changing geomagnetic latitude appear mainly through the change in L as given by equation (30). The use of inclined orbits at $\phi_g = 290^{\circ}$ produces sinusoidal motion about the magnetic north pole offset of 11° as given by equation (33). One-half of the cycle has $\lambda_m \geqq 11^{\circ}$ while the remaining one-half has $\lambda_m \leqq 11^{\circ}$, which will be denoted by subscripts + and -, respectively. The average L over each half cycle is given by

$$\bar{L}_{\pm} = \frac{r}{\cos^2 11^{\circ}}\left(1 \pm \frac{4i}{\pi} \tan 11^{\circ} + \frac{1}{2} i^2\right) \qquad (34)$$

within a small inclination angle approximation. The effects of low inclination orbits on average L values are illustrated in table III. For comparison, the integrated average electron flux for energies above 1.5 MeV for each average L value is also shown in table III. As can be seen from table III, there is a large potential for reducing the exposure by using slightly inclined circular orbits at this longitudinal location. A more complete analysis of orbit inclination effects will be made in a subsequent section.

DOSE RATES IN THE GEOSTATIONARY REGION

To assess the effects of the belt radiations on operations in the geostationary region, a knowledge of the dose rate at each point of that region of space must be known as a function of shielding. The environment is a complicated function of universal time, local time, magnetic L-shell, and magnetic-field intensity. The AE4 environmental model, as described in a previous section, will be used to derive the appropriate dose rates. The short-term fluctuations in dose rates will be represented on a statistical basis. The long-term dose averages appropriate for extensive operations in connection with the construction of space facilities will also be determined.

The doses received by an object exposed to the outer-zone electrons are strongly dependent on size, shape, and material composition. In the absence of specific configuration and material requirements, some simplifying assumptions must be made. The simplifications associated with shape and size lead to two simple possibilities: (a) dose versus depth in a semi-infinite slab taking all electrons as normally incident, as illustrated in figure 6(a), or (b) dose versus depth in a semi-infinite slab taking all electrons as isotropically incident on one side, as illustrated in figure 6(b). Assumption (a) has the advantage that it can be used to evaluate doses in any arbitrary geometry by integration over appropriate path-length distributions. For this reason doses calculated under assumption (a) are presented in the appendix for use in future analysis. Assumption (b) has the advantage that it represents meaningful estimates of dose for most applications and will be discussed extensively. For example, the results for assumption (b) approximate directly the doses in extremities like the hands or feet and these values reduced by a factor of 2 approximate the body skin dose. The adequacy of these approximations must await a more accurate analysis. The relative differences between the two calculations are shown in figure 7 where it is observed that the differences are large. Concerning the choice of materials for which the calculations are made, one is limited, by the lack of available alternative techniques, to dose within a small tissue sample embedded in an aluminum shield. Substantial differences in dose for a given shield mass can be expected by use of other materials.

The dose rates at the geomagnetic equator have been calculated using the methods of Watts and Burrell (ref. 10) for an isotropic angular dependence and

aluminum-slab shielding. The universal time dependence is represented as a statistical model, and the dose limit associated with a probability P of not exceeding that level has been calculated. The equatorial dose rate is then represented as a function of sunspot number, shield thickness, magnetic L-shell, local time, and probability P as $D_Z(X,L,\phi,P)$. The average over local time and short-term fluctuations is calculated as

$$\bar{D}(X,L) = \frac{1}{24}\int_0^{24} d\phi \int_0^1 dP\ D_Z(X,L,\phi,P) \tag{35}$$

and the L dependence for various shield thicknesses in the geostationary region is shown in figure 8. The average dose rate given by equation (35) is found to be independent of the phase of the solar cycle for shield thicknesses of interest.

The average dose rate is found to be of the following parametric form:

$$\bar{D}(X,L) = 10^{p_e(X,L)} + 10^{p_\gamma(X,L)} \tag{36}$$

where the polynomial representing the average electron dose is

$$p_e(X,L) = e_0(L) + e_1(L)X + e_2(L)X^2 + e_3(L)X^3 \tag{37}$$

with the $e_j(L)$ coefficients given in table IV for discrete L values. The coefficients at intermediate L values are found by linear interpolation. The polynomial representing the average photon dose is given by

$$p_\gamma(X,L) = \gamma_0(L) + \gamma_1(L)X \tag{38}$$

with discrete values of the $\gamma_j(L)$ coefficients given in table V where intermediate L values are obtained by linear interpolation.

From the point of view of manned operations, the dose will be allowed to accumulate behind a given shield thickness until some dose rate level is exceeded after which shelter in a more heavily shielded area will be obtained. Of interest from this point of view is the average dose rate below a given action level (represented here by the probability P that the action level is not exceeded). These average rates are found by

$$D(X,L,\leq P) = \frac{1}{24}\int_0^{24} d\phi \int_0^P dP'\ D_Z(X,L,\phi,P') \tag{39}$$

and the dependence of these restricted averages on shield thickness L and action level denoted by P is shown in figures 9 to 16. Again the average over all local times does not exhibit noticeable solar cycle dependence.

The average dose rate as a function of local time is given by

$$\bar{D}_Z(X,L,\phi) = \int_0^1 dP' \, D_Z(X,L,\phi,P') \tag{40}$$

and is found to have the following functional form:

$$\bar{D}_Z(X,L,\phi) = \bar{D}(X,L)\frac{10^{b_Z(X,L)\cos\frac{\pi}{12}(\phi-11)}}{F\left[b_Z(X,L)\right]} \tag{41}$$

where

$$b_Z(X,L) = b(X,L) - \frac{0.71(0.089788Z^{1.4})}{1 + 0.089788Z^{1.4}} \tag{42}$$

with

$$b(X,L) = \left[\sum_{j=0}^{2} b_j(L)X^j\right]_{>0} \tag{43}$$

The subscripted term in brackets is defined as

$$\left[Z\right]_{>0} = \begin{cases} Z & Z > 0 \\ 0 & Z \leq 0 \end{cases} \tag{44}$$

The $b_j(L)$ coefficients are given in table VI for discrete L values. Linear interpolation is used for intermediate values.

The analytical representation of AE4 dose rates presented in this section agrees with the values calculated from the representation of the electron environment given by equations (6), (8), and (12) to within 10 percent. The absolute accuracy of these analytical representations is not precisely known.

DOSE RATES FOR CIRCULAR GEOSYNCHRONOUS ORBITS

The dose rate is a function of shielding, orbital position, and local time. In the case of geosynchronous circular orbits, the orbital position is likewise a function of local time. One may consider that, since the location and dose-rate variation are periodic in local time, the initial orbital phase may be chosen to form a coalescence so as to minimize exposure, especially during extravehicular activity. Closer examination shows, however, that the initial orbital phase advances during the course of the solar year and any possible advantage from such a coalescence is completely destroyed after 6 months only to be

reestablished 6 months later. The progression of the local time variation for different seasons of the solar year is shown for orbits inclined by 10° and geographic longitude at 290° for solar minimum (Z = 0) in figure 17, and for solar maximum (Z = 100) in figure 18. The starting phase of each orbit is shown in the figures. Clearly, the local time variation cannot be used to reduce the exposure significantly, especially at epochs other than solar minimum.

The only reliable means to reduce exposure (besides the utilization of short-term fluctuations) for geosynchronous operations appear through the use of inclined circular orbits. The dose rates for $\phi_g = 290°$ will be composed of a 12-hr period of relatively low exposure followed by 12 hr of high exposure. The dose rate is mainly determined by the geographic latitude (that is, the L-shell corresponding to that latitude). A given latitude will, in the course of 1 solar year, correspond to all possible local times. The latitude is a function of the orbit phase, as given by equation (23) or equation (26) for small inclination. The pertinent quantity is the average dose rate as seen at a given orbital phase (that is, fixed latitude), which is shown in figures 19 to 24 for various inclinations and geographic longitudes of 20° and 290°. The orbital phase in figures 19 to 24 corresponds to the time during the completion of one geosynchronous orbit similar to those shown in figure 5. As can be seen in figures 19 to 24, persistent dose-rate variations are produced which can be used to control exposure during extravehicular activity for which heavy shielding cannot be provided.

If orbit inclination is to be used to control exposure, then the average ambient exposure within the habitat and the average exposure during work shifts outside the habitat are of interest. It is assumed that work periods are of a 12-hr duration (that is, two 6-hr work shifts) with the remaining 12 hr spent in the habitat. The 12-hr work period is taken at the lull in the radiation field as seen in figures 19 to 24. For $\phi_g = 20°$, the work periods would be taken as alternating 6 hr on, followed by 6 hr off. For $\phi_g = 290°$, there would be two 6-hr shifts back-to-back, followed by 12 hr off.

The dose rate averaged over the entire orbit is shown in figures 25 and 26 as a function of shield thickness for various inclinations. Since a worker will spend time at different locations (different shielding) during the radiation highs and lows, the 12-hr averages of the dose rates during these periods of high and low exposure have been calculated and are shown in figures 27 to 30.

DOSES FOR GEOSYNCHRONOUS OPERATIONS AND SHIELD REQUIREMENTS

The career exposure limits and rate constraints which are presently used for mission planning and analysis (ref. 11) are shown in table VII. Nominal shield requirements and operational constraints are to be determined so that the limits in table VII are not exceeded. The analysis of shield requirements is complicated by the time line taken by the astronaut within three distinct shielded areas; namely, the space suit, the habitat, and under extreme conditions a heavily shielded radiation shelter. The shield thickness for each mission segment is to be determined by meeting dose constraints as well as other requirements, such as the need to minimize the habitat or radiation shelter weight, or the need to maximize the time spent on extravehicular activity (EVA), or the

need to maximize the astronaut's maneuverability and dexterity during EVA. The principal questions concern the number of days required to reach the exposure limits during EVA, the fraction of the permissible exposure received while living in the habitat, the limiting biological factors and whether personal shielding can be utilized, and finally the impact of a sudden solar particle increase on shield requirements. Information useful for the resolution of these questions will now be derived and preliminary shield thicknesses will be determined.

The dose constraints relate to the doses received by four body organs as given in table VII. For present purposes, the doses are estimated as follows:

$$D_{BFO}(X) \approx D(X + 5) \tag{45}$$

$$D_{skin}(X) \approx \frac{1}{2} D(X) \tag{46}$$

$$D_{lens}(X) \approx \frac{1}{2} D(X + 0.3) \tag{47}$$

$$D_{testes}(X) \approx D(X + 3) \tag{48}$$

where $D(X)$ denotes the dose at depth X in an aluminum slab for isotropic incident electrons and BFO denotes blood-forming organ. The adequacy of these approximations is to be determined. The variable X in equations (45) to (48) denotes the external shield thickness. The numerical values on the right-hand sides of equations (45) to (48) approximately account for self-shielding.

Space-Suit Shielding

The space-suit requirements will be determined by the desire to maximize the amount of time spent on EVA. Aside from the need for a 1-gram-per-square-centimeter-thick helmet as dictated by the limiting factor during an extreme median energy solar event (ref. 11), the space-suit thickness will be used mainly for protection from the outer-zone electrons. A conservative shield design taking no advantage of ceasing work activity during extreme fluctuations in the electron intensities is assumed here. The actual dose received can be reduced by at least a factor of 2 by ceasing EVA during the 10 to 20 percent most intense days as can be seen from figures 15 and 16 (see discussion of eq. (39) in connection with figs. 15 and 16). Assuming that the work shifts are for all days, the number of days required to reach the quarterly exposure limits have been calculated for each of the critical body organs and the results are given in figures 31 to 36.

It is seen in figures 31 to 36 that the skin dose is the limiting factor during EVA operations. The minimum space-suit shield requirements calculated from the figures by requiring that there be 90 days of shifts per quarter are shown in table VIII. The shielding required for two shifts per day (each astro-

naut works only one shift) during the radiation maximum is shown in the third column with the requirements at radiation minimum shown in column 4. The shield requirements for an average shift are shown in the last column of table VIII.

The required space-suit shielding shown in table VIII is in most cases rather thick and may prove to be an excessive limitation on the astronaut's ability to perform useful work functions. If the most extreme days of the belt fluctuations are avoided, then great reductions in space-suit requirements are realized. If only 70 percent of the days are worked (approximately equivalent to a 5-day work week), then exposure is reduced by a factor of 3.85. The corresponding space-suit requirements are given in table IX.

It should be further noted that 90 percent of the exposure is received on the one-half of the days that are most extreme. Hence, the shield requirements listed even in table IX are more than those which are required for the one-half of the least extreme days. Again, a graduated set of space suits is clearly indicated to provide maximum maneuverability on the least intense days with a heavier shielded suit for the more intense days (ref. 1).

Habitat Shielding

The habitat is the normal living quarters in which the bulk of the astronaut's time in space will be spent. Since dose limits during EVA will be approached, the habitat must be nearly radiation free. For the purpose of determining habitat shield requirements, the fraction of the quarterly exposure limits received within a habitat each quarter has been calculated as a function of habitat wall thickness. These results are shown in figures 37 and 38 for various orbit inclinations and the two geographic locations.

It is noted from the figures that the organs which are most exposed in proportion to their exposure constraints within the habitat are those which are least exposed during EVA. This is the result of the large dose gradients (due to penetrating electrons) during EVA as opposed to the more uniform exposure (from photons) within the habitat. It is seen in figures 37 and 38 that the testes dose is the limiting factor within the habitat and that personal shielding could be used to advantage to control exposure.

Since it is considered that the main exposure of the astronaut is to be during EVA, the exposure within the habitat must be made negligibly small (less than 10 percent of the exposure constraint). If an aluminum wall structure (or other low-atomic-number material) is used throughout, then wall thicknesses in excess of 6 g/cm^2 will be required. More efficient would be the use of a high-atomic-number material as an inner wall liner to eliminate the bremsstrahlung produced in the outer habitat wall. The total wall thickness can probably, in this way, be reduced to 2 g/cm^2, or less. The accurate determination of such a multilayered wall structure is beyond our present capability to calculate. Some preliminary efforts along these lines have been made (ref. 12), but techniques are lacking for the general optimum shield design problem.

CONCLUDING REMARKS

The use of local time variations, work stoppages during extreme highs of the short-term fluctuations, and orbit inclination to minimize exposure and space-suit shield requirements during extravehicular activity (EVA) for near geostationary operations have been considered utilizing the AE4 environmental model. It is found that local time variations cannot be effectively utilized at solar minimum and are not of sufficient magnitude at epochs other than solar minimum. Large reductions in exposure and space-suit requirements are obtained by the use of work stoppages during extreme highs of the short-term fluctuations. The impact of work stoppages on work activity must yet be evaluated. Exposure and space-suit shield reductions also result by using slightly inclined orbits. The habitat walls, if constructed of low-atomic-number materials, will be excessively thick. Construction utilizing high-atomic-number materials as an inner wall liner will probably reduce the wall thickness to near 2 g/cm^2. Personal shielding of the testes within the habitat may prove to be advantageous.

Extensive tables and graphs are presented for future analysis of shield requirements for operations in the geostationary regions.

Langley Research Center
National Aeronautics and Space Administration
Hampton, VA 23665
February 8, 1977

APPENDIX

ELECTRON DOSE RATES FOR NORMAL INCIDENCE

The average equatorial dose rates taking all electrons as normally incident on an aluminum slab have been calculated as a function of depth in the slab. These results may be used in calculations of doses utilizing path-length data in human geometry. The dose rates are represented as L-dependent polynomials as follows:

$$D(X,L) = 10^{p_e(X,L)} + 10^{p_\gamma(X,L)} \tag{A1}$$

where the polynomial representing the average electron dose is

$$p_e(X,L) = \sum_{j=0}^{3} a_j(L)X^j \tag{A2}$$

and the polynomial representing the average photon dose is given by

$$p_\gamma(X,L) = d_0(L) + d_1(L)X \tag{A3}$$

The $a_j(L)$ and $d_j(L)$ coefficients are listed in table X for discrete values of L. Intermediate values may be found by numerical interpolation.

REFERENCES

1. Wilson, John W.; and Denn, Fred M.: Preliminary Analysis of the Implications of Natural Radiations on Geostationary Operations. NASA TN D-8290, 1976.

2. Singley, G. Wayne; and Vette, James I.: The AE4 Model of the Outer Radiation Zone Electron Environment. NSSDC 72-06, NASA Goddard Space Flight Center, 1972.

3. Williams, Donald J.: Outer Zone Electrons. Radiation Trapped in the Earth's Magnetic Field, Billy M. McCormac, ed., Gordon & Breach, Sci. Publ., Inc., 1966, pp. 263-283.

4. Paulikas, G. A.; and Blake, J. B.: The Particle Environment at the Synchronous Altitude. Models of the Trapped Radiation Environment. Volume VII: Long-Term Time Variations. NASA SP-3024, 1971, pp. 51-67.

5. Vette, James I.: Summary of Particle Populations in the Magnetosphere. NASA TM X-63673, 1969.

6. Vette, James I.; Lucero, Antonio B.; and Wright, Jon A.: Models of the Trapped Radiation Environment. Volume III: Electrons at Synchronous Altitudes. NASA SP-3024, 1967.

7. Vette, James I.; Lucero, Antonio B.; and Wright, Jon A.: Models of the Trapped Radiation Environment. Volume II: Inner and Outer Zone Electrons. NASA SP-3024, 1966.

8. Singley, G. Wayne; and Vette, James I.: A Model Environment for Outer Zone Electrons. NASA TM X-69989, 1972.

9. McIlwain, Carl E.: Magnetic Coordinates. Radiation Trapped in the Earth's Magnetic Field, Billy M. McCormac, ed., Gordon & Breach, Sci. Publ., Inc., 1966, pp. 45-61.

10. Watts, John W., Jr.; and Burrell, M. O.: Electron and Bremsstrahlung Penetration and Dose Calculation. NASA TN D-6385, 1971.

11. Space Science Board: Radiation Protection Guides and Constraints for Space-Mission and Vehicle-Design Studies Involving Nuclear Systems. Natl. Acad. Sci. - Natl. Res. Counc., 1970.

12. Morel, Jim E.: Doses to a Thin Silicon Slab Behind Aluminum, Aluminum-Tantalum, and Aluminum-Lead Shields for Isotropic Fission Electrons. AFWL Tech. Note DYT TN-75-1, U.S. Air Force, Sept. 1975.

TABLE I.- COEFFICIENTS FOR MEAN-LOG FLUX AT VARIOUS L-SHELLS

L	μ_0	μ_1	μ_2	μ_3
6.6	7.4678	-2.5881	0.7205	-0.1164
7.0	7.4324	-2.9967	.8799	-.1375
7.5	7.3091	-3.5252	1.1859	-.1935
8.0	7.1356	-4.5104	1.9030	-.3631
9.0	6.2440	-4.8491	1.4469	-.3122
10.0	5.4778	-7.4778	5.8300	-5.0747

TABLE II.- COEFFICIENTS FOR LOG-FLUX STANDARD DEVIATION

FOR VARIOUS L-SHELLS

L	σ_0	σ_1	σ_2	σ_3
6.6	0.1449	0.6542	-0.2532	0.0241
7.0	.1480	.6641	-.2946	.0327
7.5	.2640	.3853	-.1903	.0174
8.0	.3617	.1230	-.0846	.0008
9.0	.7613	-1.2424	.9042	.2492
10.0	.8183	-.7068	-.9643	0

TABLE III.- EFFECTS OF ORBIT INCLINATION ON EXPOSURE AT $\phi_g = 290^o$

i, deg	$\bar{L}_+$, Earth radii	Flux,* electrons/cm^2-sec	$\bar{L}_-$, Earth radii	Flux,* electrons/cm^2-sec
0	6.85	1.0×10^5	6.85	1.0×10^5
10	7.30	3.3×10^4	6.67	1.7×10^5
20	8.03	3.7×10^3	6.77	1.3×10^5
30	8.74	6.1×10	6.91	9.0×10^4

*Flux of electrons with energy above 1.5 MeV.

TABLE IV.- COEFFICIENTS FOR AVERAGE ELECTRON DOSE AT VARIOUS L-SHELLS

L	e_0	e_1	e_2	e_3
6.6	4.3863	-4.3108	1.6899	-0.5651
7.0	4.3338	-5.4413	2.7325	-.9034
7.5	4.1988	-7.0768	4.7296	-1.6784
8.0	3.8256	-8.4001	6.3887	-2.4633
9.0	3.1901	-13.2579	11.6860	-5.6497
10.0	2.5052	-21.7532	27.2432	-36.5023

TABLE V.- COEFFICIENTS FOR AVERAGE PHOTON DOSE AT VARIOUS L-SHELLS

L	γ_0	γ_1
6.6	0.1045	-0.0835
7.0	-.0900	-.0834
7.5	-.3447	-.0837
8.0	-.7083	-.0840
9.0	-1.5021	-.0885
10.0	-2.4492	-.0937

TABLE VI.- COEFFICIENTS FOR DOSE-RATE LOCAL TIME VARIATION

L	b_0	b_1	b_2
6.6	-0.0535	0.3454	-0.1794
7.0	-.0679	.3916	-.2206
7.5	-.0438	.3433	-.2095
8.0	-.0367	.3664	-.2676
9.0	-.0202	.4677	-.6041
10.0	-.0462	.9452	-2.1375

TABLE VII.- SUGGESTED EXPOSURE LIMITS AND EXPOSURE ACCUMULATION RATE CONSTRAINTS FOR UNIT REFERENCE RISK CONDITIONS

Constraint	Ancillary reference risks				
	Primary reference risk (rem at 5 cm)	Bone marrow (rem at 5 cm)	Skin (rem at 0.1 mm)	Ocular lens (rem at 3 mm)	Testes (rem at 3 cm)
1-year average daily rate		0.2	0.6	0.3	0.1
30-day maximum		25	75	37	13
Quarterly maximum[a]		35	105	52	18
Yearly maximum		75	225	112	38
Career limit	400	400	1200	600	200

[a]May be allowed for two consecutive quarters followed by 6 months of restriction from further exposure to maintain yearly limit.

TABLE VIII.- MINIMUM SPACE-SUIT SHIELD REQUIREMENTS FOR SHIFTS DURING RADIATION MAXIMUM, MINIMUM, AND AVERAGE

ϕ_g, deg	i, deg	Shield thickness, g/cm^2 aluminum		
		Maximum	Minimum	Average
290	0	0.90	0.90	0.90
290	10	1.06	.68	.94
290	20	1.03	.56	.92
290	30	.94	.50	.83
20	0	1.15	1.15	1.15
20	10	1.07	.97	1.03
20	20	1.01	.62	.90
20	30	.93	.21	.82

TABLE IX.- MINIMUM SPACE-SUIT SHIELD REQUIREMENTS FOR 30-PERCENT WORK LOSS PER QUARTER FOR WORKING SHIFTS DURING RADIATION MAXIMUM, MINIMUM, AND AVERAGE

ϕ_g, deg	i, deg	Shield thickness, g/cm^2 aluminum		
		Maximum	Minimum	Average
290	0	0.69	0.69	0.69
290	10	.82	.49	.72
290	20	.80	.40	.70
290	30	.72	.35	.63
20	0	.86	.86	.86
20	10	.83	.74	.79
20	20	.78	.45	.68
20	30	.72	.14	.62

TABLE X.- PARAMETERS FOR THE CALCULATION OF DOSE RATE IN AN ALUMINUM SLAB FOR NORMAL INCIDENCE

L	a_0	a_1	a_2	a_3	d_0	d_1
6.6	4.7662	-3.7310	1.0868	-0.2927	-0.2819	0.0112
7.0	4.7053	-4.7646	1.9443	-.5320	-.4677	.0125
7.5	4.4561	-5.4529	2.3675	-.6121	-.7142	.0141
8.0	4.1526	-7.0018	4.1130	-1.2859	-1.0681	.0158
9.0	3.7010	-12.9946	12.1489	-6.0786	-1.8593	.0169
10.0	2.8740	-18.8603	17.9546	-17.5813	-2.8004	.0154

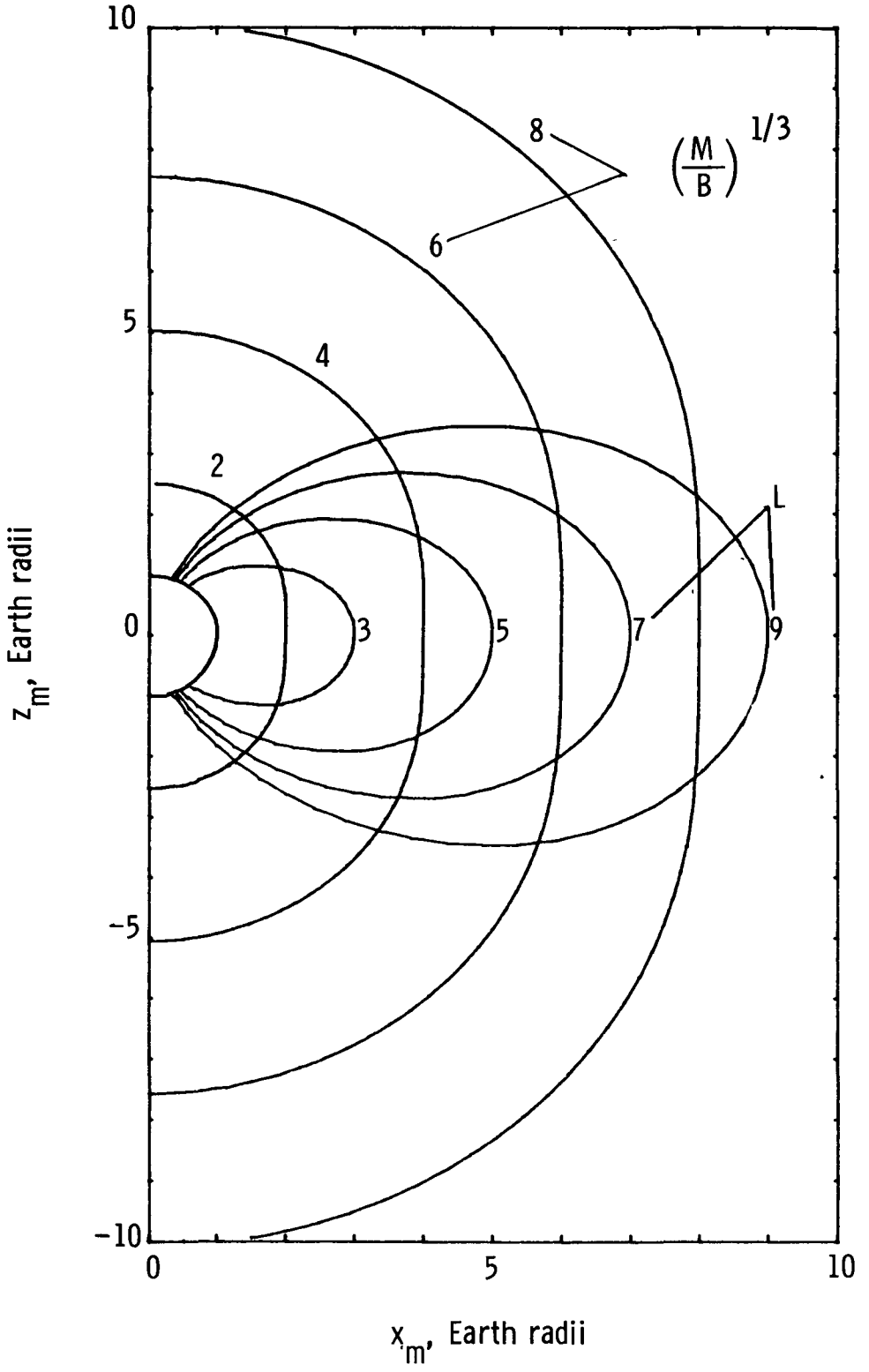

Figure 1.- Intersection of B and L surfaces of the geomagnetic dipole field with the right half of the (X_m, Z_m) plane. The B surfaces are labeled by $(M/B)^{1/3}$ in units of Earth radii where M is the geomagnetic dipole moment.

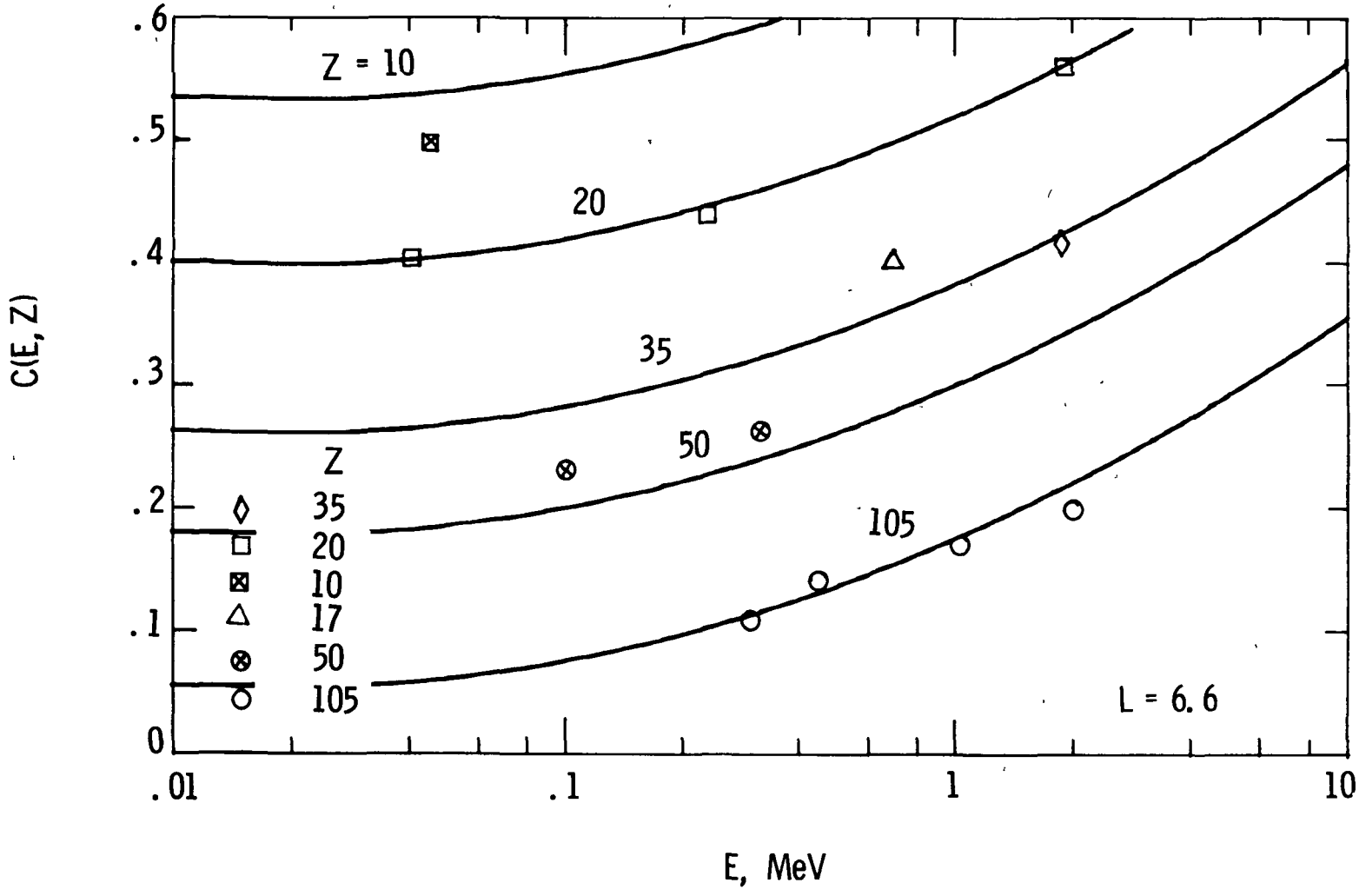

Figure 2.- Coefficient of average local time variation at L = 6.6 as a function of electron energy for different shifted sunspot numbers Z, as given by equation (12) in comparison to measurements taken from figure 60 of reference 8.

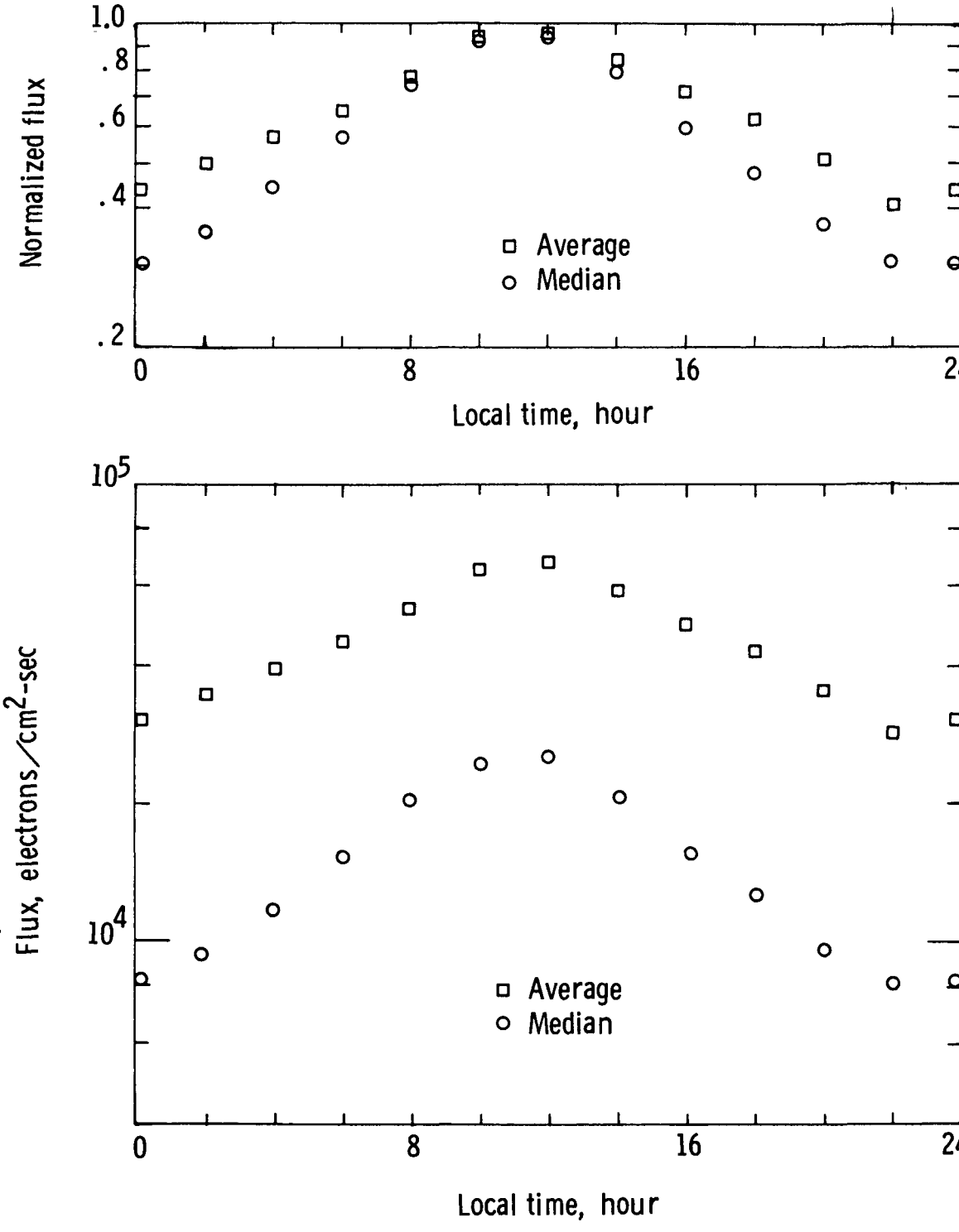

Figure 3.- Local time variations at geostationary altitude as measured by Paulikas and Blake (ref. 4) near solar maximum. Top graph shows the flux normalized to unity at the eleventh hour.

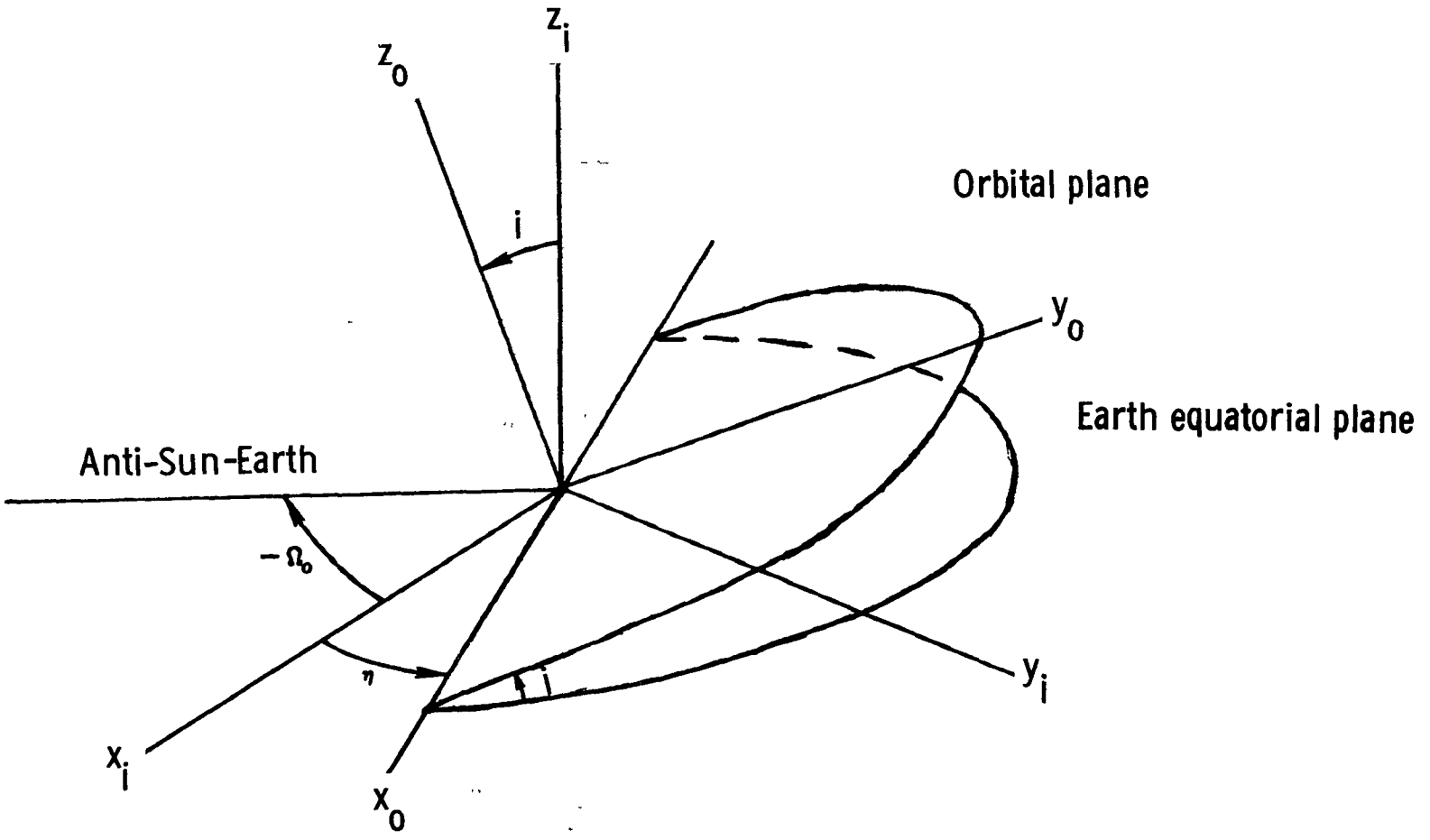

Figure 4.- Relation of inertially oriented coordinate systems defined in the orbital plane and in the Earth's equatorial plane.

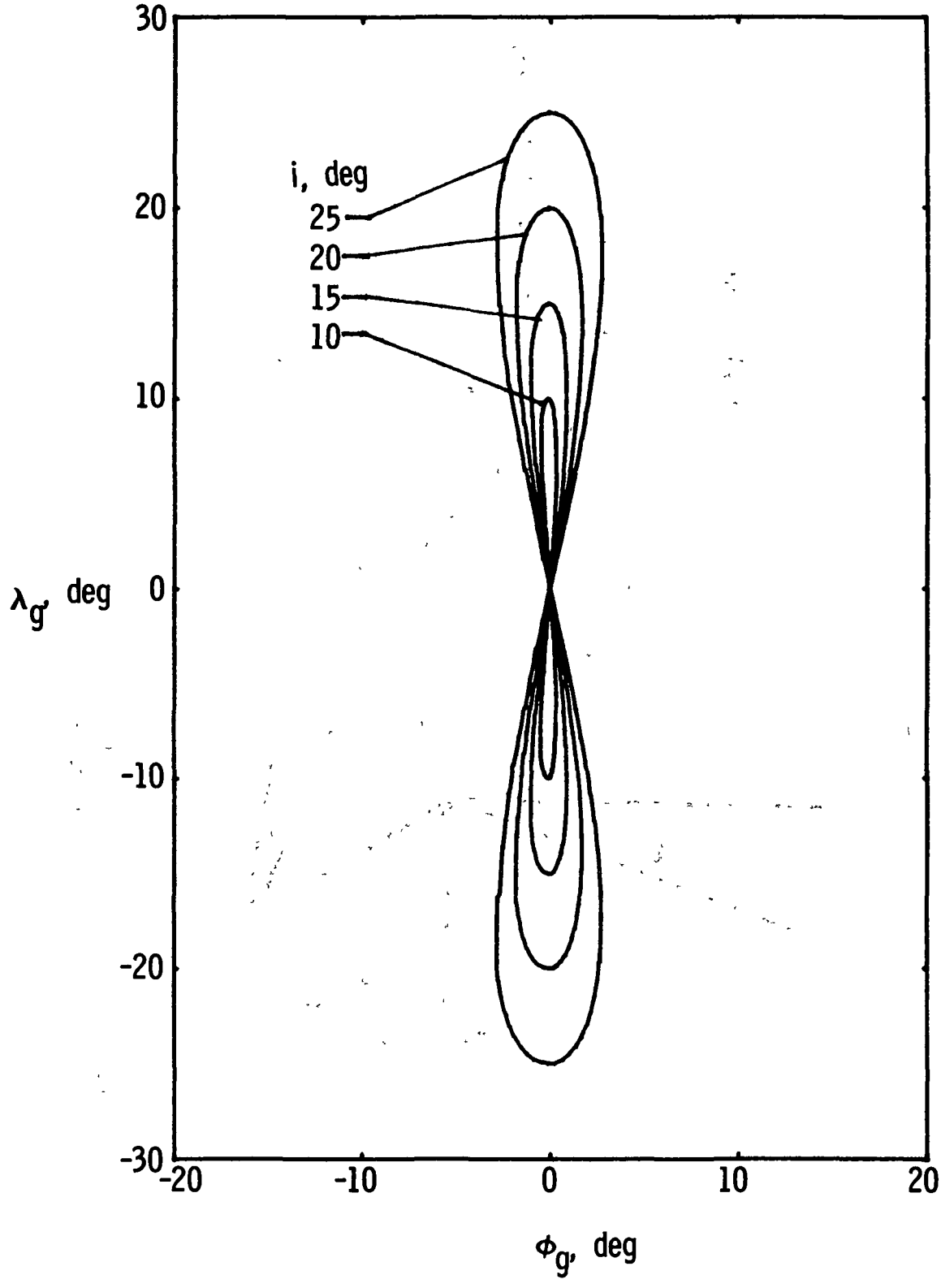

Figure 5.- Geographic trajectory of slightly inclined geosynchronous circular orbits over Greenwich at the four indicated inclinations.

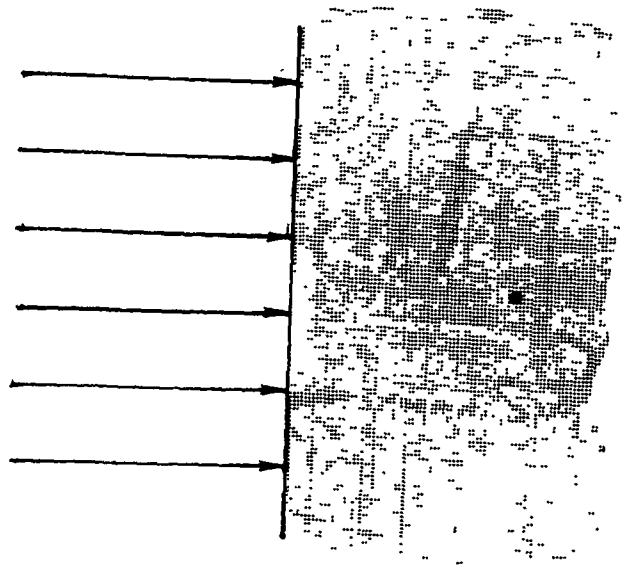

(a) Normal incidence.

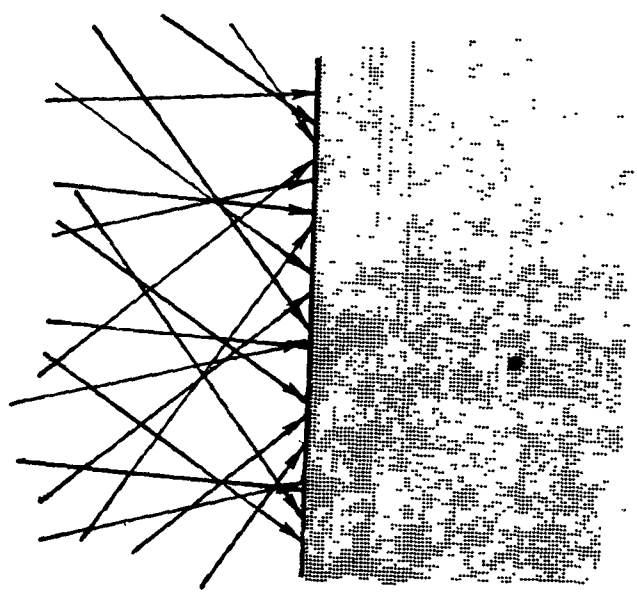

(b) Isotropic incidence.

Figure 6.- Slab geometry used in the present calculations showing electron trajectories incident from the left.

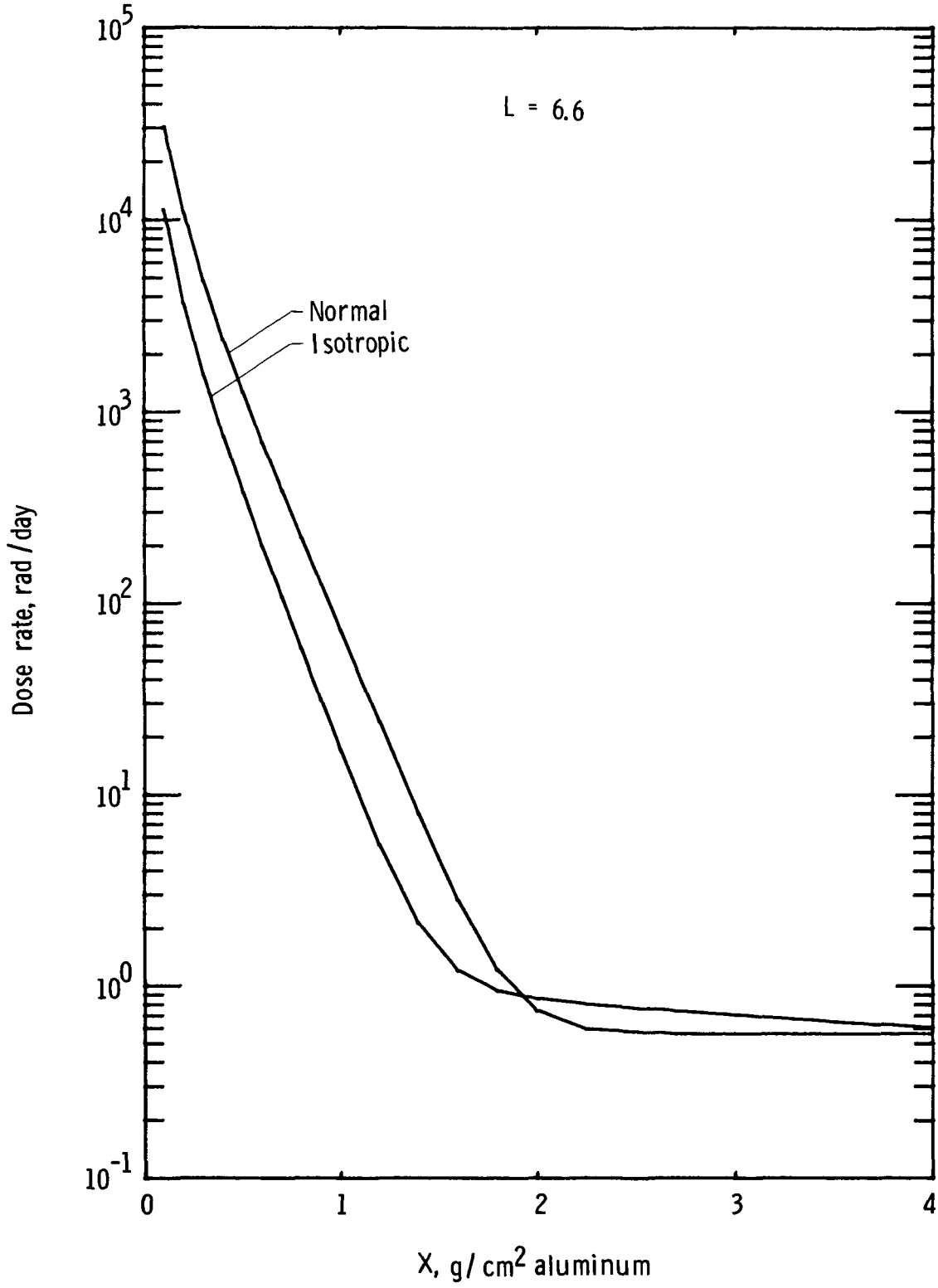

Figure 7.- Geostationary average dose rates behind an aluminum slab for normal and isotropic incidence.

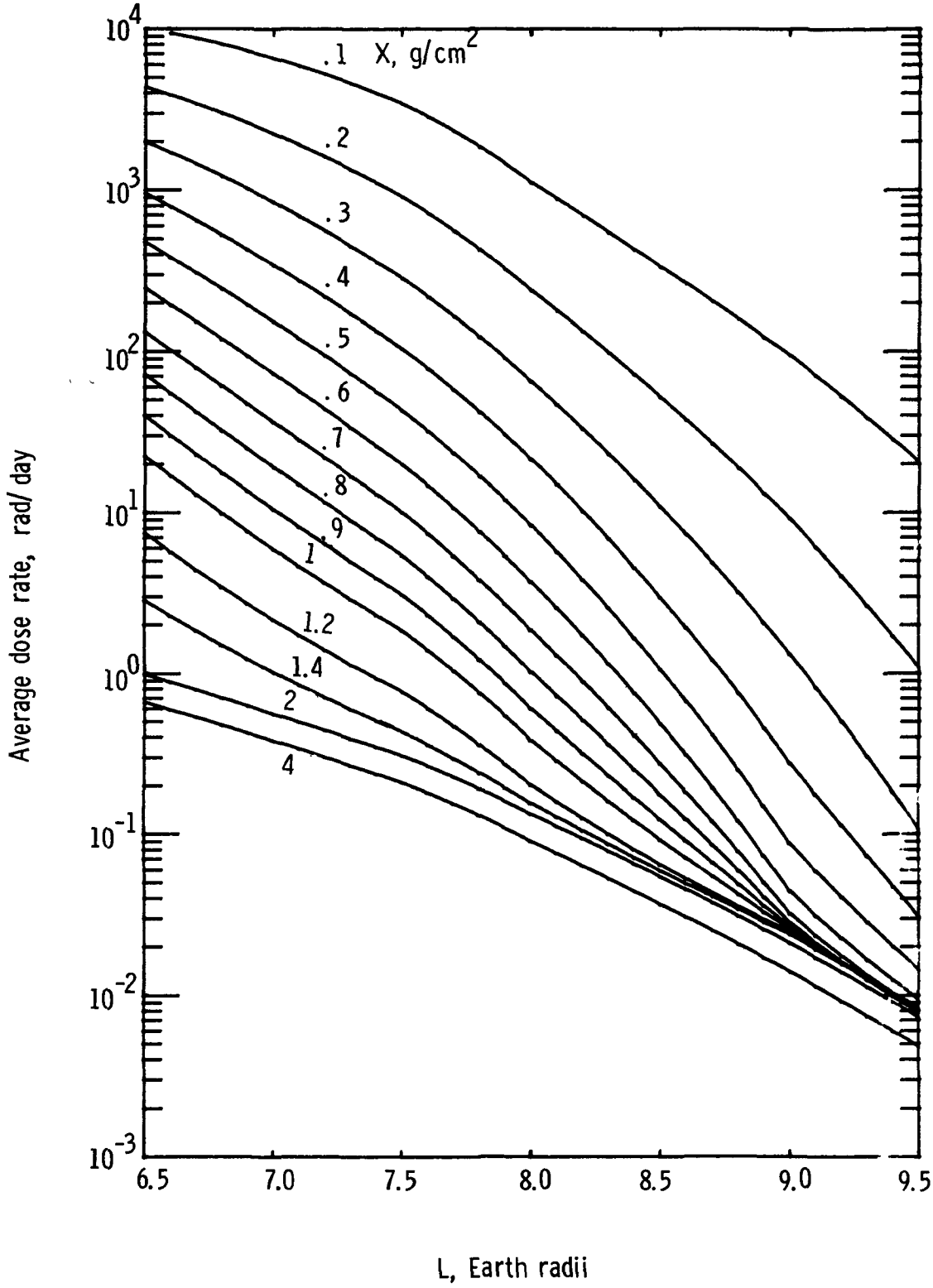

Figure 8.- Equatorial average dose rate as a function of L-shell behind various aluminum-shield thicknesses.

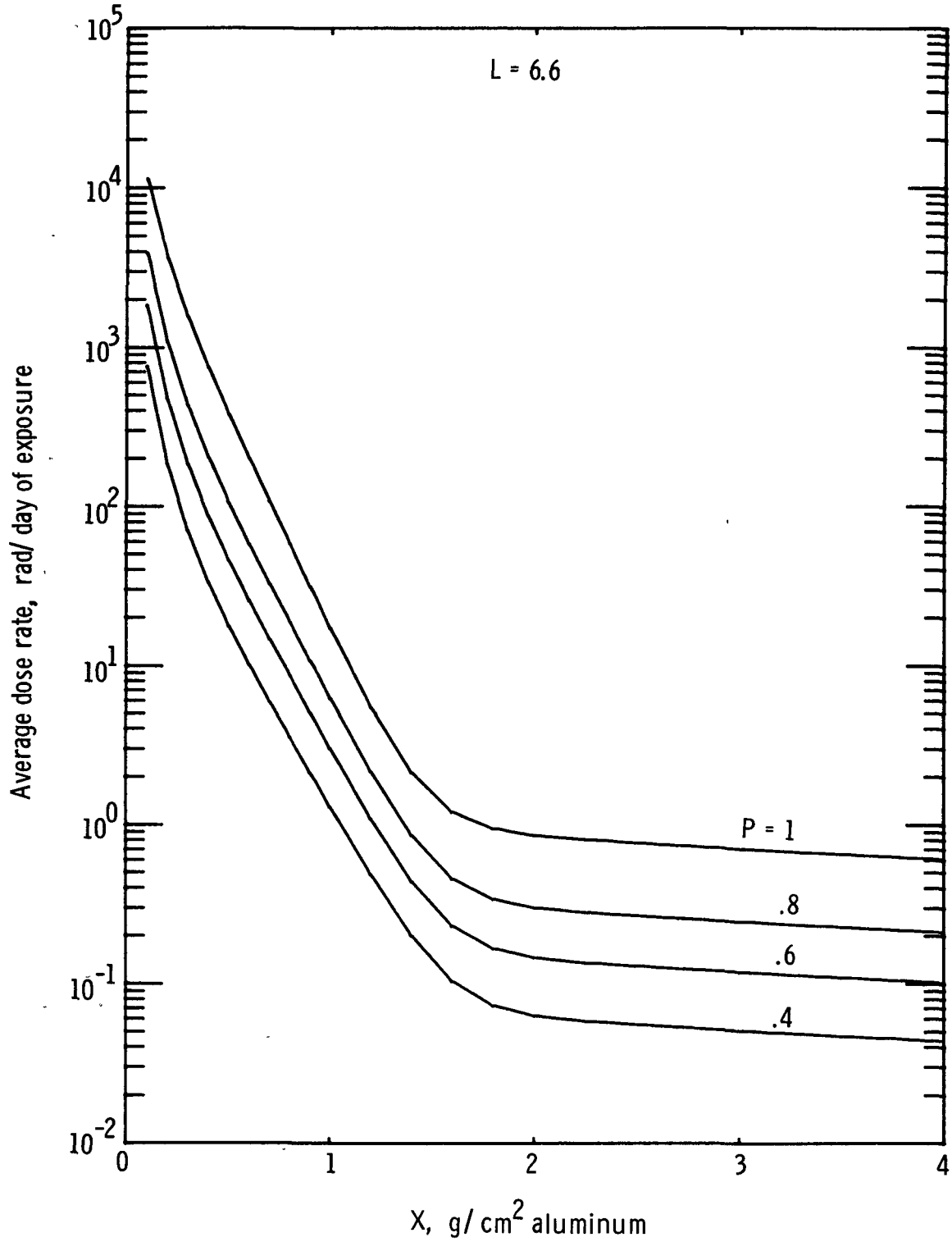

Figure 9.- Restricted average dose rates at L = 6.6 as a function of shield thickness for selected probability levels denoted by P.

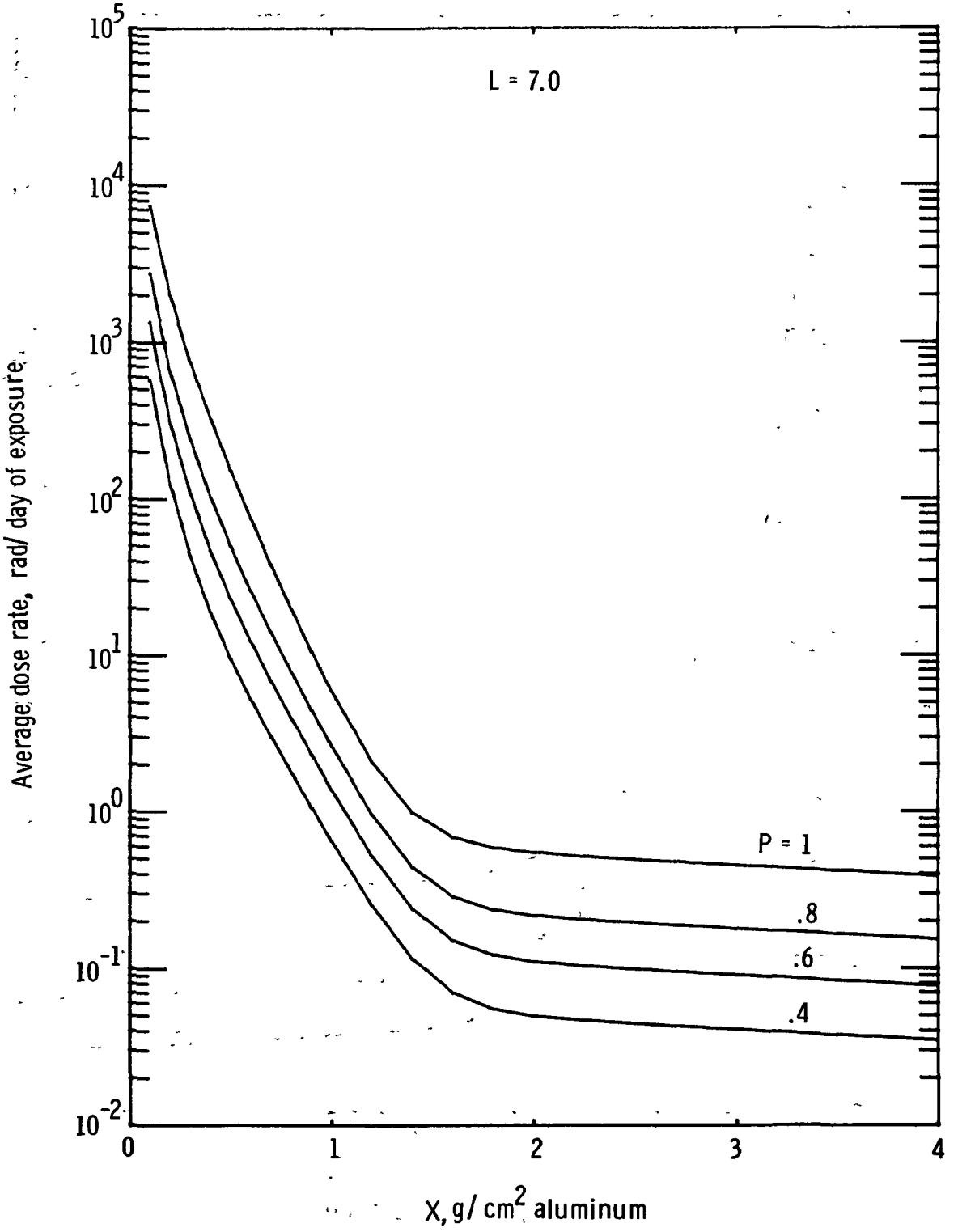

Figure 10.- Restricted average dose rates at L = 7.0 as a function of shield thickness for selected probability levels denoted by P.

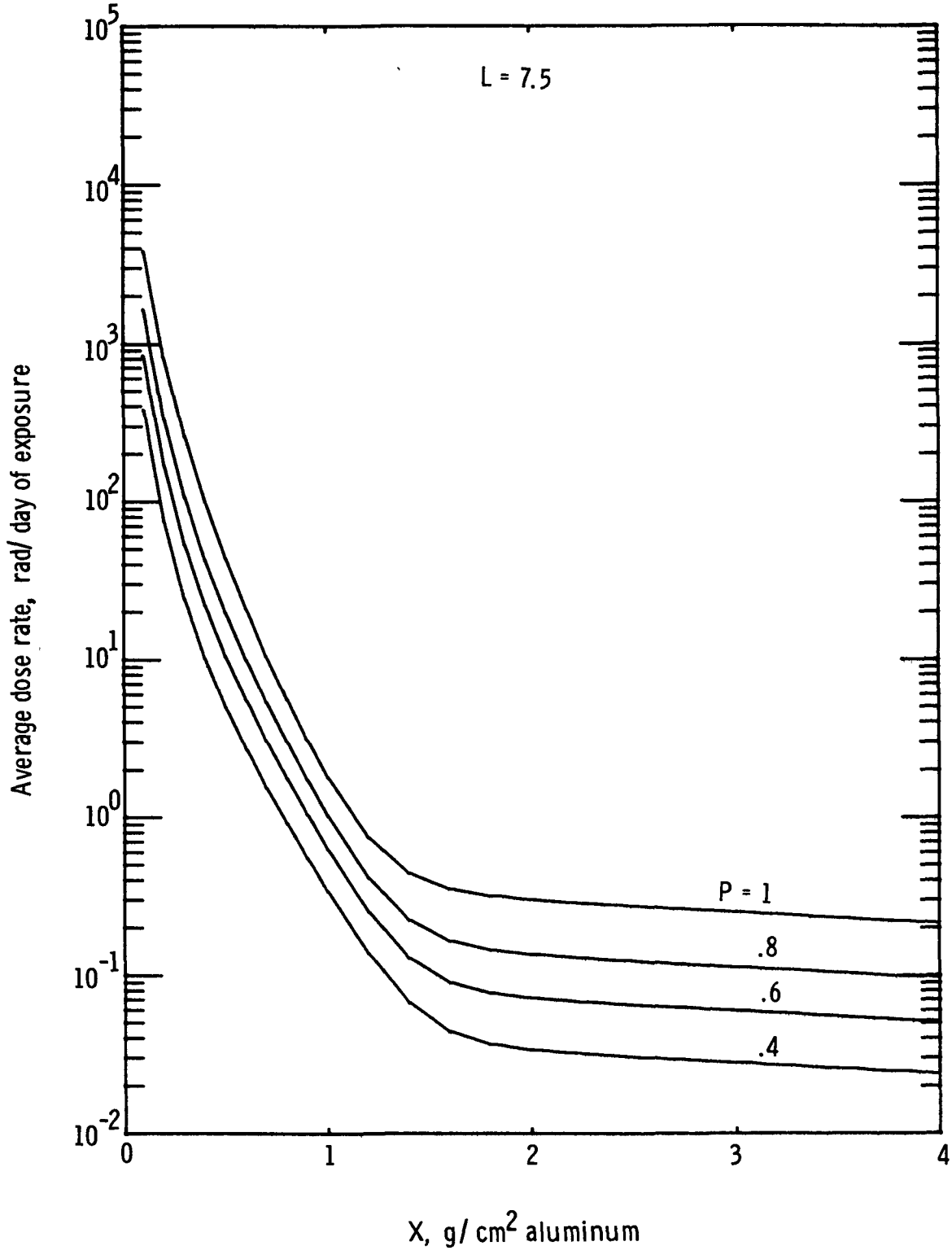

Figure 11.- Restricted average dose rates at L = 7.5 as a function of shield thickness for selected probability levels denoted by P.

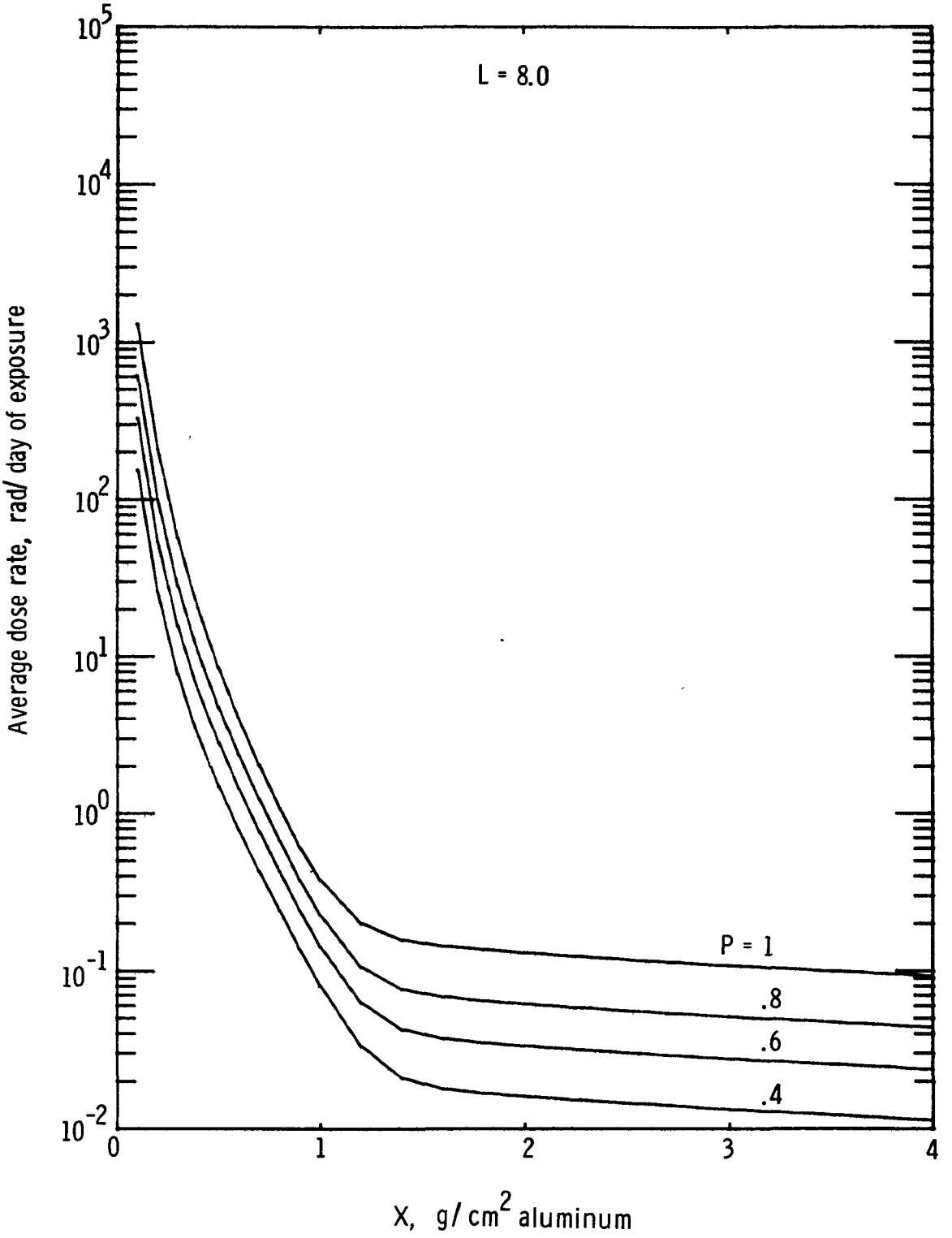

Figure 12.- Restricted average dose rates at L = 8.0 as a function of shield thickness for selected probability levels denoted by P.

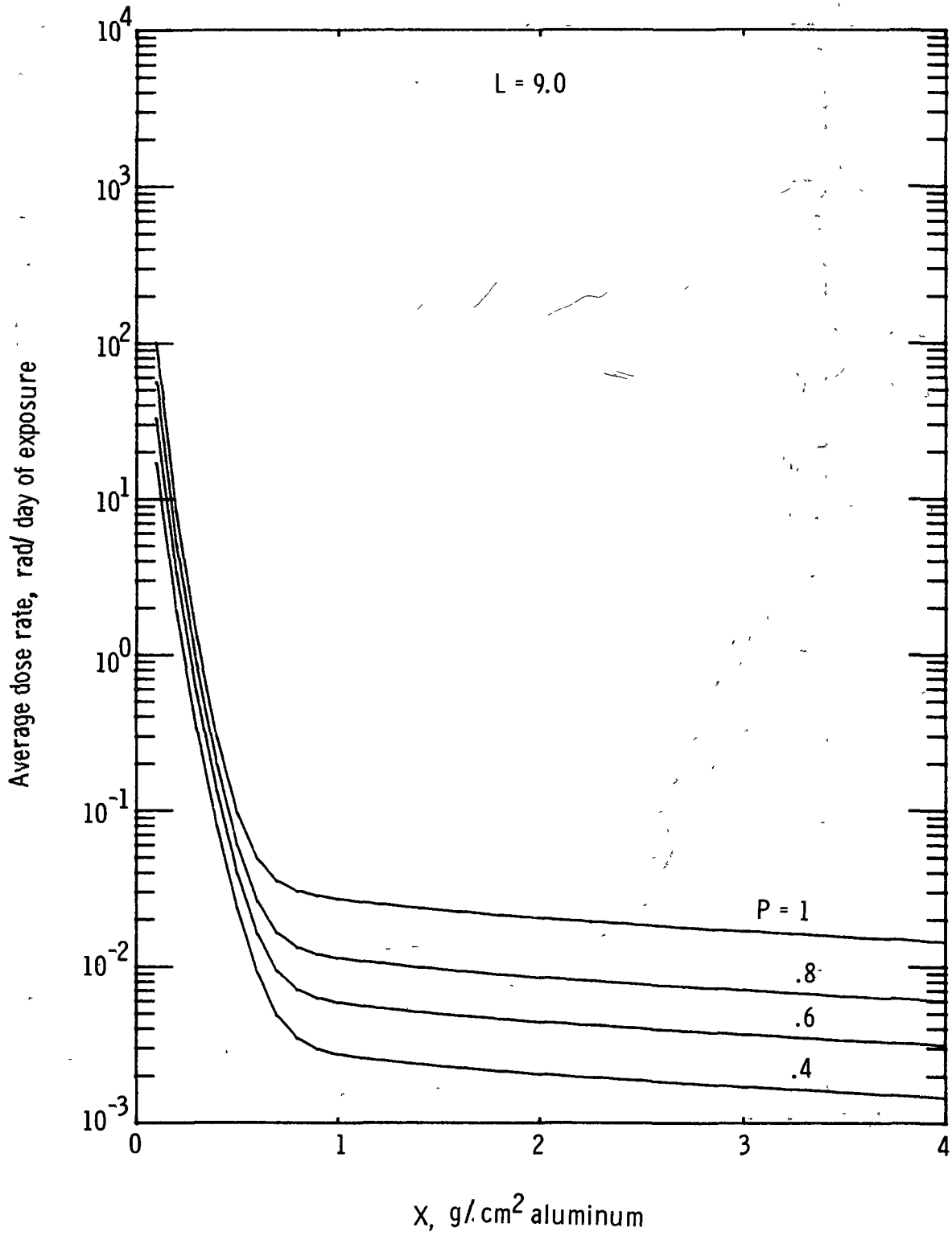

Figure 13.- Restricted average dose rates at L = 9.0 as a function of shield thickness for selected probability levels denoted by P.

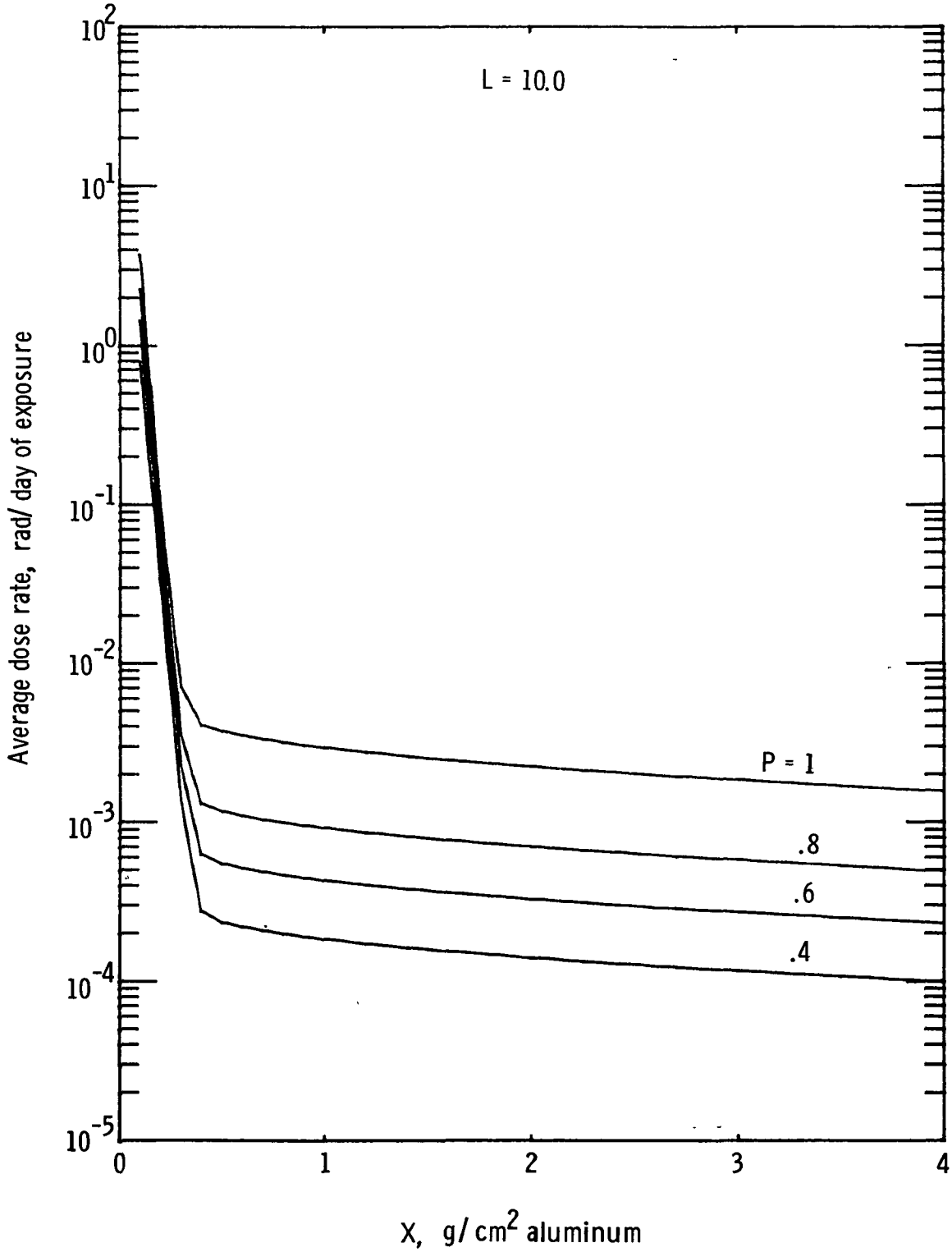

Figure 14.- Restricted average dose rates at L = 10.0 as a function of shield thickness for selected probability levels denoted by P.

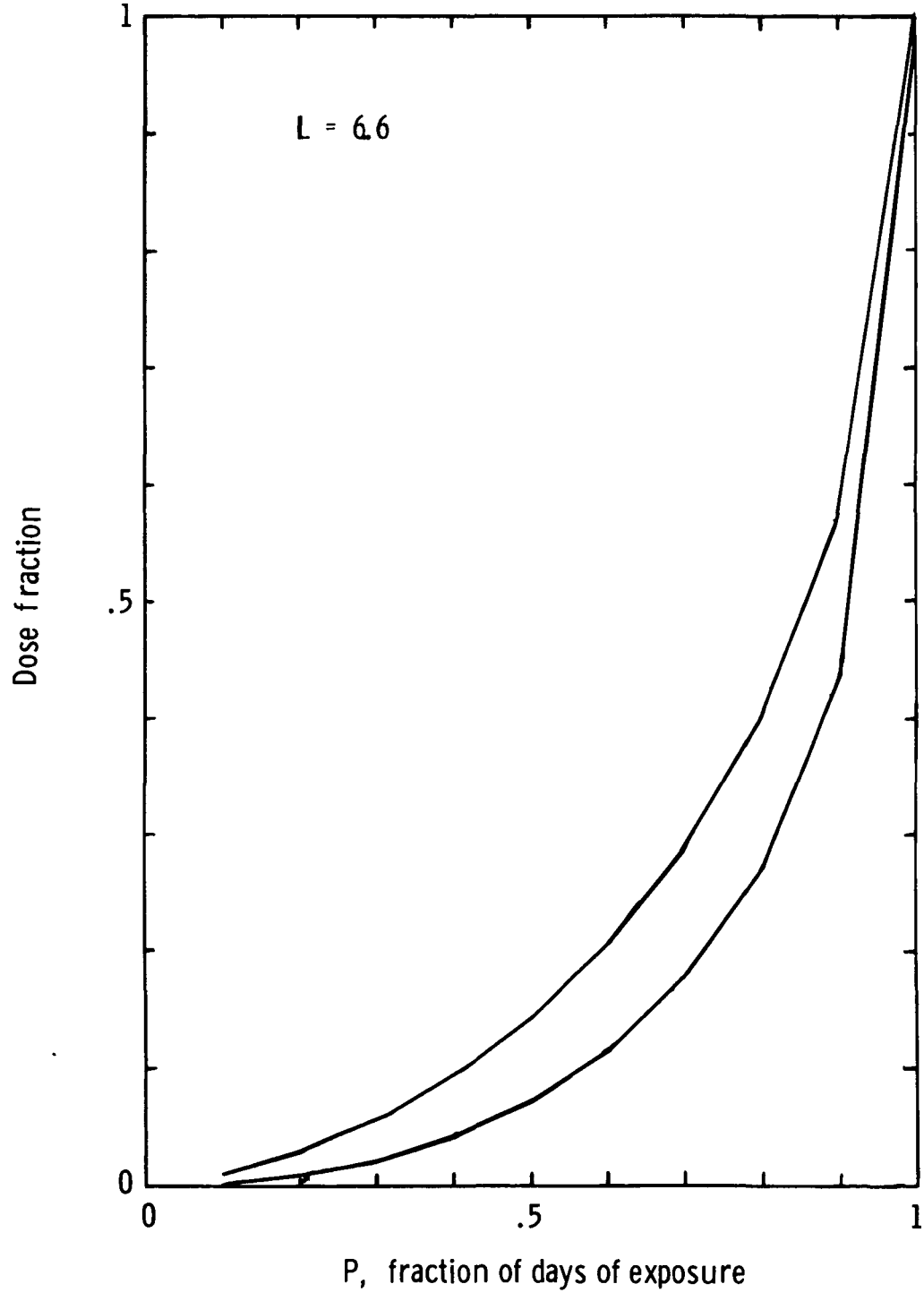

Figure 15.- Fraction of average dose received at L = 6.6 by working only the P fraction of lowest-exposure days. The two curves show the range of dose fractions for shield thicknesses between 0.1 and 4 g/cm^2.

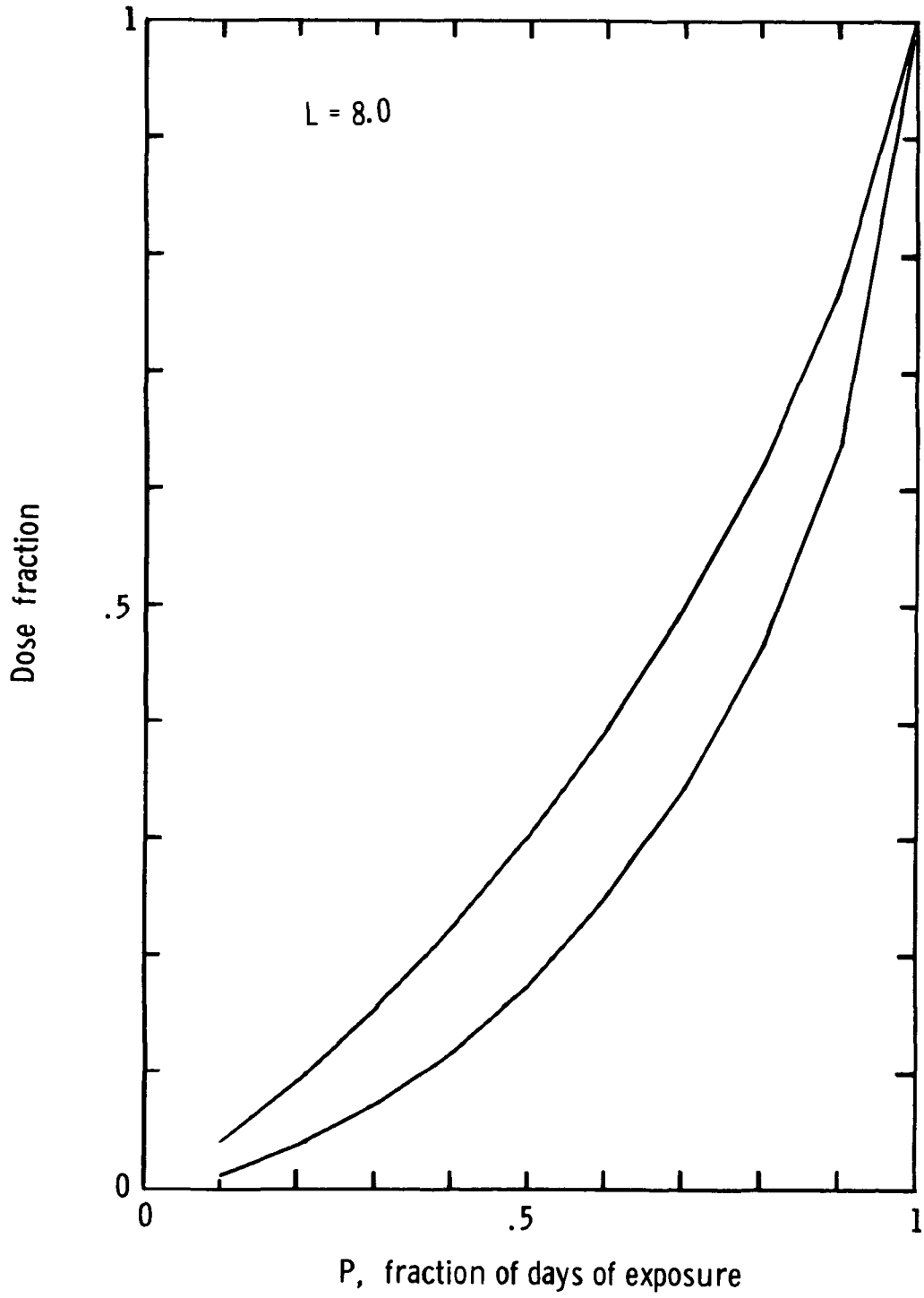

Figure 16.- Fraction of average dose received at L = 8.0 by working only the P fraction of lowest-exposure days. The two curves show the range of dose fractions for shield thicknesses between 0.1 and 4 g/cm^2.

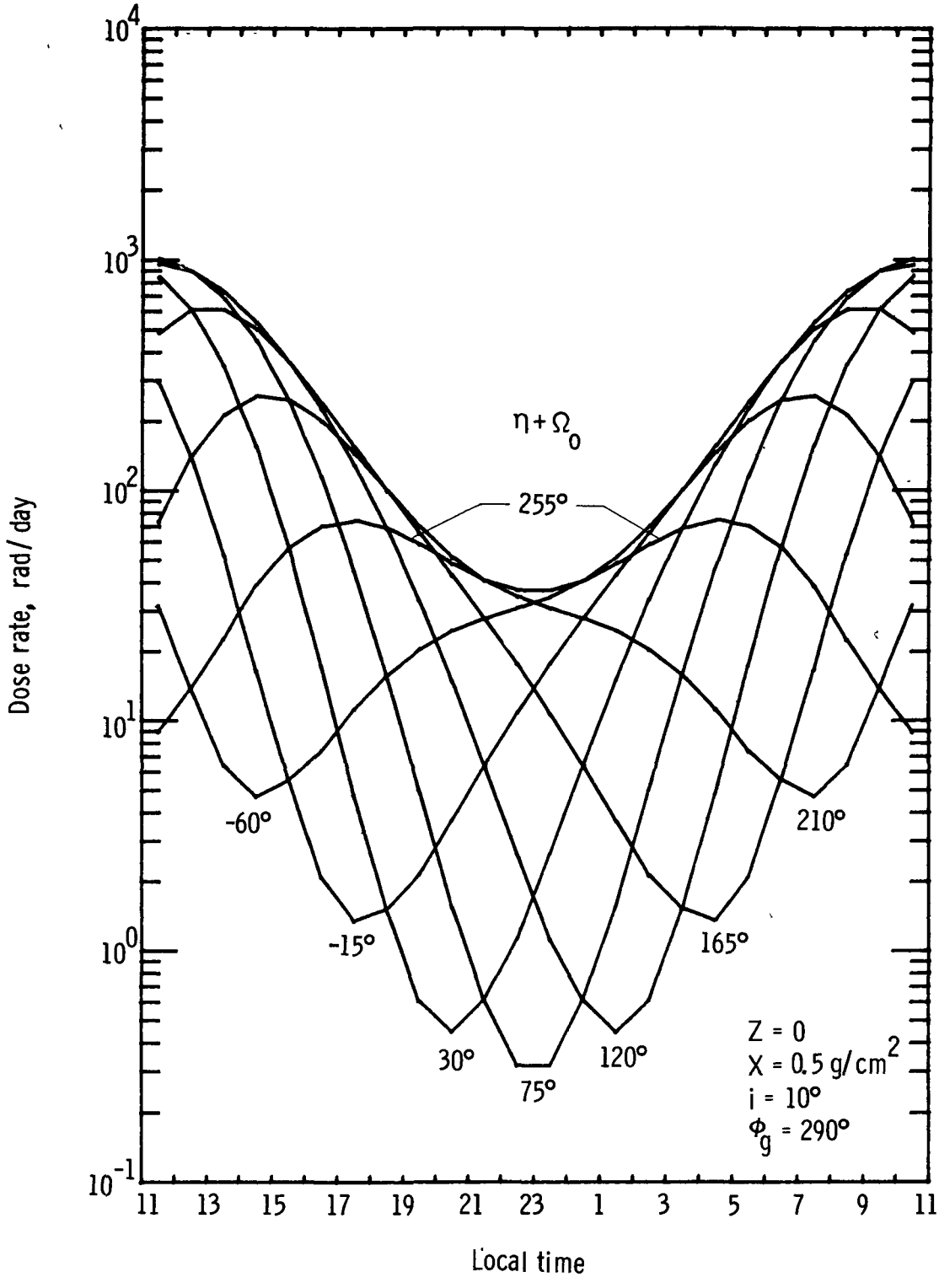

Figure 17.- Average local time variations during solar minimum at various times during the solar year (that is, different values of $\eta + \Omega_0$ as indicated).

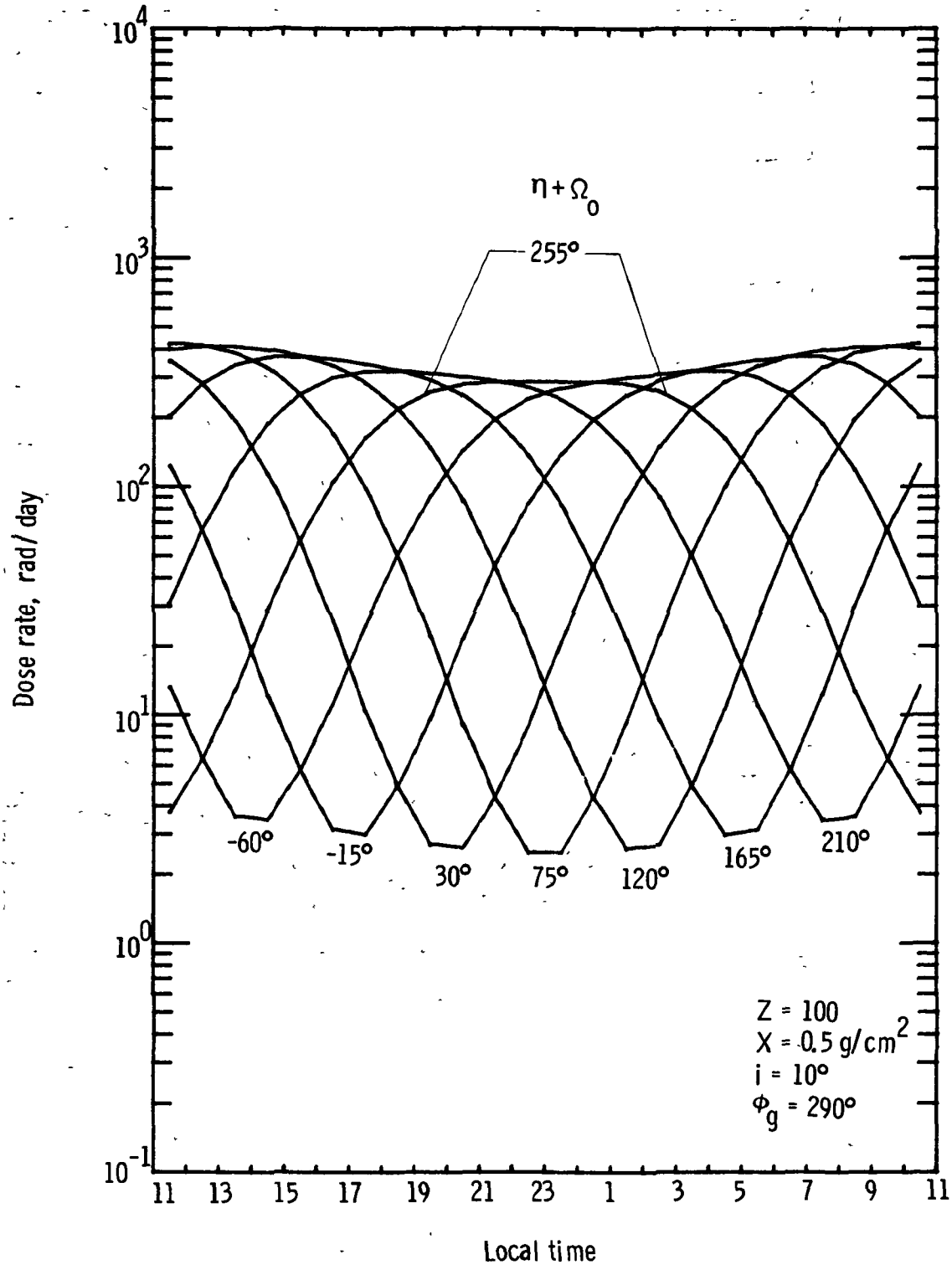

Figure 18.- Average local time variations during solar maximum at various times during the solar year (that is, different values of $\eta + \Omega_0$ as indicated).

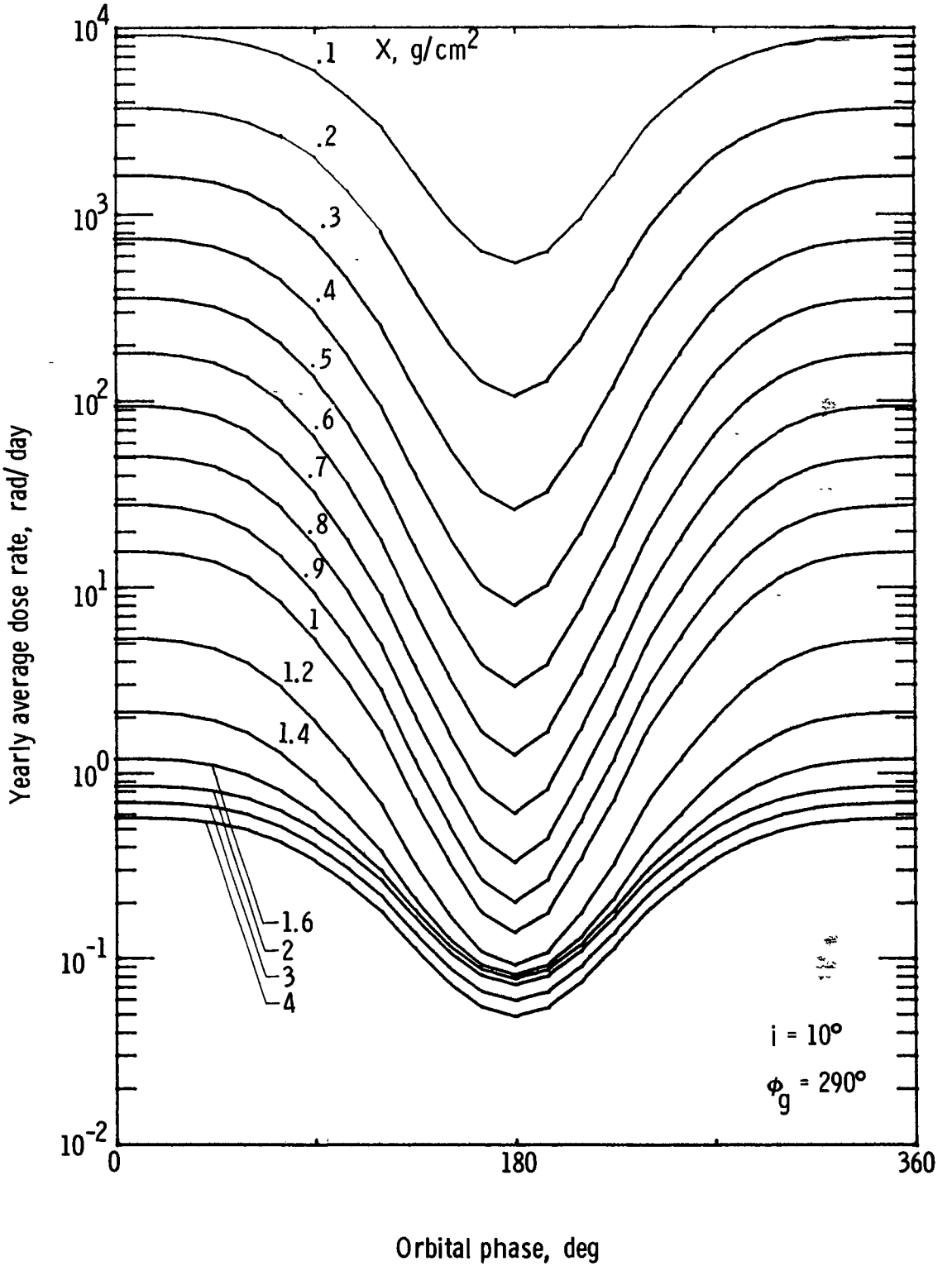

Figure 19.- Yearly average dose rate as a function of orbital phase for a satellite located near $\phi_g = 290^\circ$ in a 10° inclined orbit. The shield thickness is indicated in the figure for each curve.

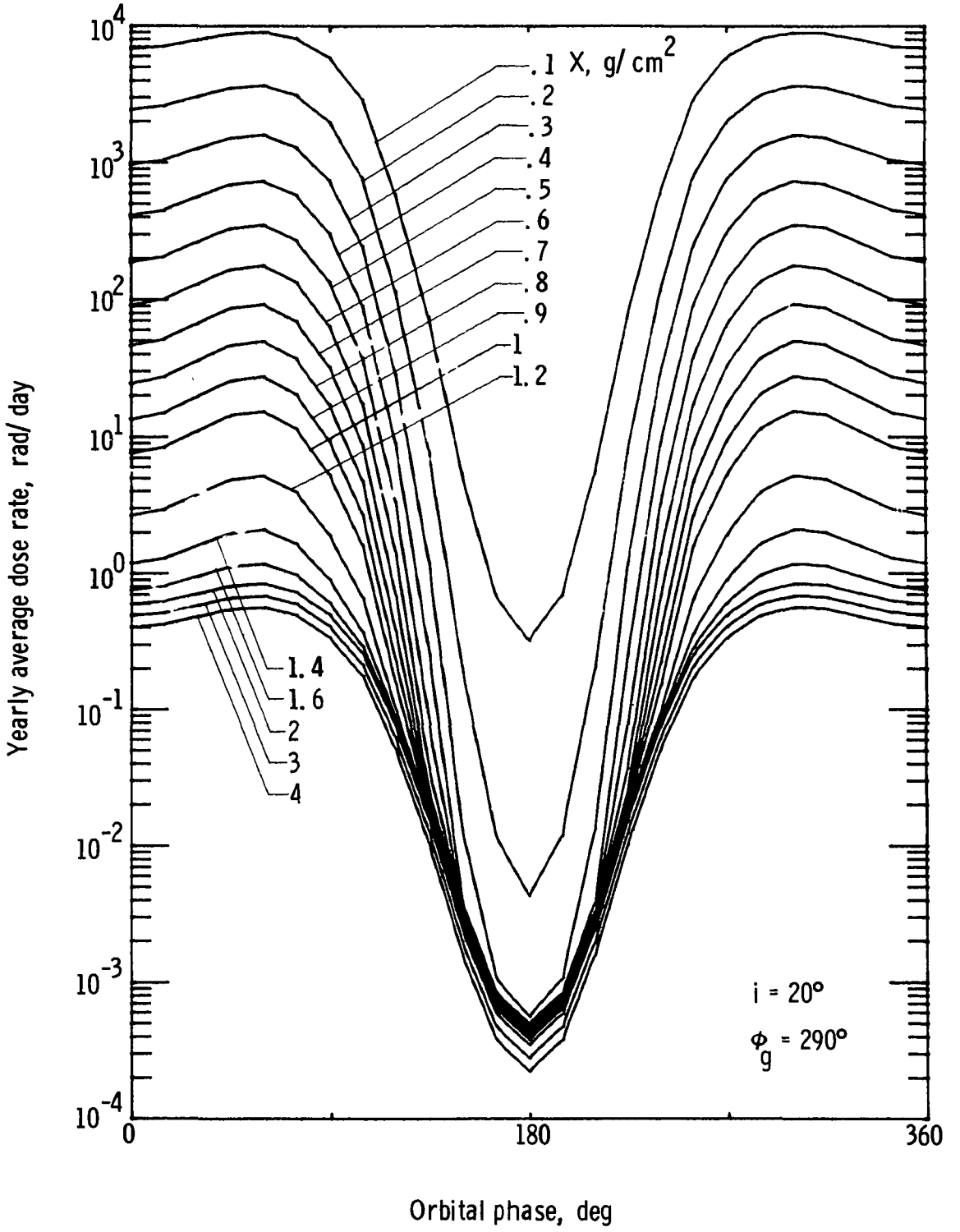

Figure 20.- Yearly average dose rate as a function of orbital phase for a satellite located near $\phi_g = 290°$ in a 20° inclined orbit. The shield thickness is indicated in the figure for each curve.

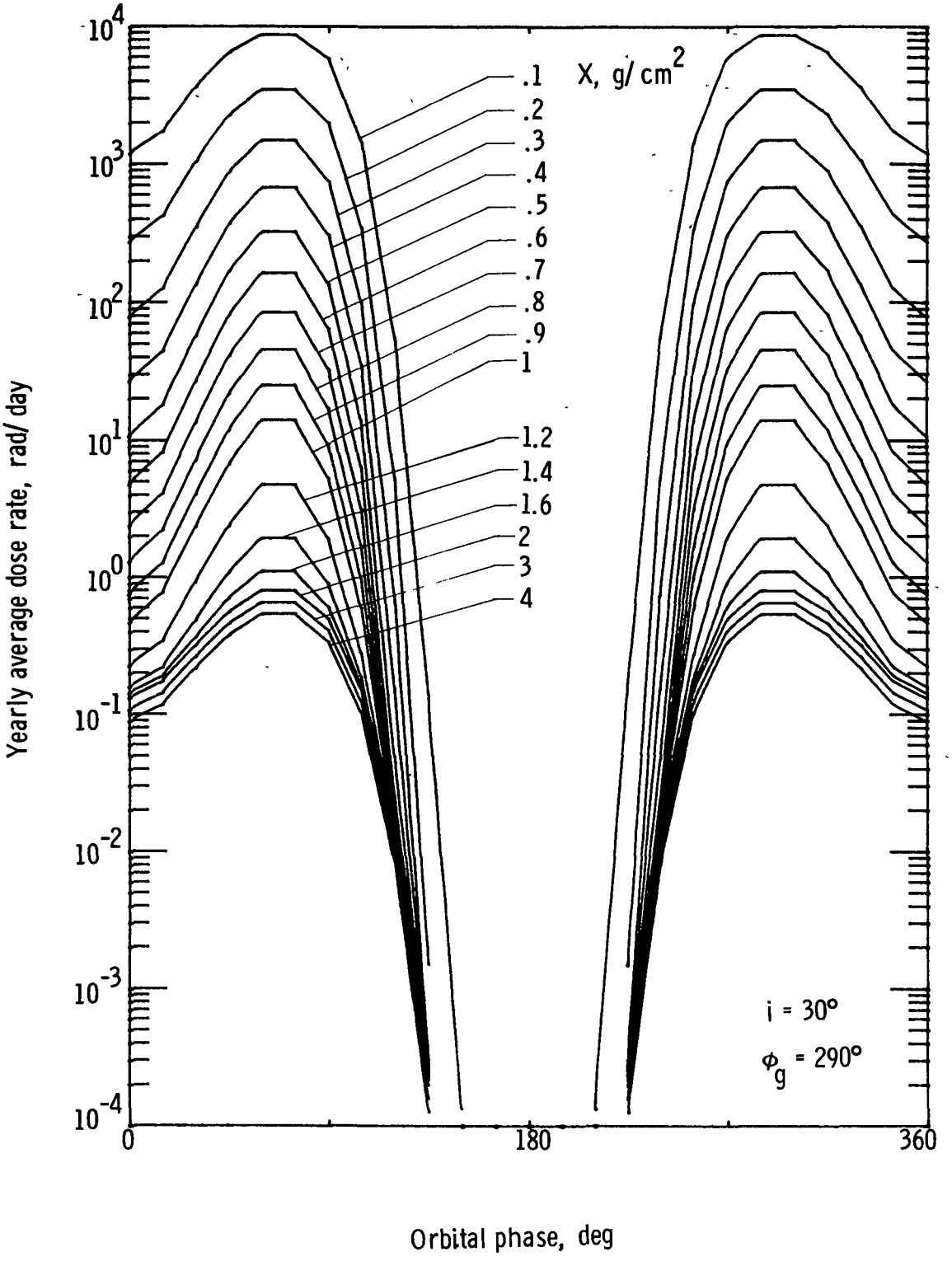

Figure 21.- Yearly average dose rate as a function of orbital phase for a satellite located near $\phi_g = 290°$ in a 30° inclined orbit. The shield thickness is indicated in the figure for each curve.

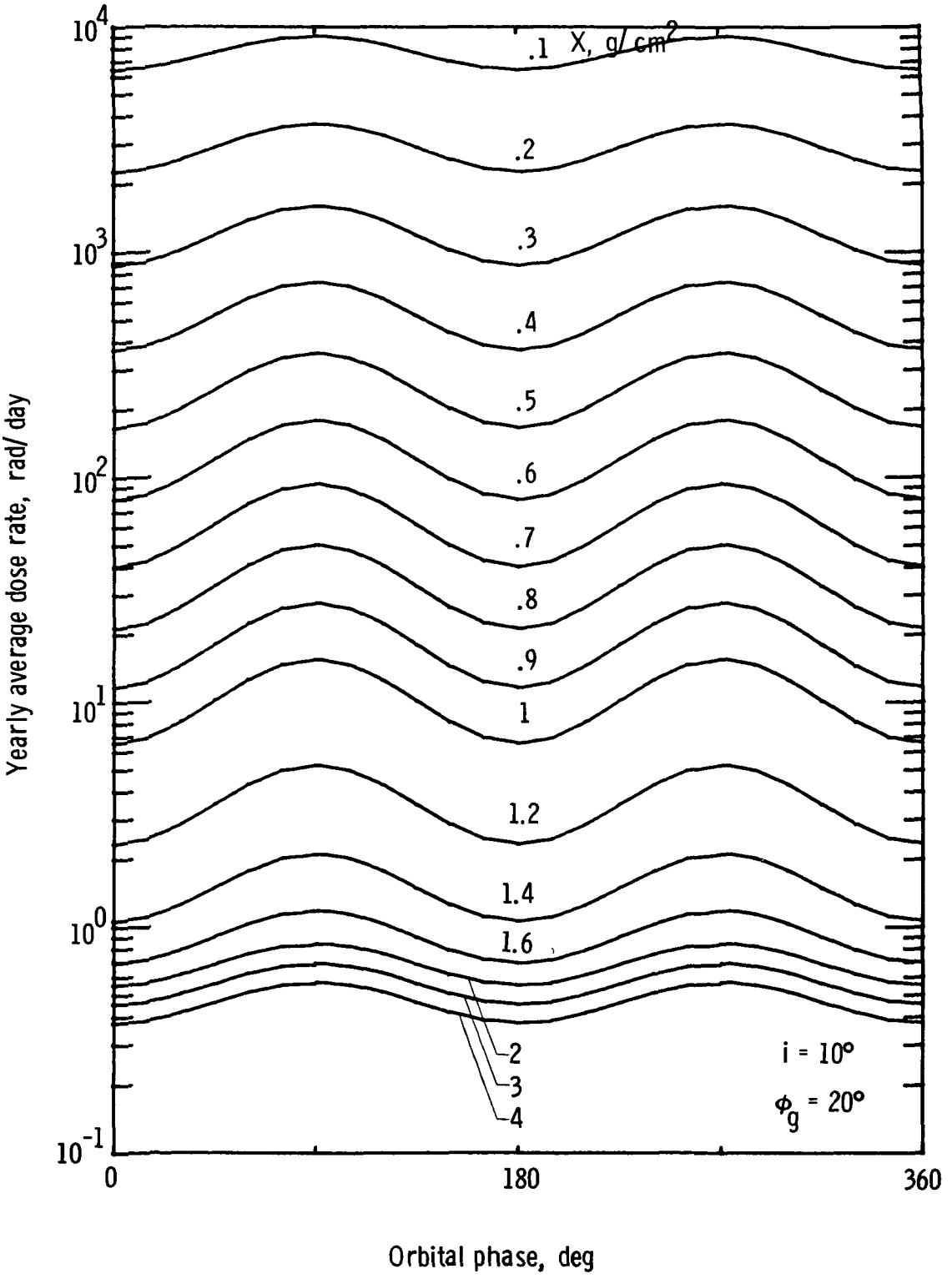

Figure 22.- Yearly average dose rate as a function of orbital phase for a satellite located near $\phi_g = 20°$ in a 10° inclined orbit. The shield thickness is indicated in the figure for each curve.

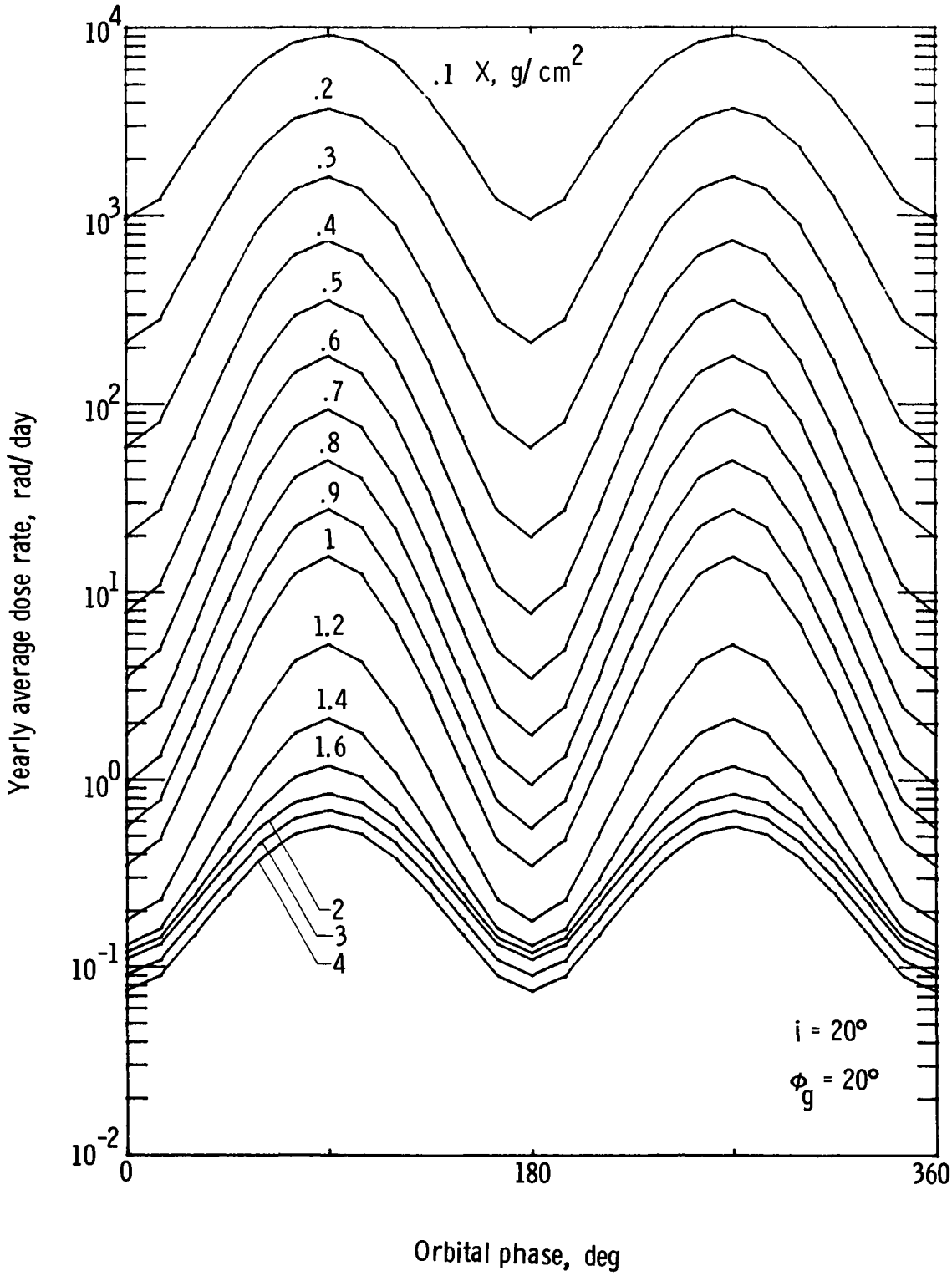

Figure 23.- Yearly average dose rate as a function of orbital phase for a satellite located near $\phi_g = 20°$ in a 20° inclined orbit. The shield thickness is indicated in the figure for each curve.

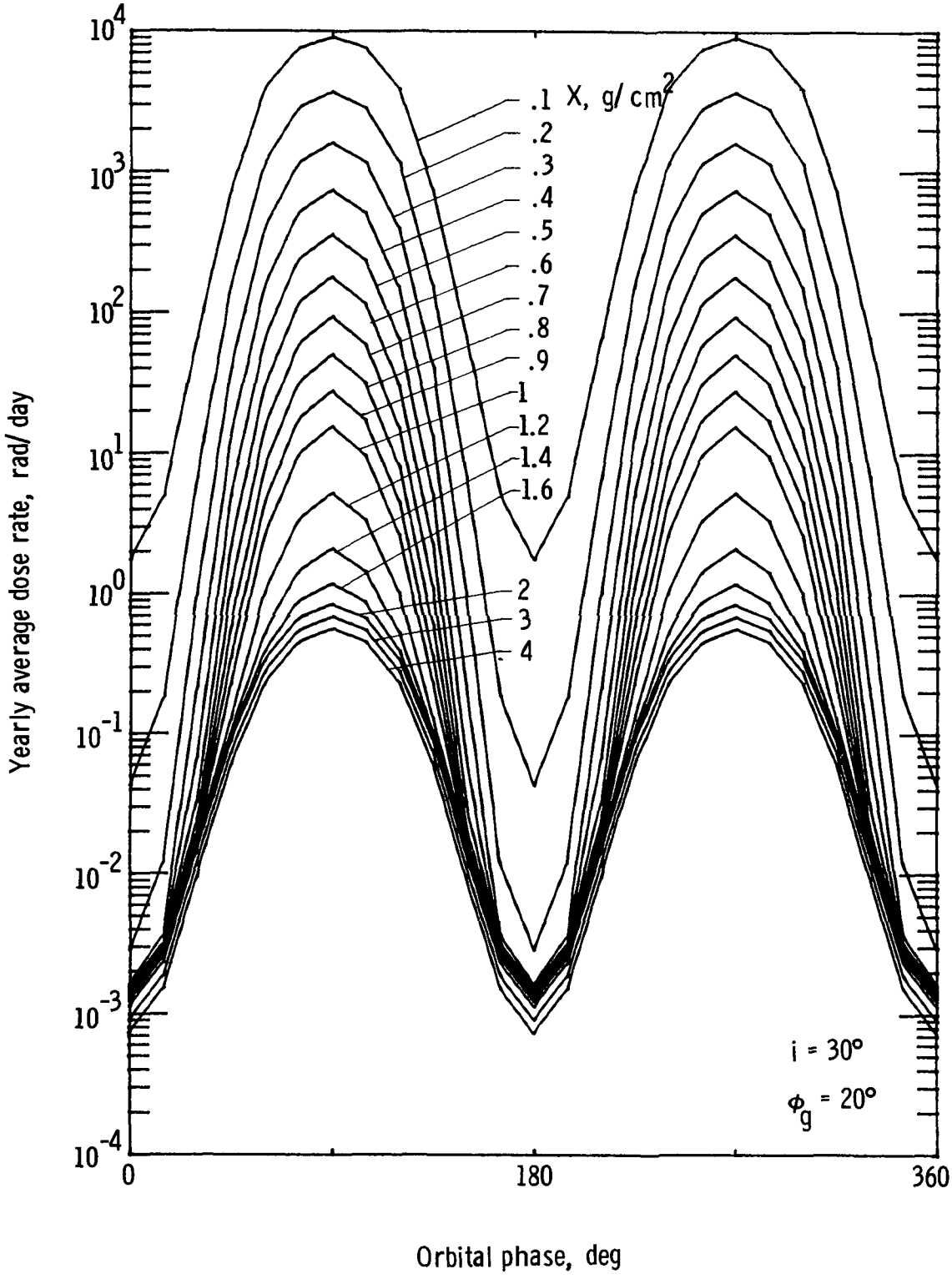

Figure 24.- Yearly average dose rate as a function of orbital phase for a satellite located near $\phi_g = 20°$ in a 30° inclined orbit. The shield thickness is indicated in the figure for each curve.

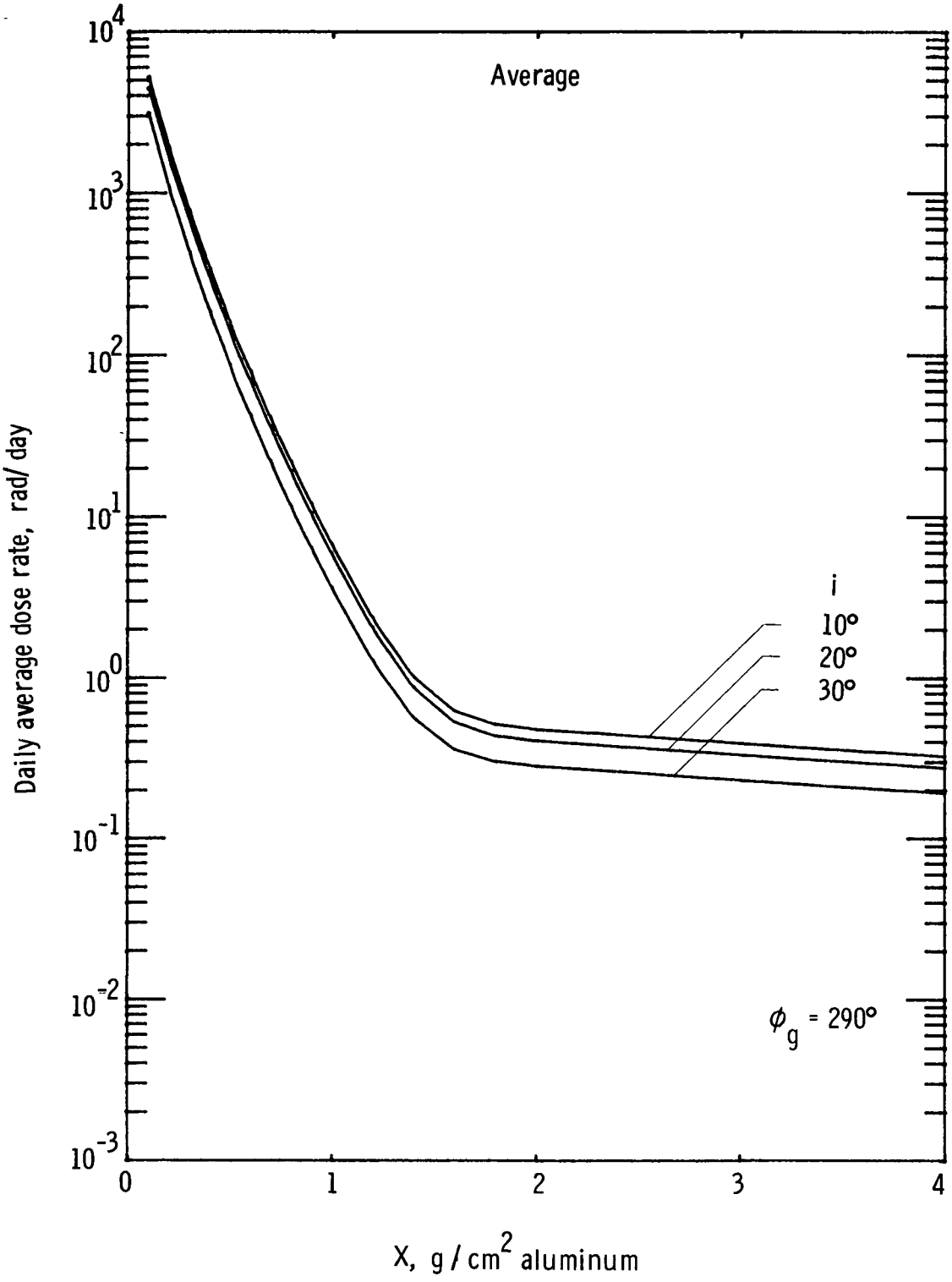

Figure 25.- Daily average dose rate for geosynchronous orbit over ϕ_g = 290° for various orbit inclinations.

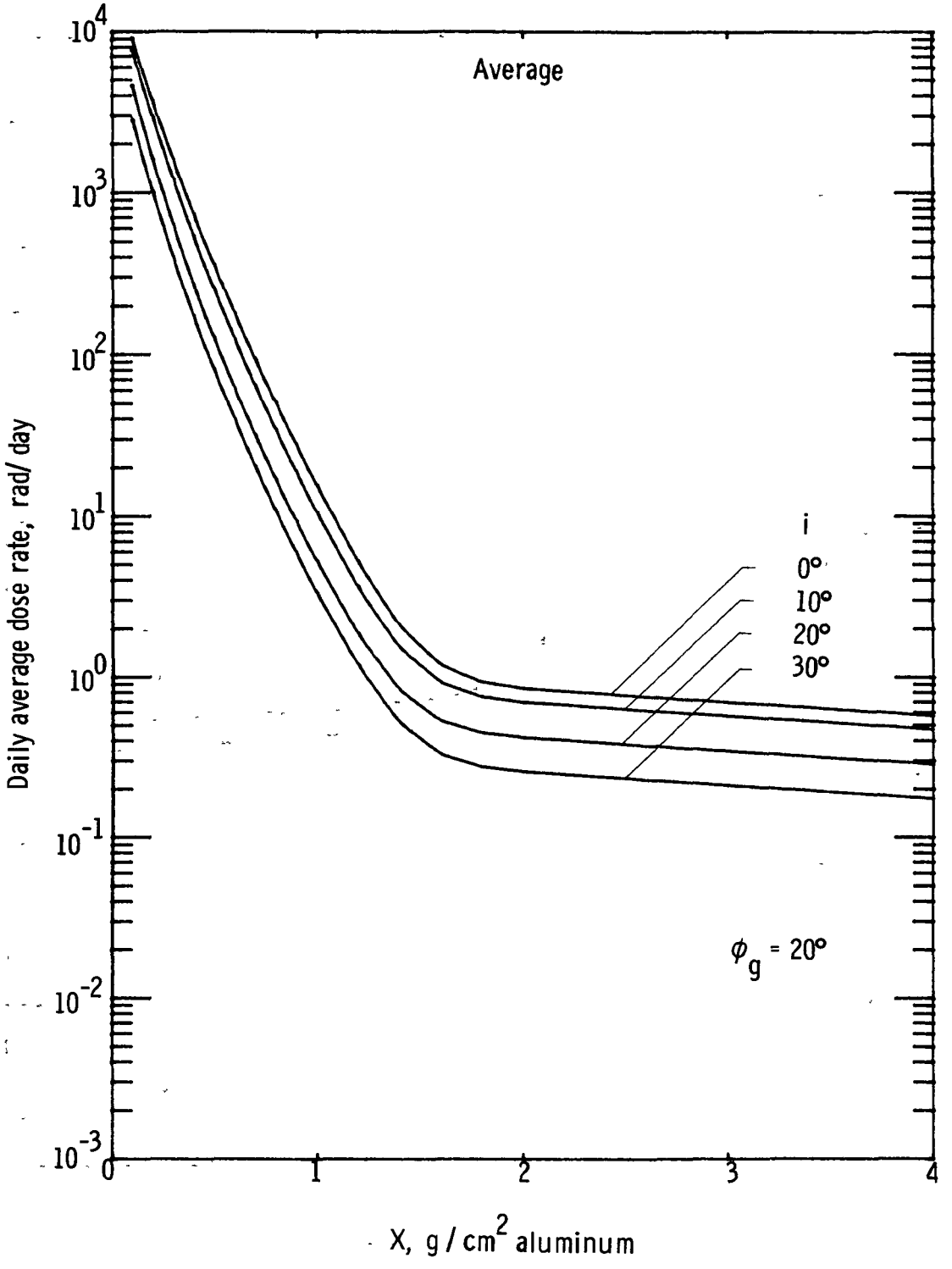

Figure 26.- Daily average dose rate for geosynchronous orbit over ϕ_g = 20° for various orbit inclinations.

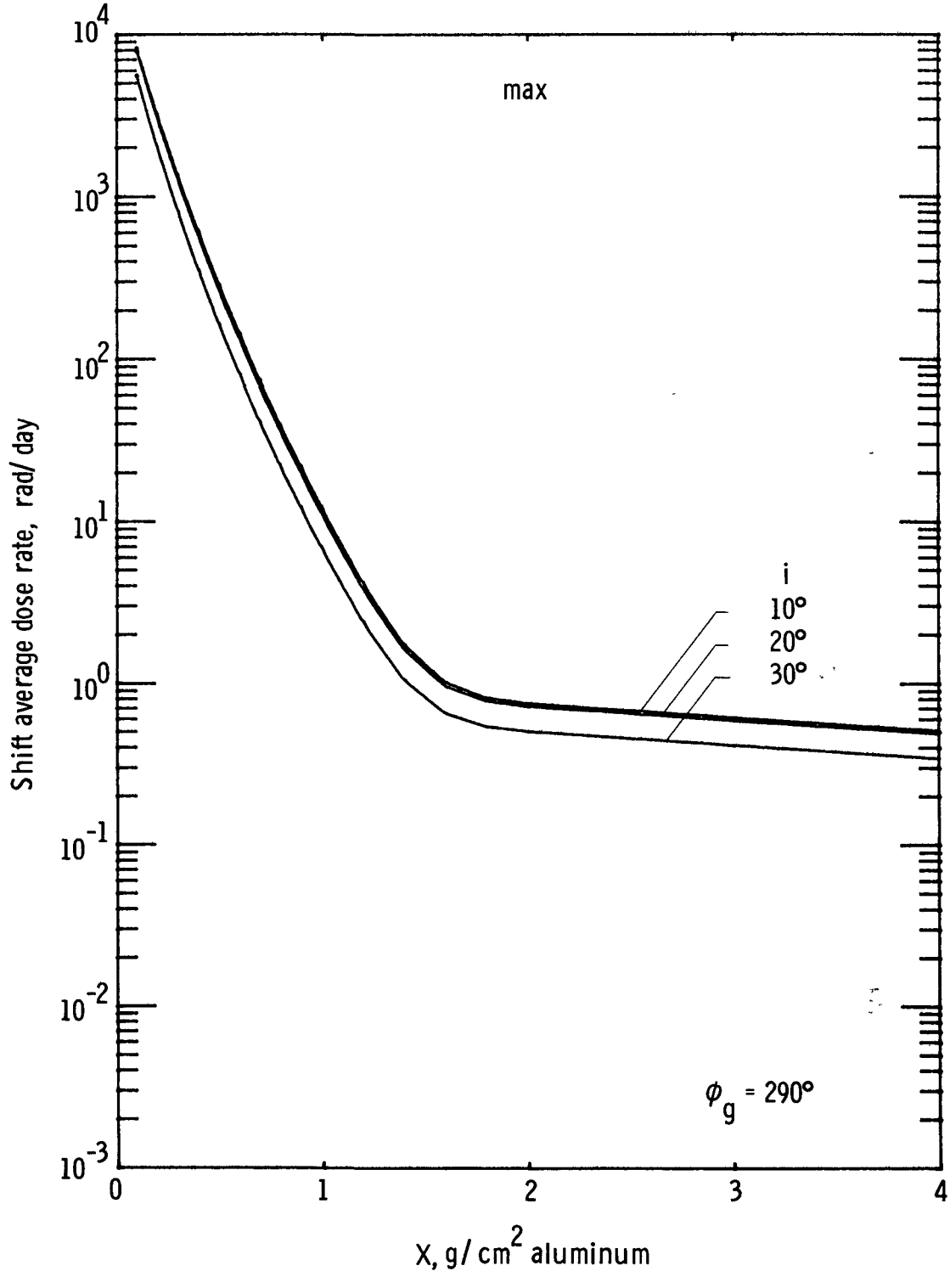

Figure 27.- Shift average dose rate for geosynchronous orbit over ϕ_g = 290° during shifts of maximum exposure for various orbit inclinations.

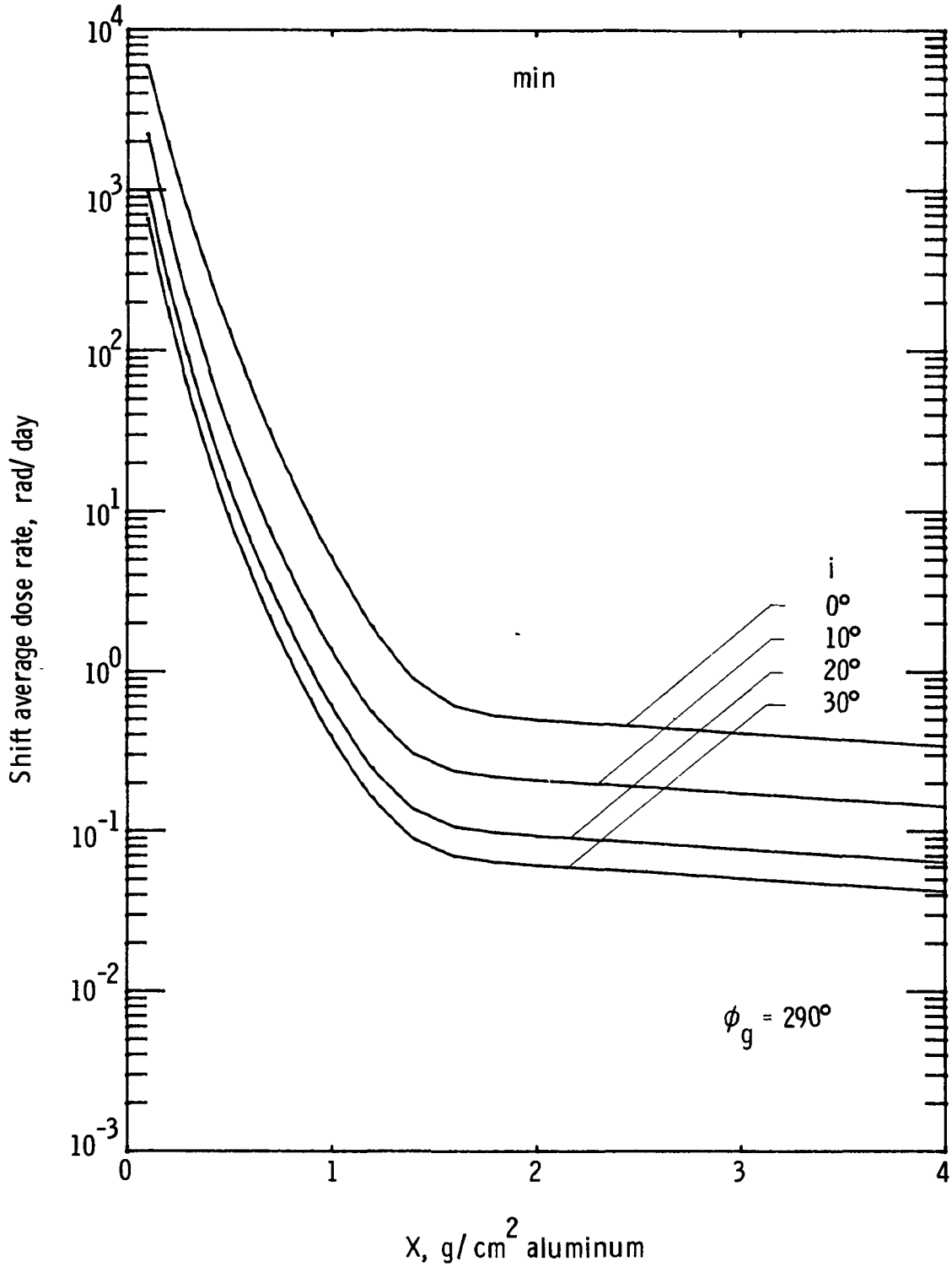

Figure 28.- Shift average dose rate for geosynchronous orbit over ϕ_g = 290° during shifts of minimum exposure for various orbit inclinations.

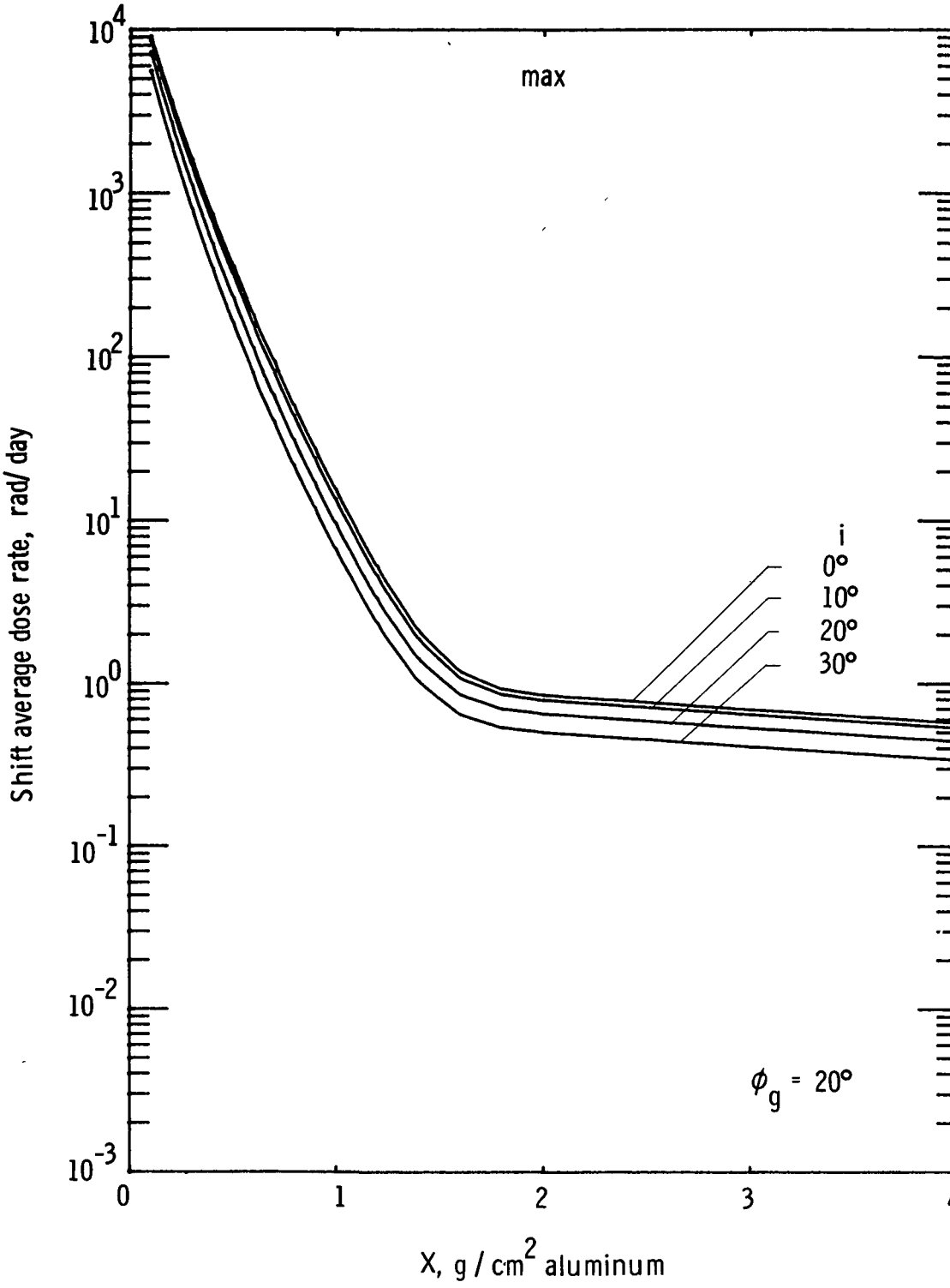

Figure 29.- Shift average dose rate for geosynchronous orbit over ϕ_g = 20° during shifts of maximum exposure for various orbit inclinations.

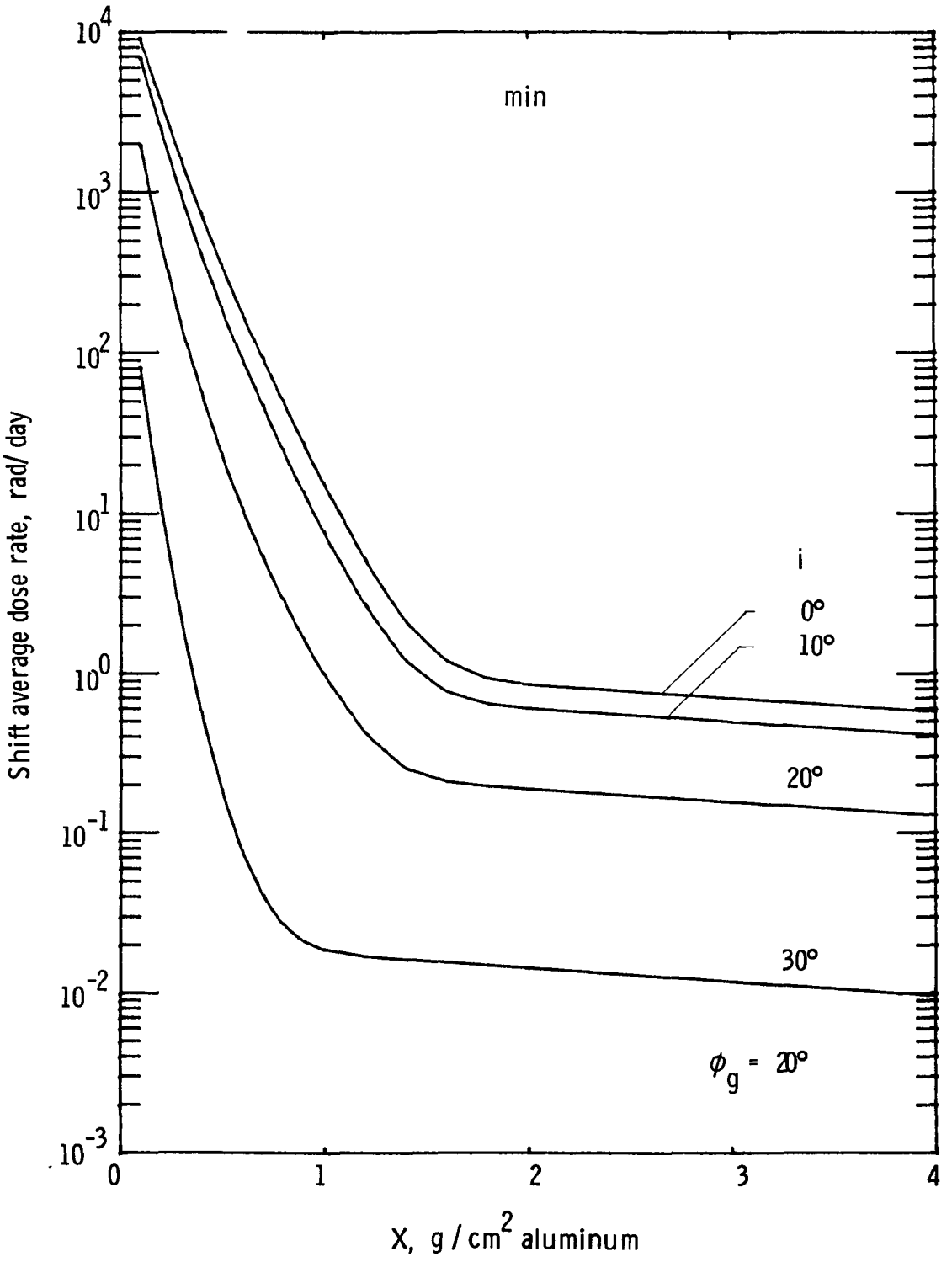

Figure 30.- Shift average dose rate for geosynchronous orbit over ϕ_g = 20° during shifts of minimum exposure for various orbit inclinations.

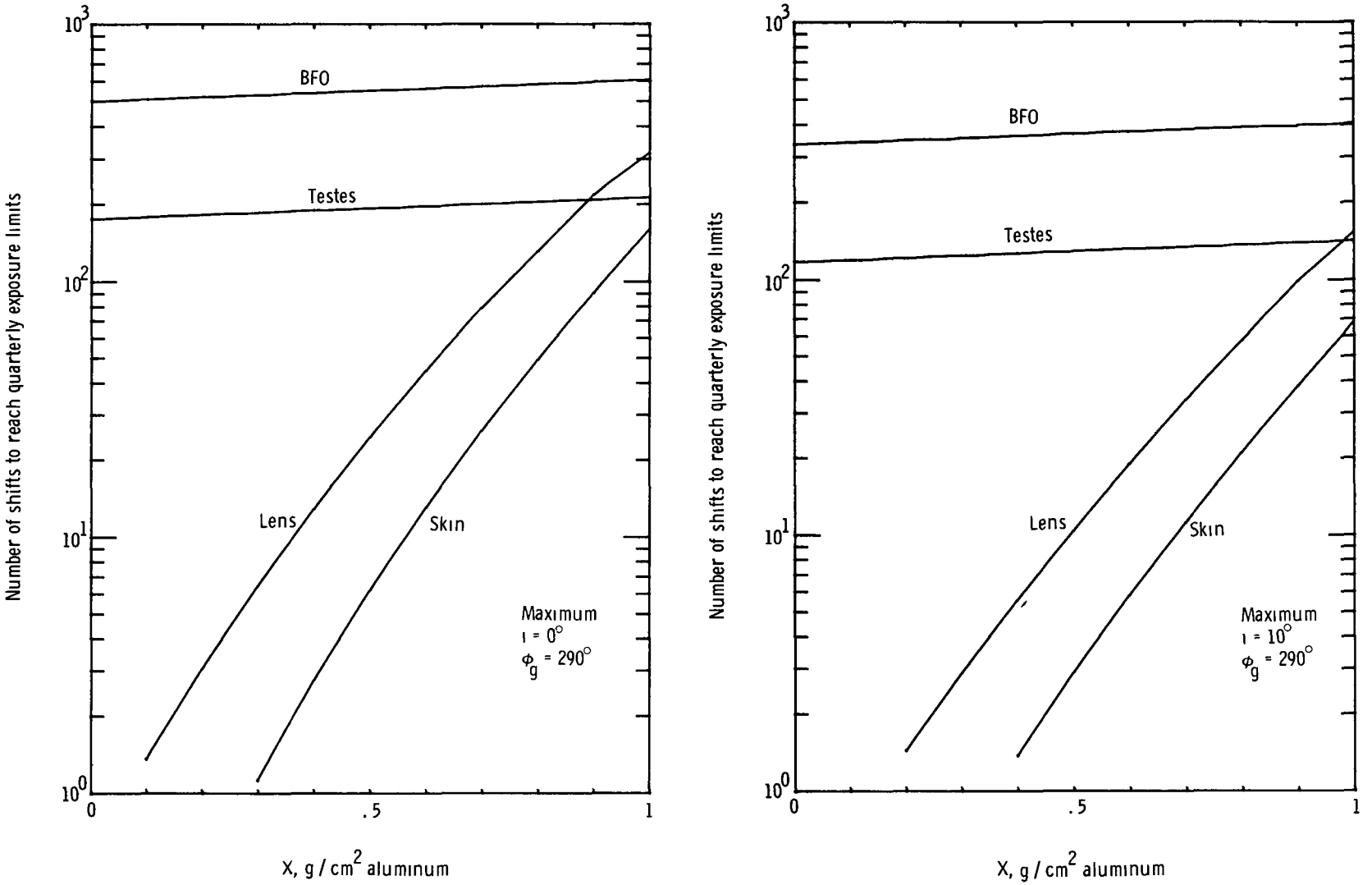

(a) 0° inclination.

(b) 10° inclination.

Figure 31.- Number of 6-hr shifts during periods of maximum exposure required to reach the quarterly exposure limit for each of four critical organs during EVA operations at the geosynchronous location of ϕ_g = 290° and various inclinations.

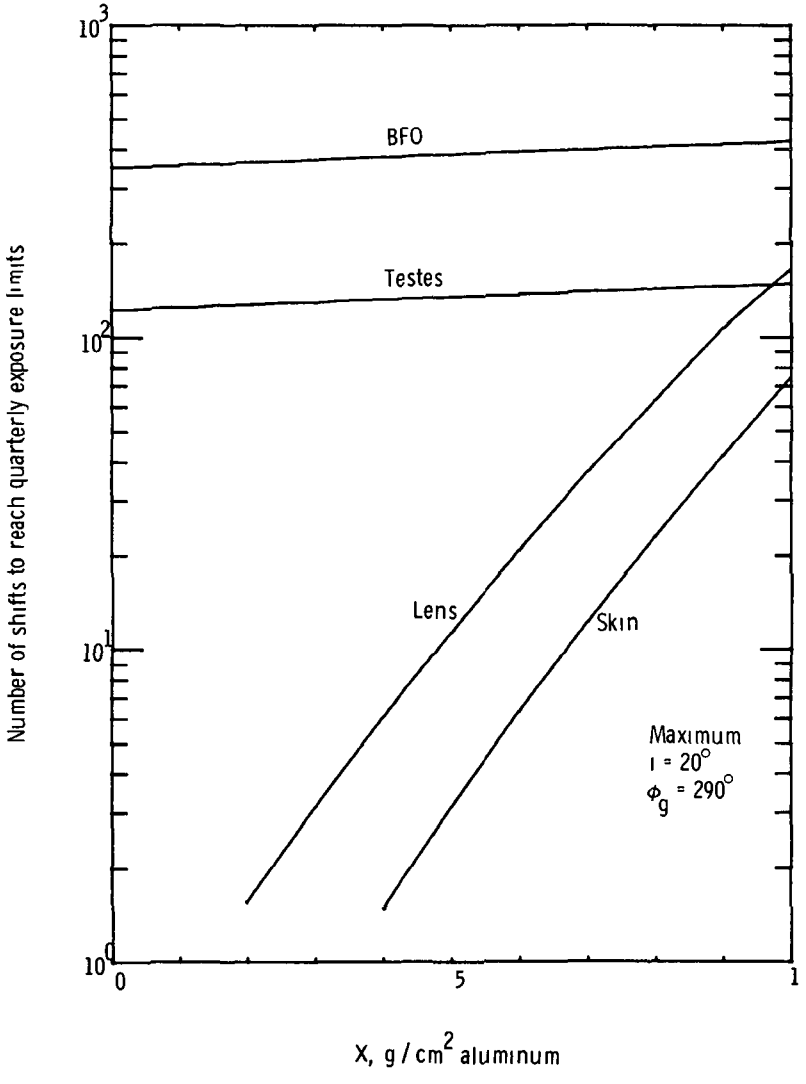

(c) 20° inclination.

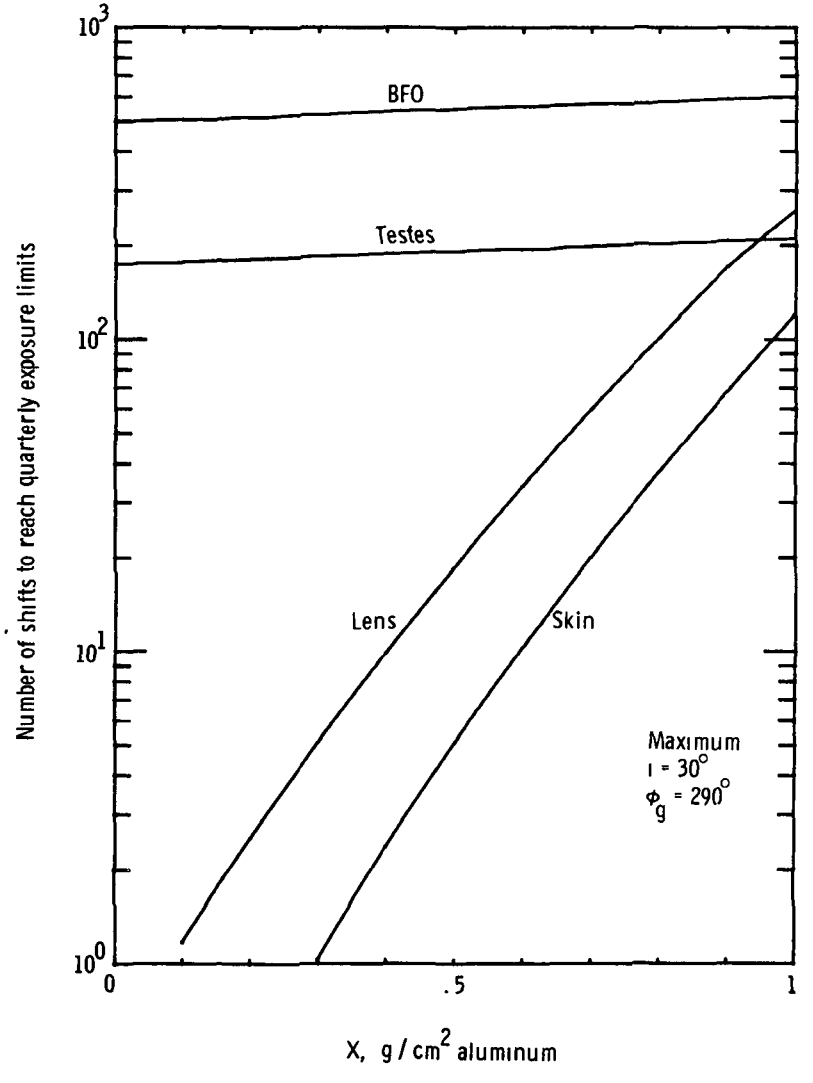

(d) 30° inclination.

Figure 31.- Concluded.

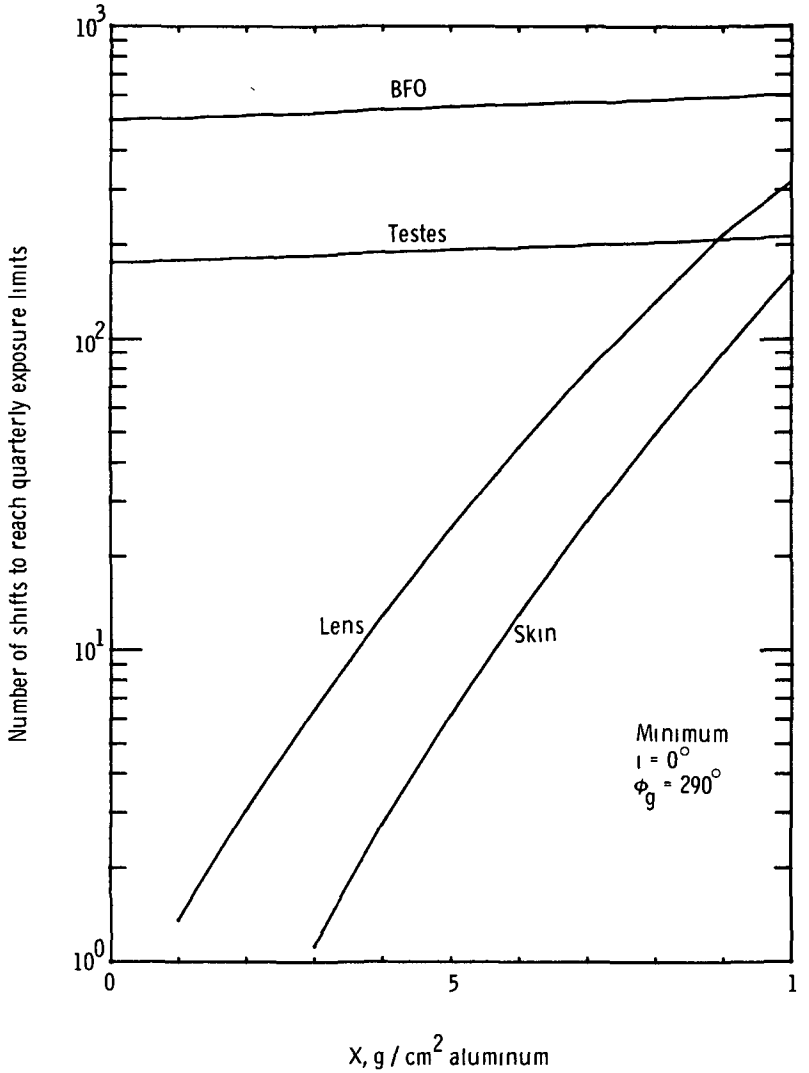

(a) 0° inclination.

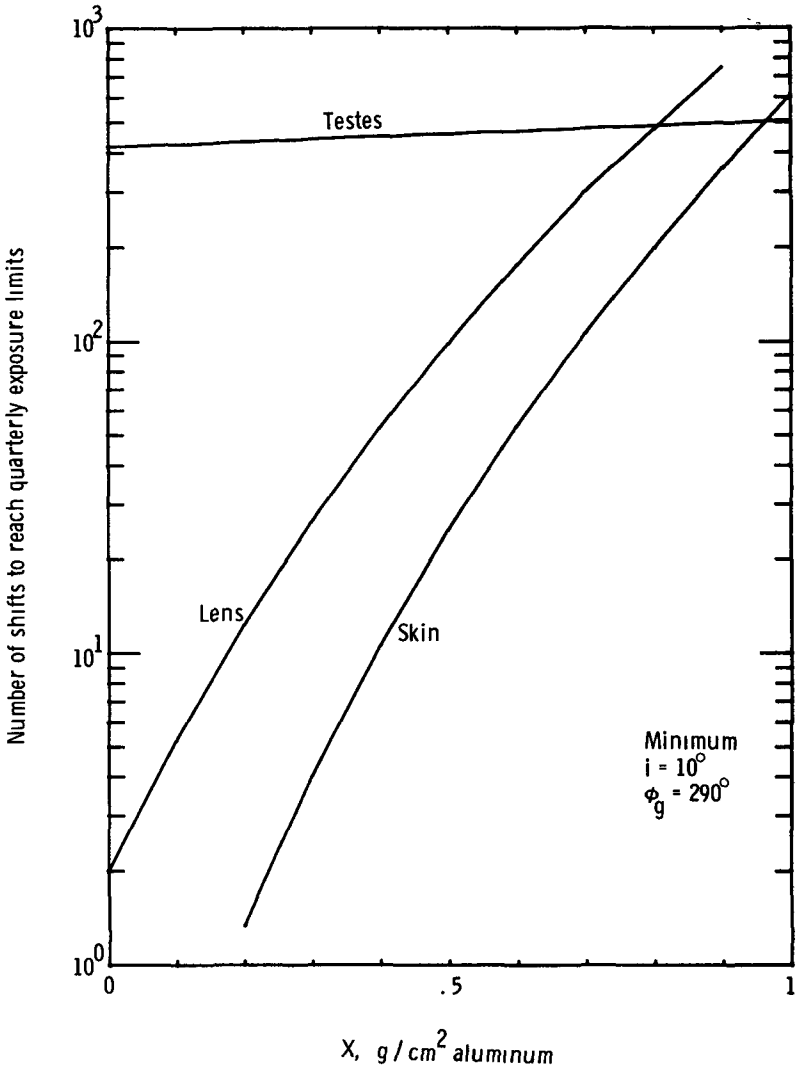

(b) 10° inclination.

Figure 32.- Number of 6-hr shifts during periods of minimum exposure required to reach the quarterly exposure limit for each of four critical organs during EVA operations at the geosynchronous location of ϕ_g = 290° and various inclinations.

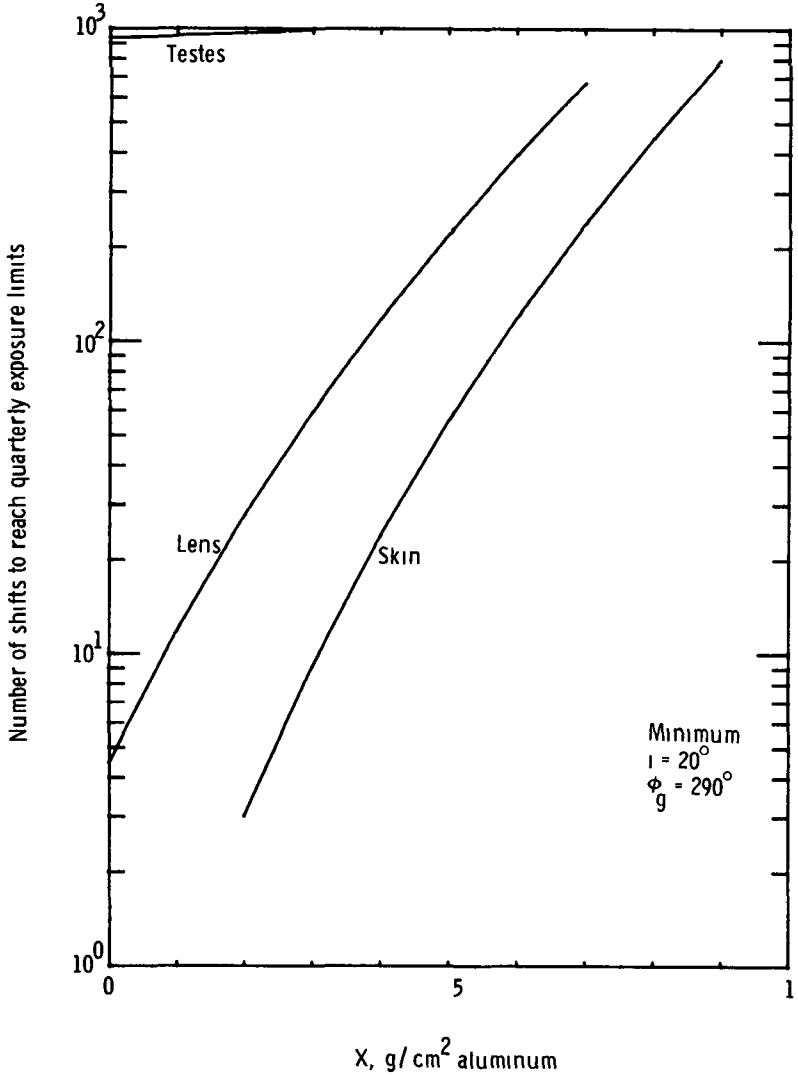

(c) 20° inclination.

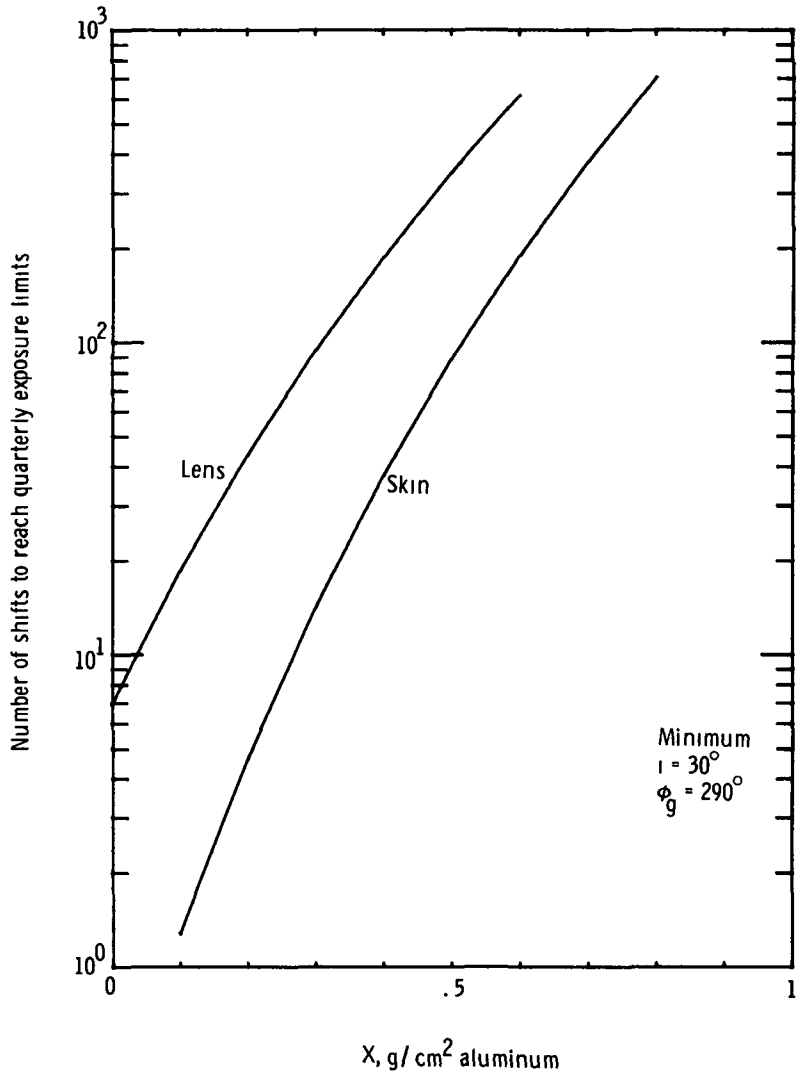

(d) 30° inclination.

Figure 32.- Concluded.

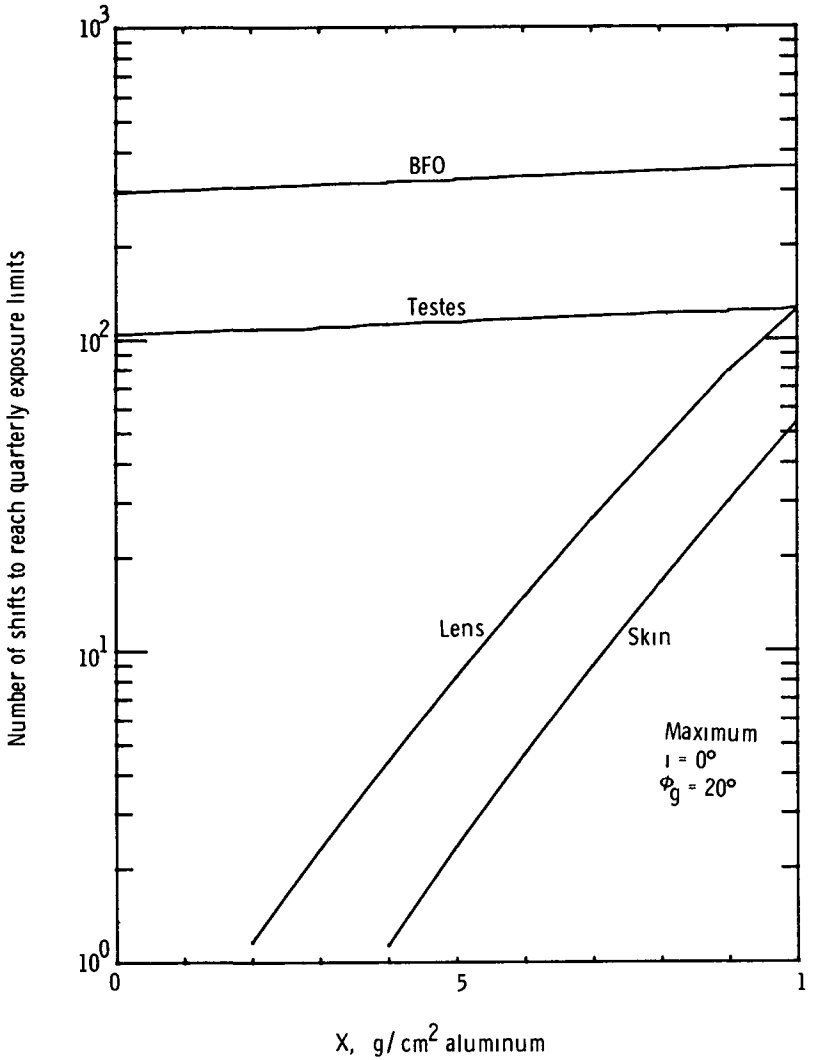

(a) 0° inclination.

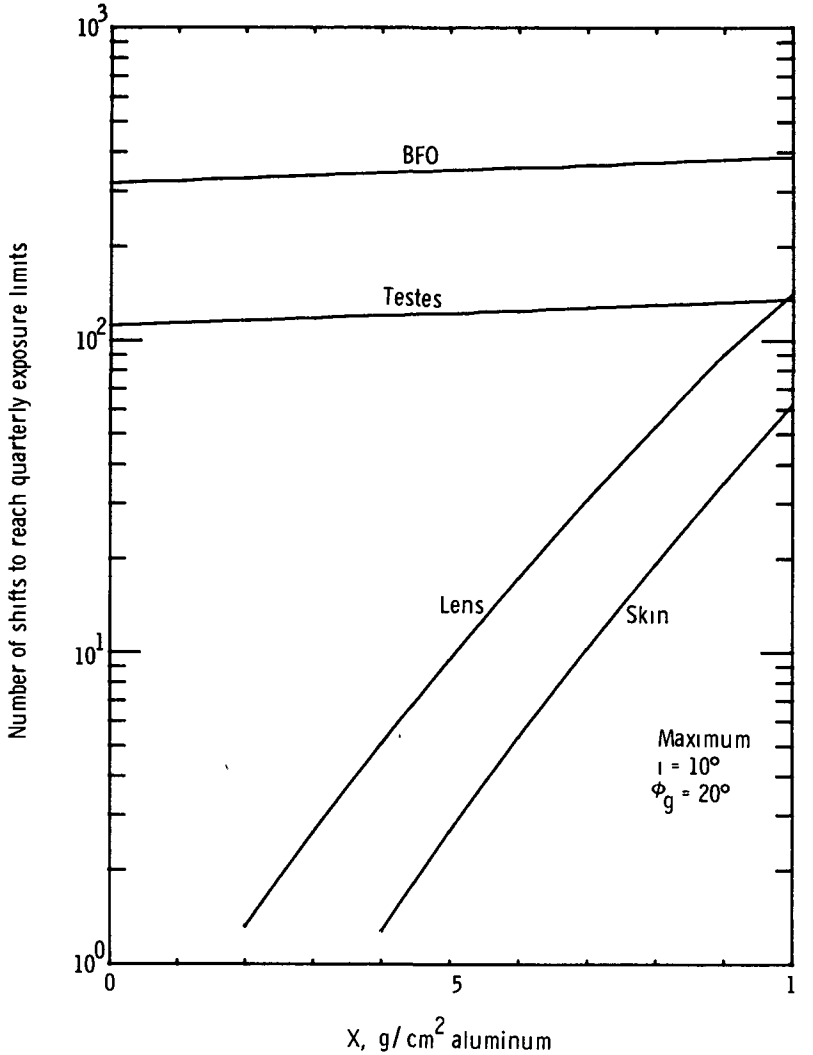

(b) 10° inclination.

Figure 33.- Number of 6-hr shifts during periods of maximum exposure required to reach the quarterly exposure limit for each of four critical organs during EVA operations at the geosynchronous location of $\phi_g = 20°$ and various inclinations.

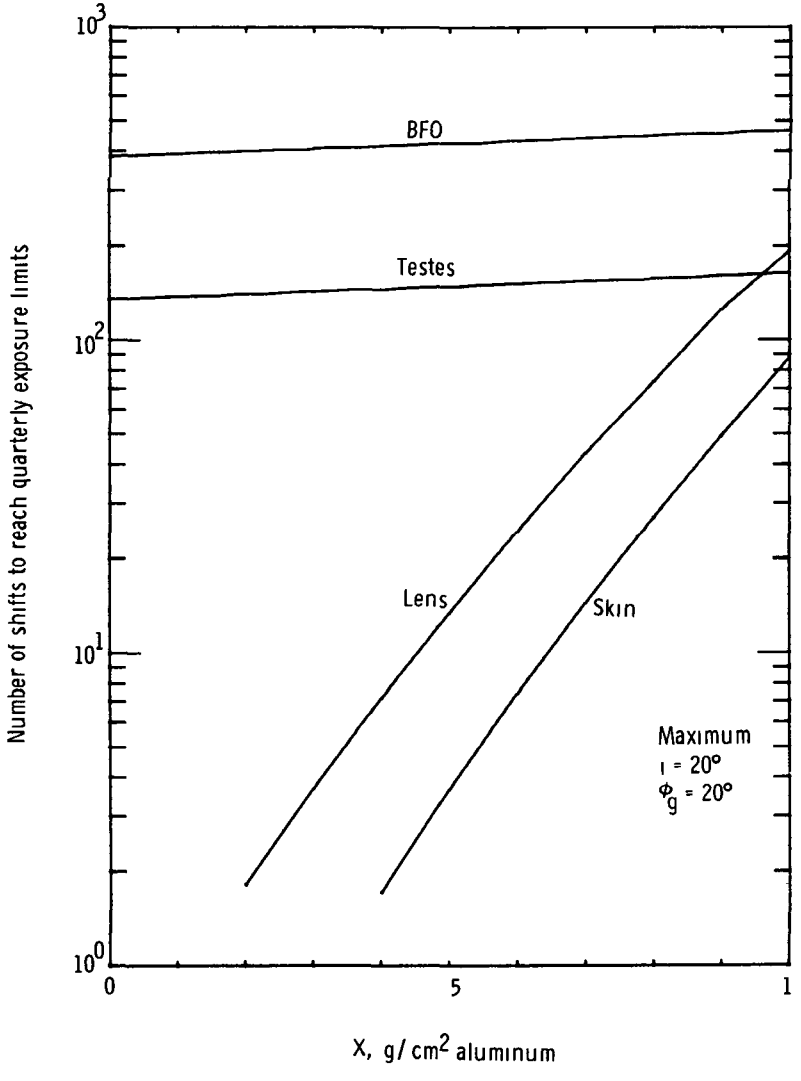

(c) 20° inclination.

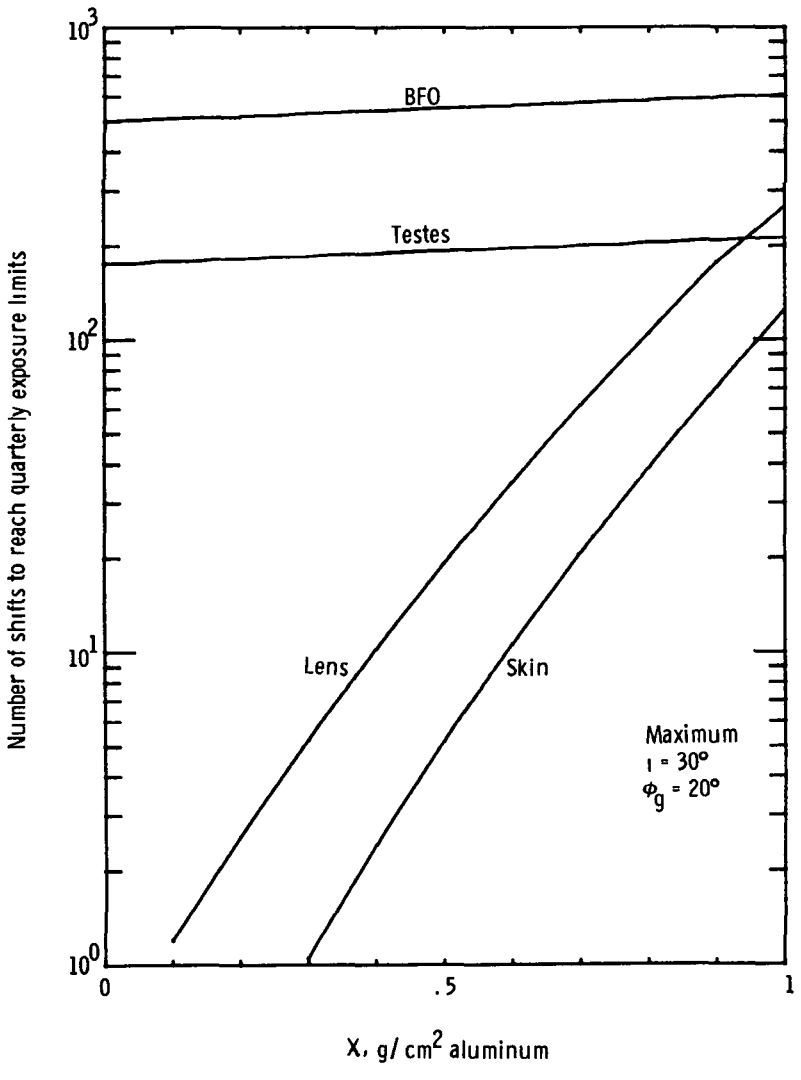

(d) 30° inclination.

Figure 33.- Concluded.

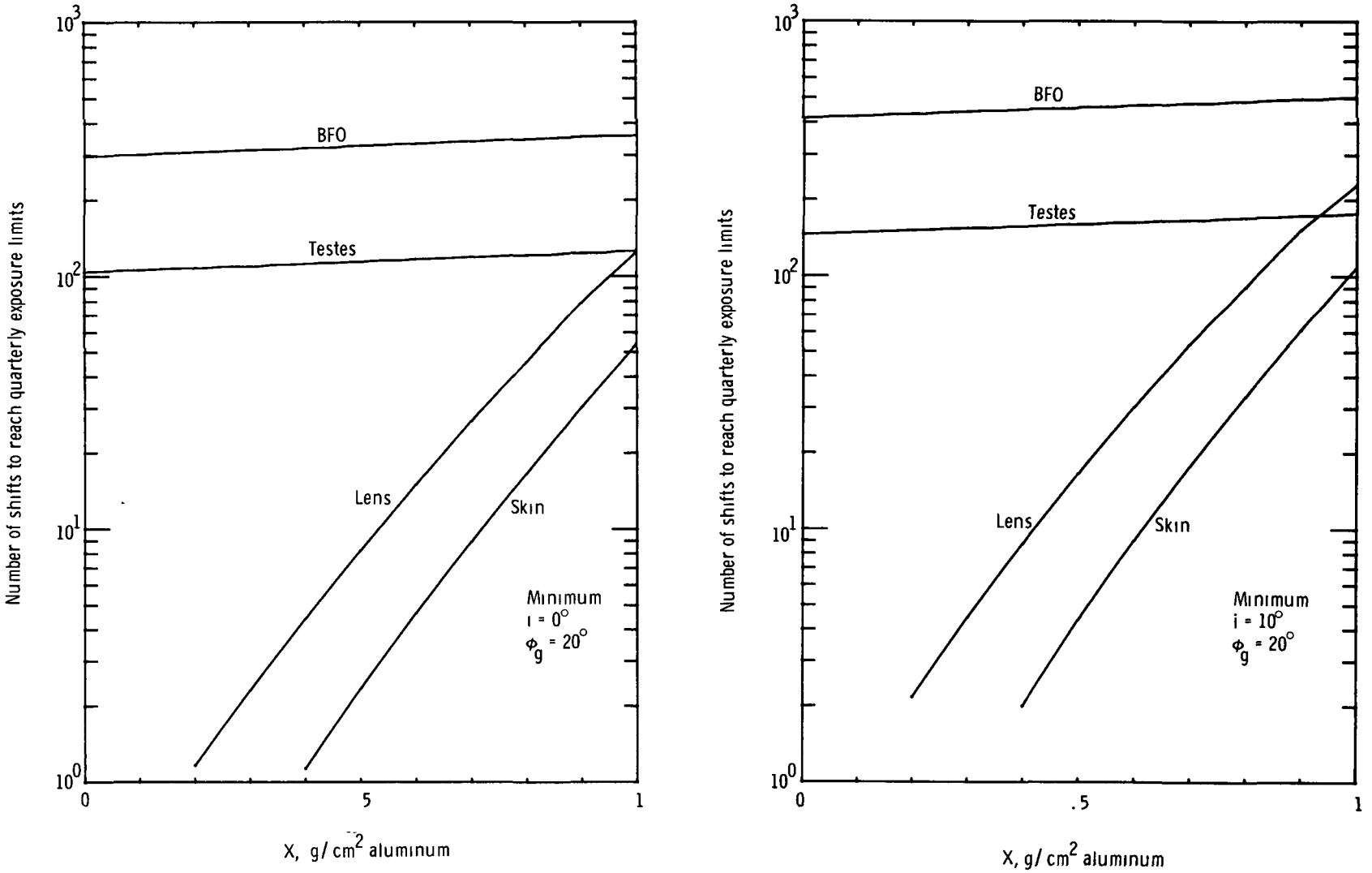

(a) 0° inclination.

(b) 10° inclination.

Figure 34.- Number of 6-hr shifts during periods of minimum exposure required to reach the quarterly exposure limit for each of four critical organs during EVA operations at the geosynchronous location of $\phi_g = 20°$ and various inclinations.

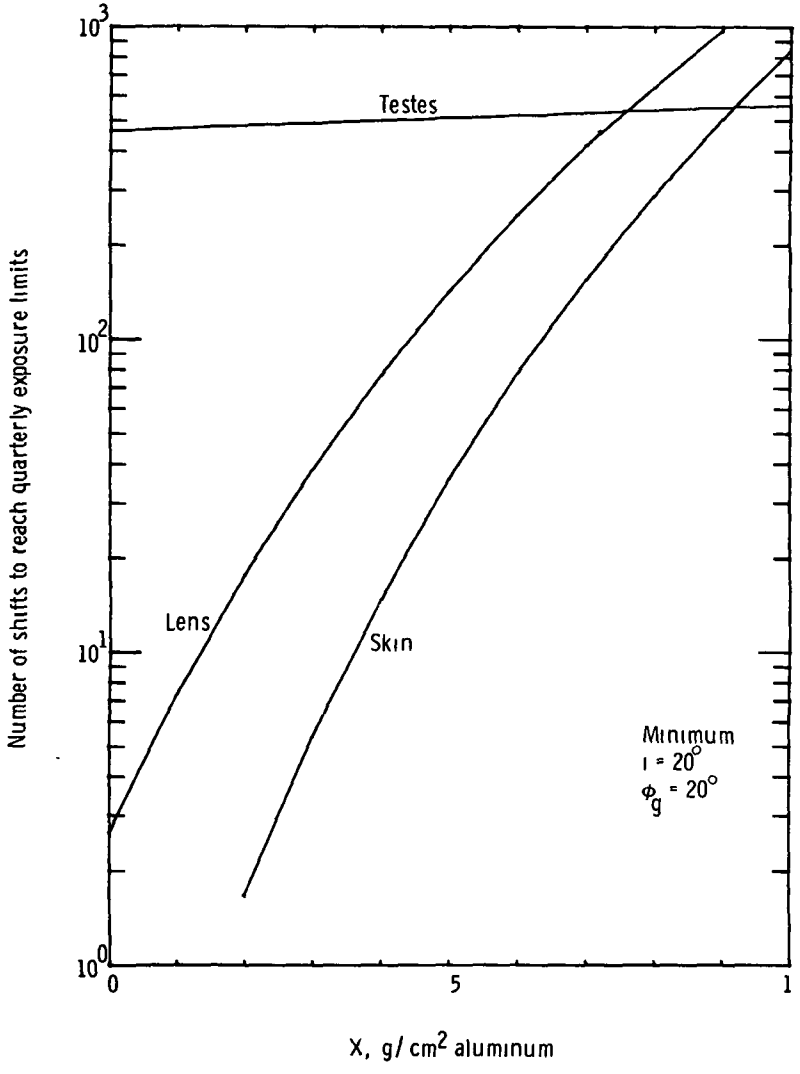

(c) 20° inclination.

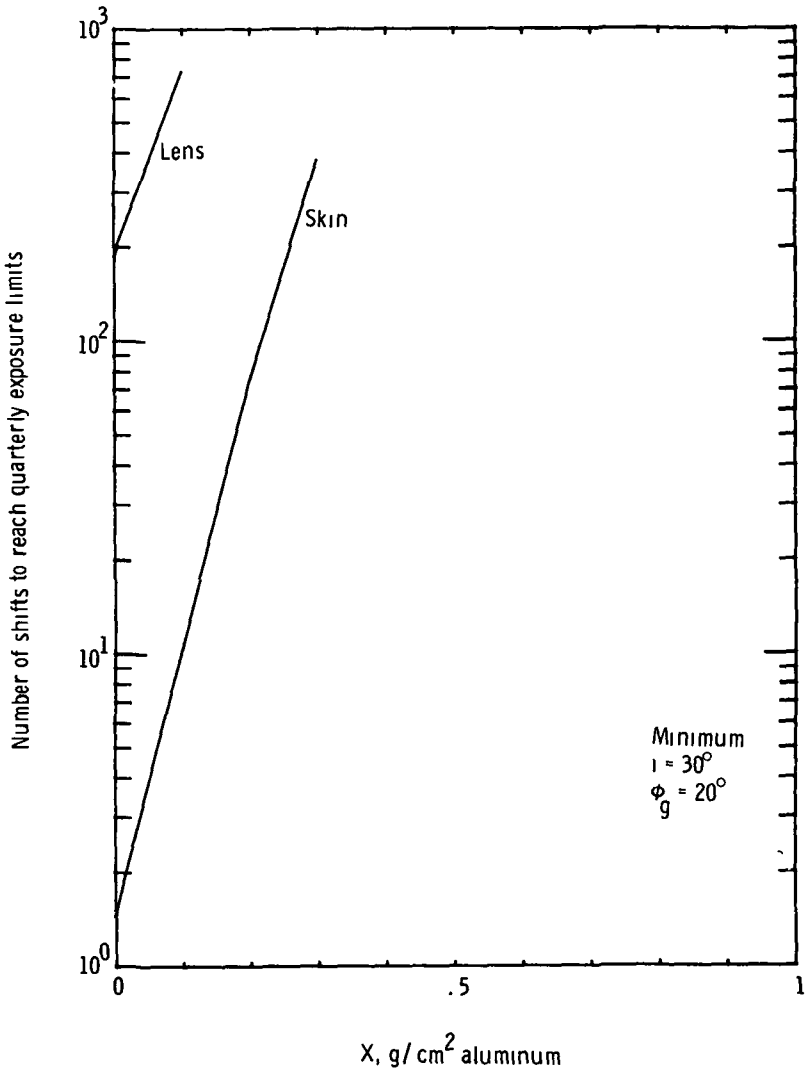

(d) 30° inclination.

Figure 34.- Concluded.

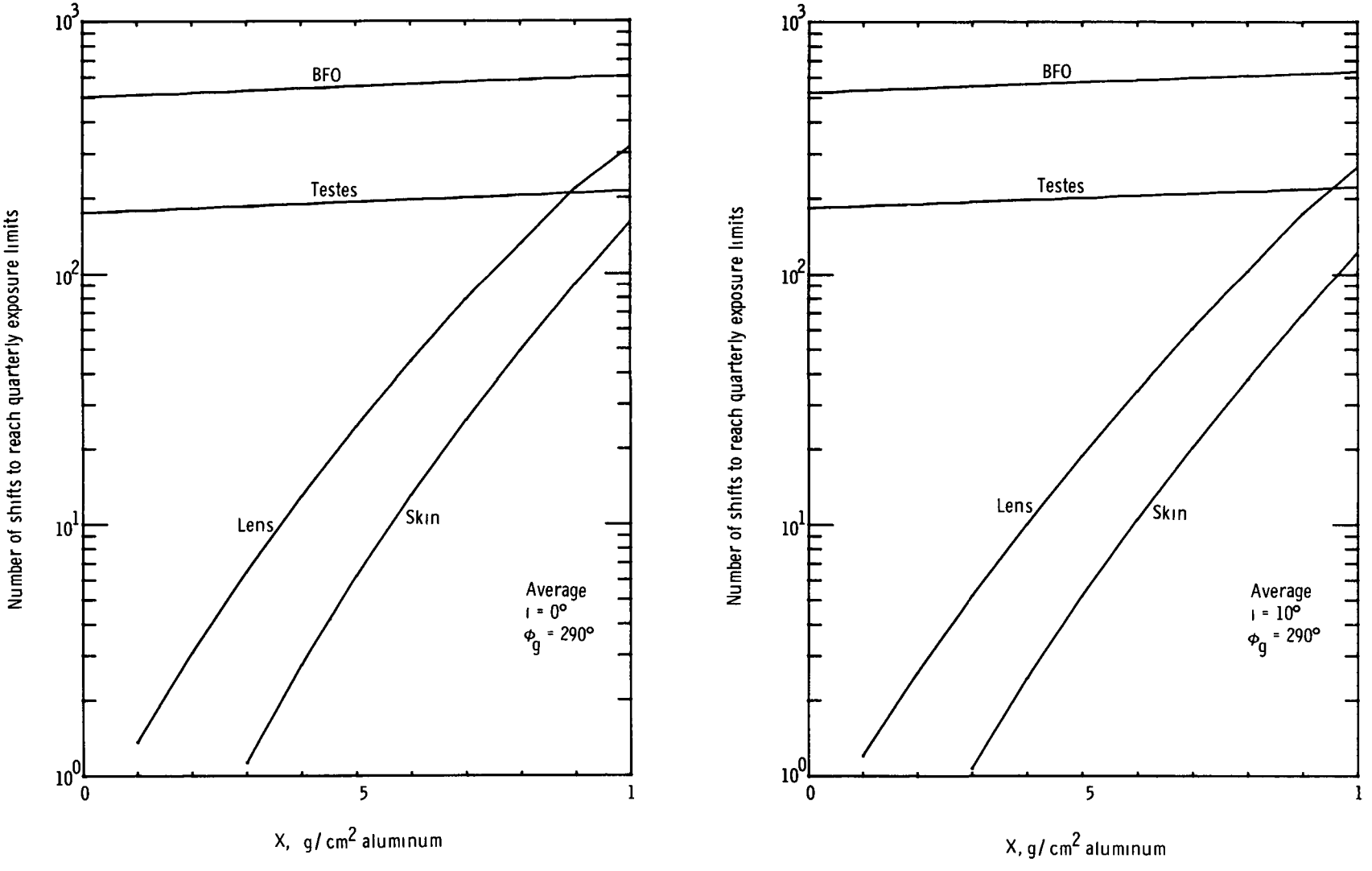

(a) 0° inclination.

(b) 10° inclination.

Figure 35.- Number of 6-hr shifts at daily average exposure rates required to reach the quarterly exposure limit for each of four critical organs during EVA operations at the geosynchronous location of ϕ_g = 290° and various inclinations.

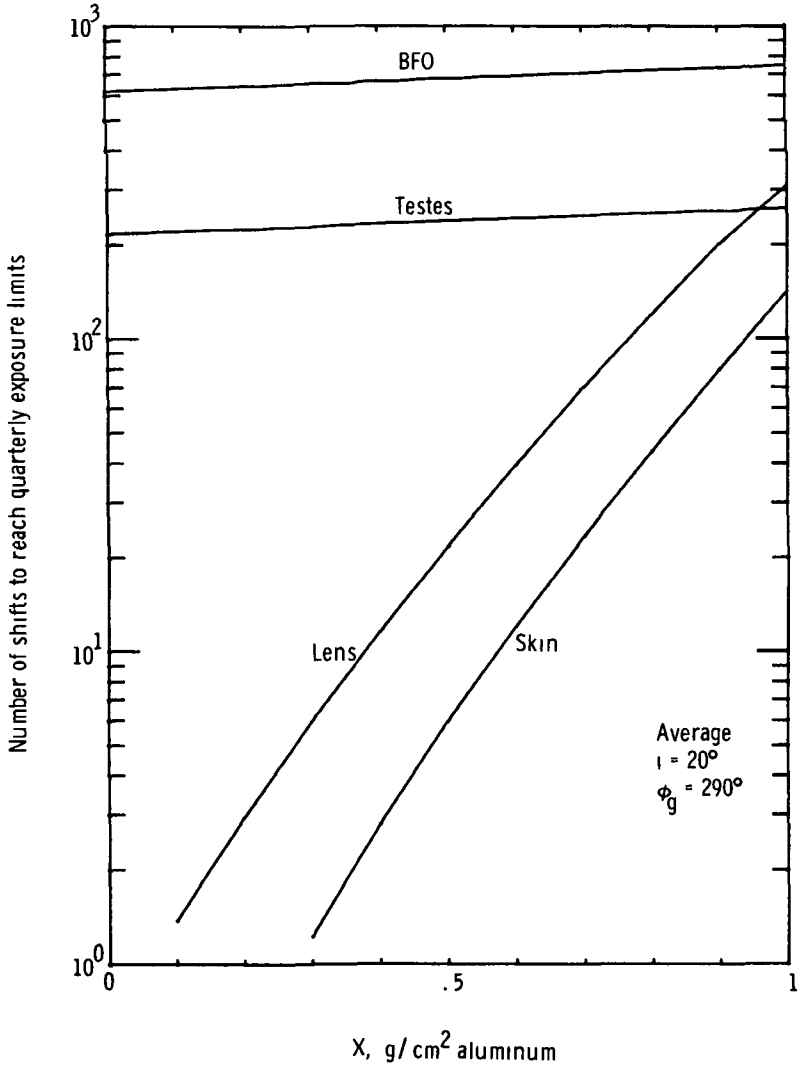

(c) 20° inclination.

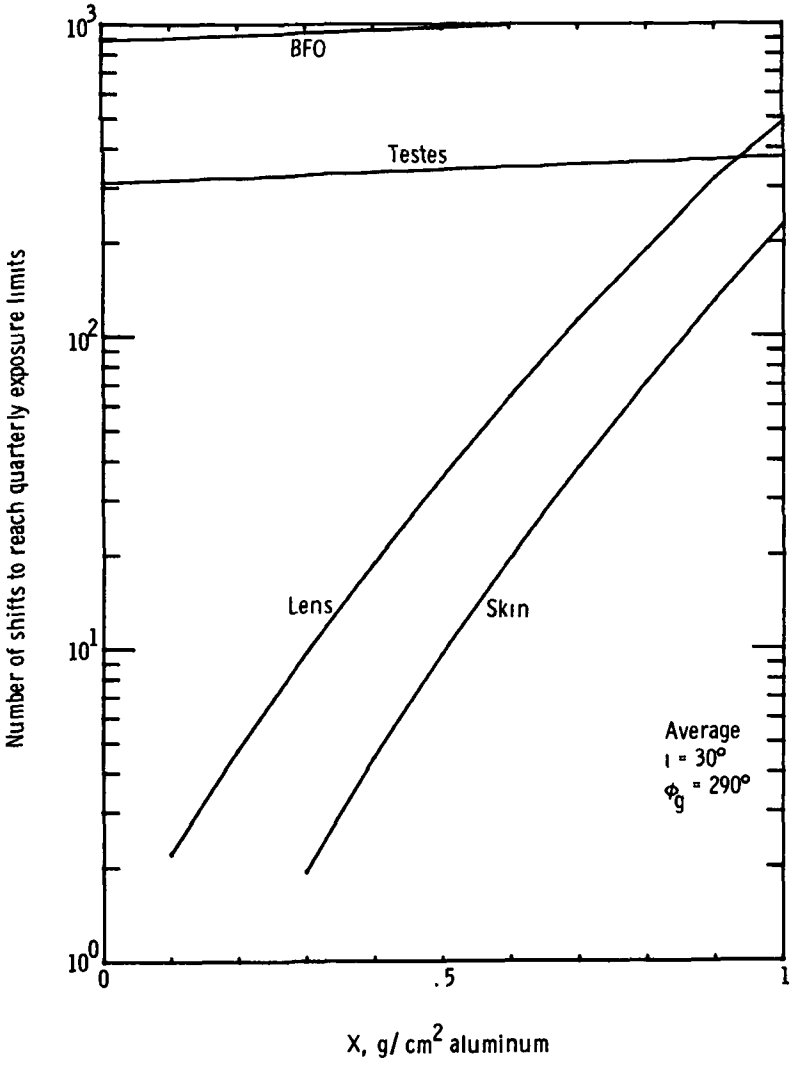

(d) 30° inclination.

Figure 35.- Concluded.

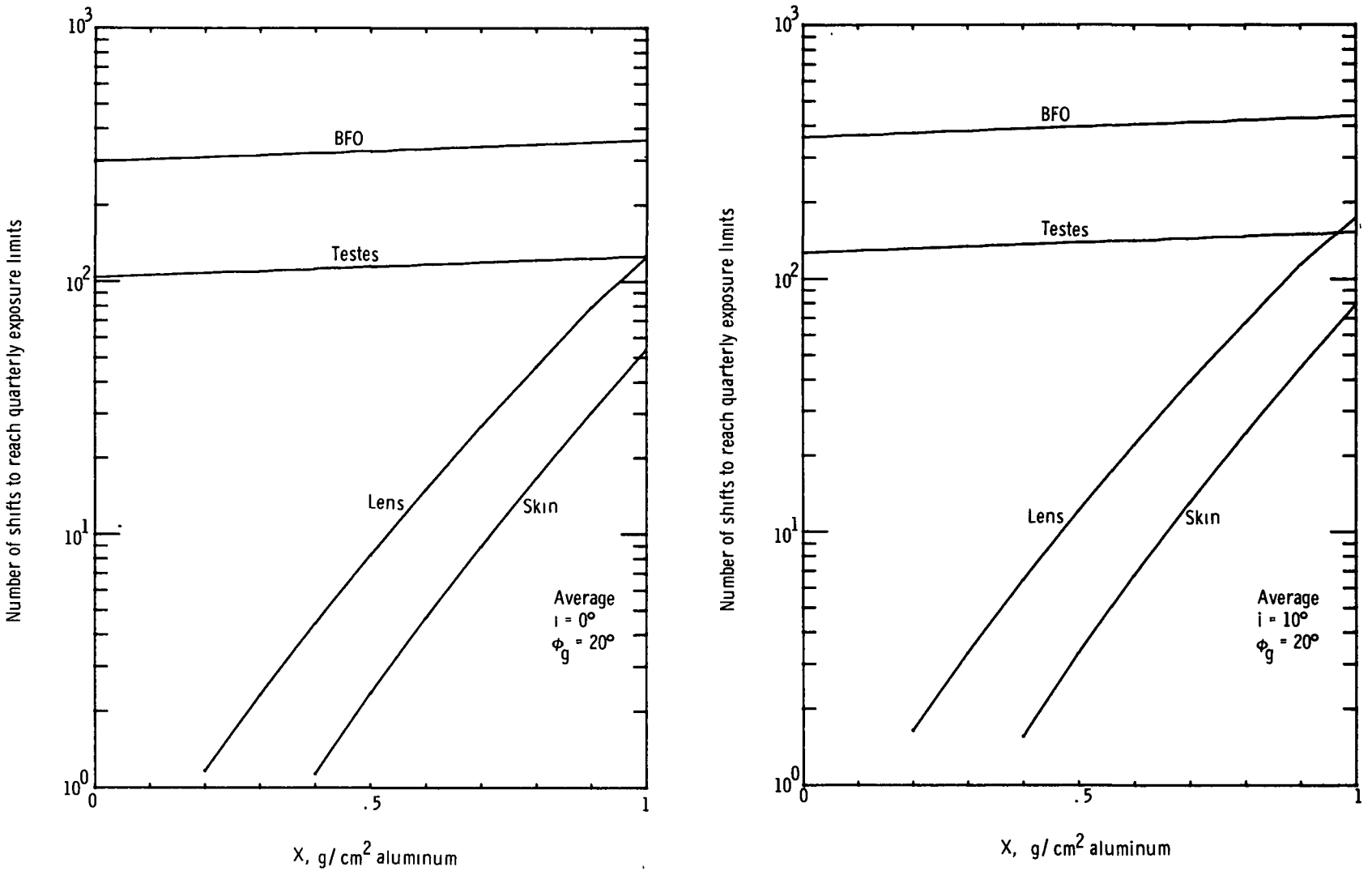

(a) 0° inclination.

(b) 10° inclination.

Figure 36.- Number of 6-hr shifts at daily average exposure rates required to reach the quarterly exposure limit for each of four critical organs during EVA operations at the geosynchronous location of ϕ_g = 20° and various inclinations.

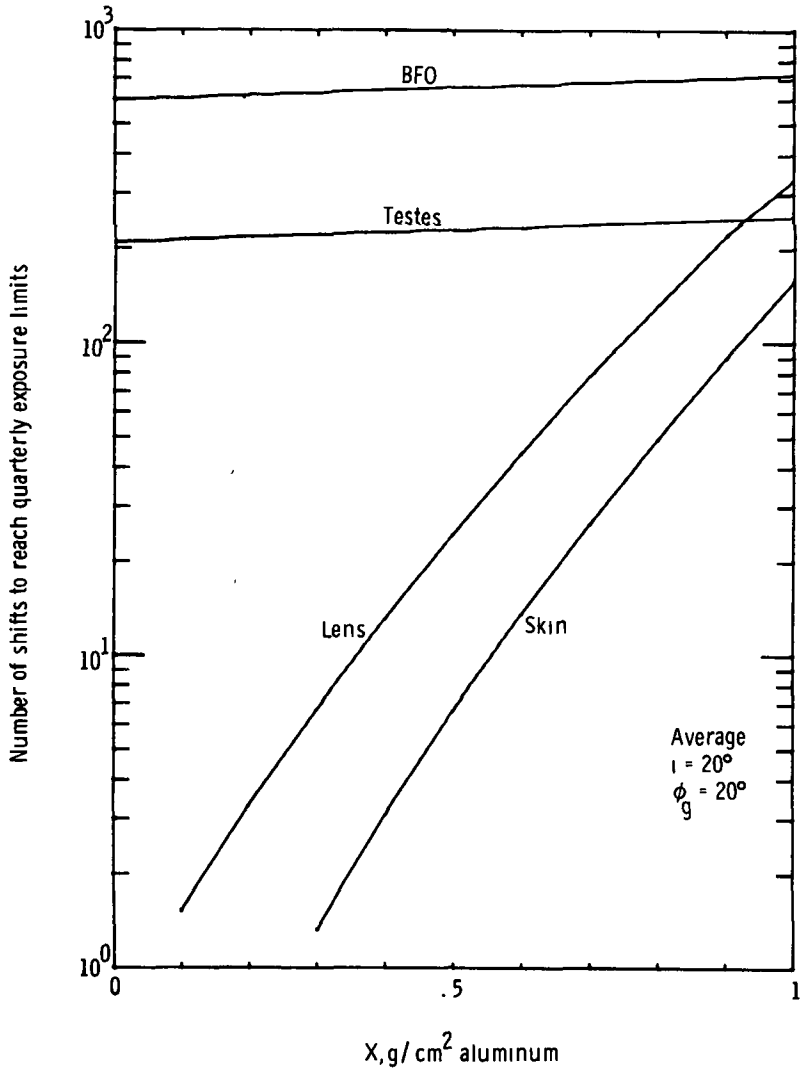

(c) 20° inclination.

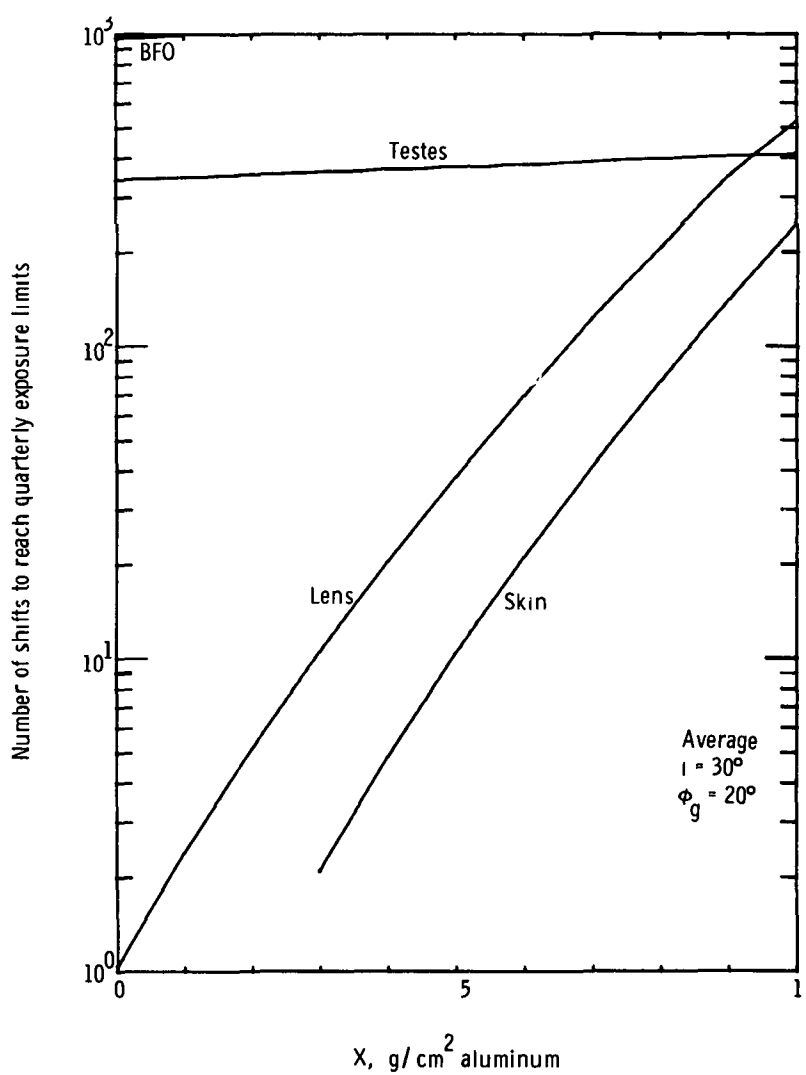

(d) 30° inclination.

Figure 36.- Concluded.

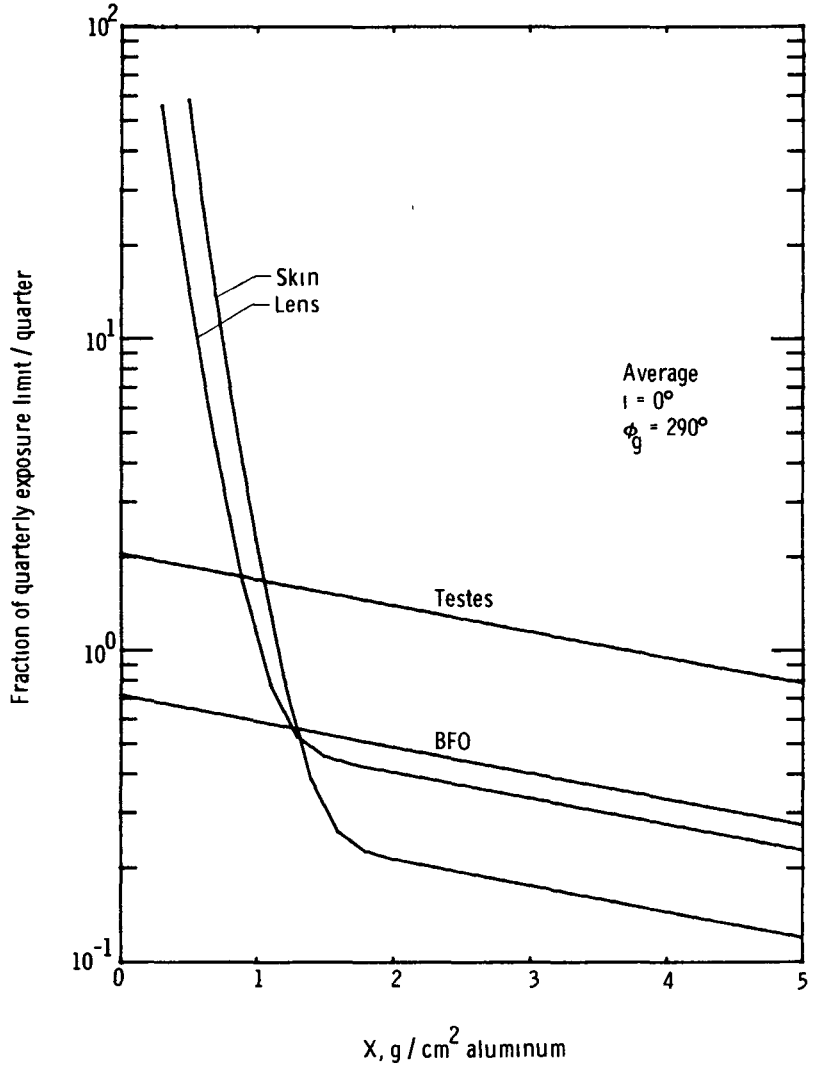

(a) 0° inclination.

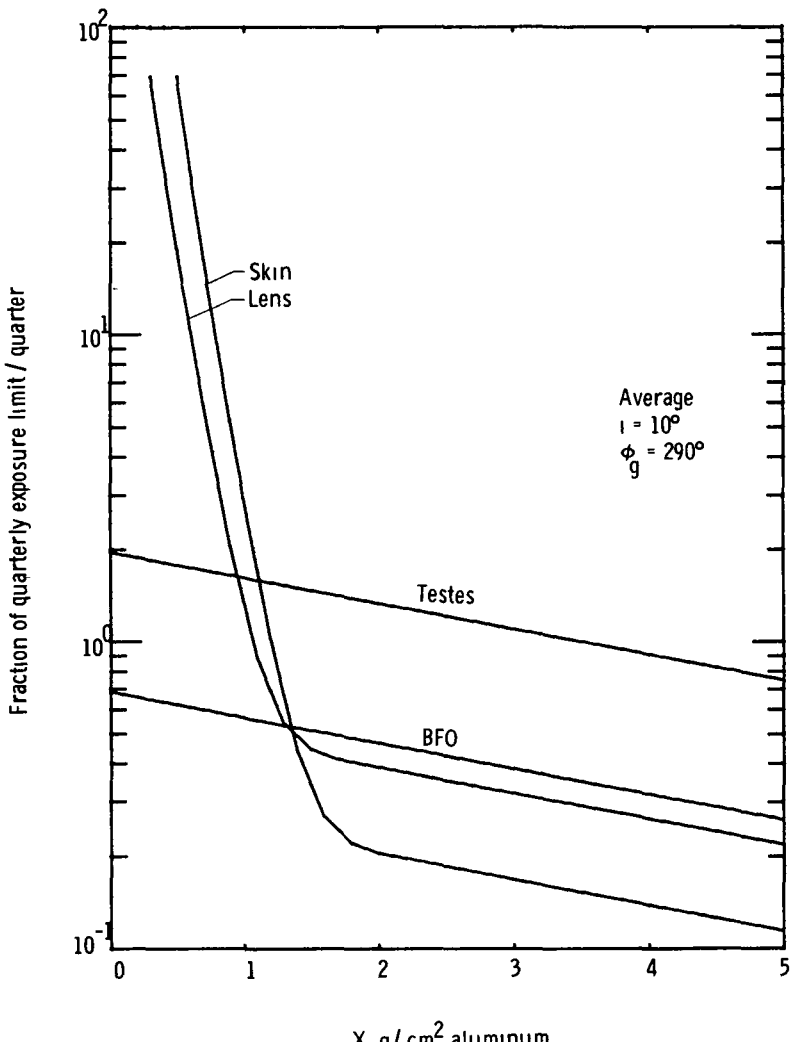

(b) 10° inclination.

Figure 37.- Fraction of quarterly exposure limit obtained per quarter for four critical organs during operations at the geosynchronous location of ϕ_g = 290° and various orbit inclinations.

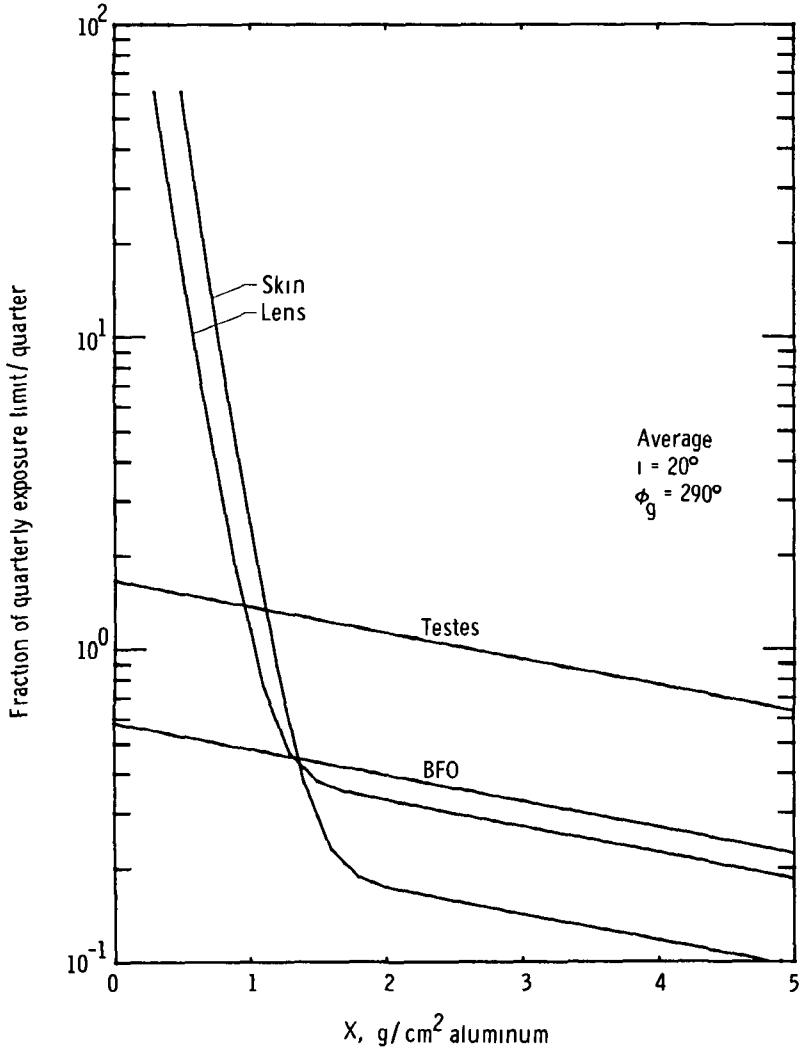

(c) 20° inclination.

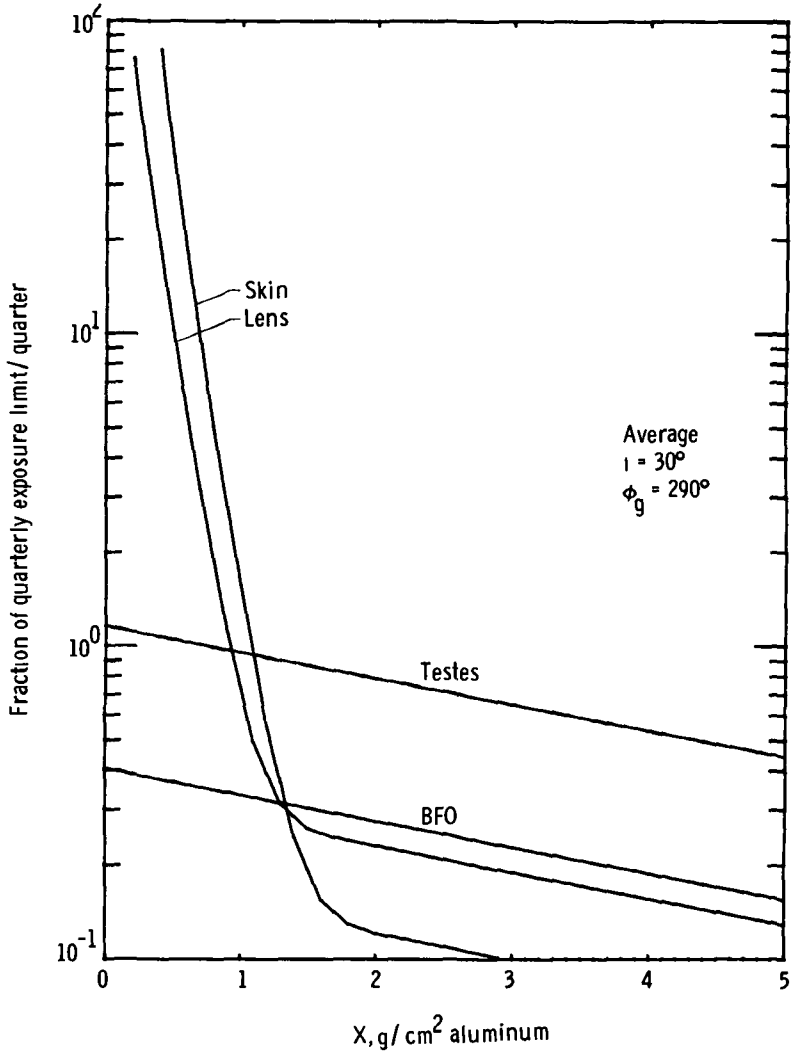

(d) 30° inclination.

Figure 37.- Concluded.

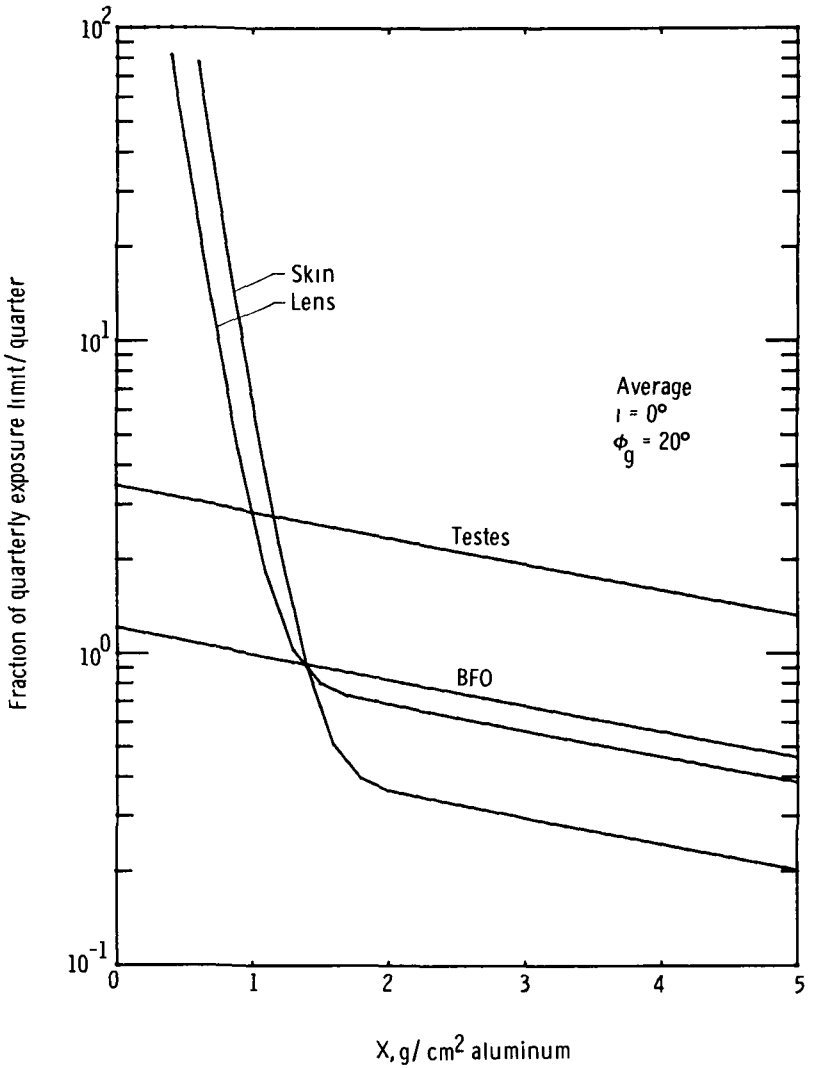

(a) 0° inclination.

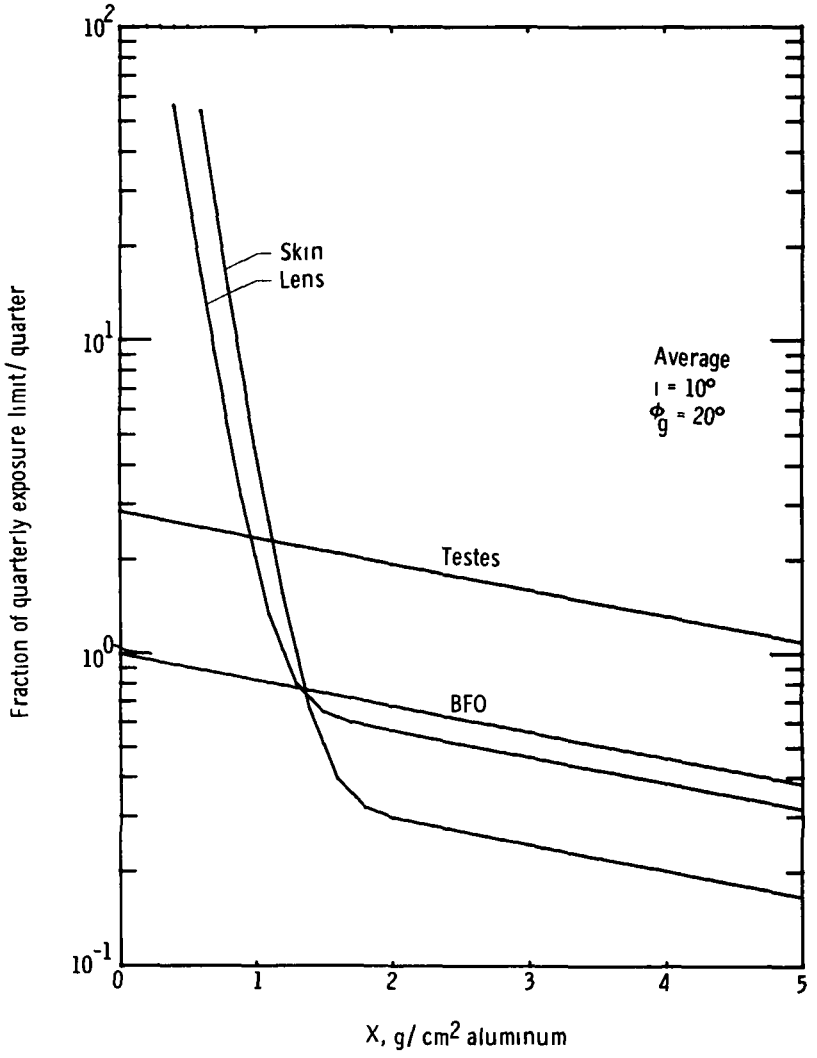

(b) 10° inclination.

Figure 38.- Fraction of quarterly exposure limit obtained per quarter for four critical organs during operations at the geosynchronous location of $\phi_g = 20°$ and various orbit inclinations.

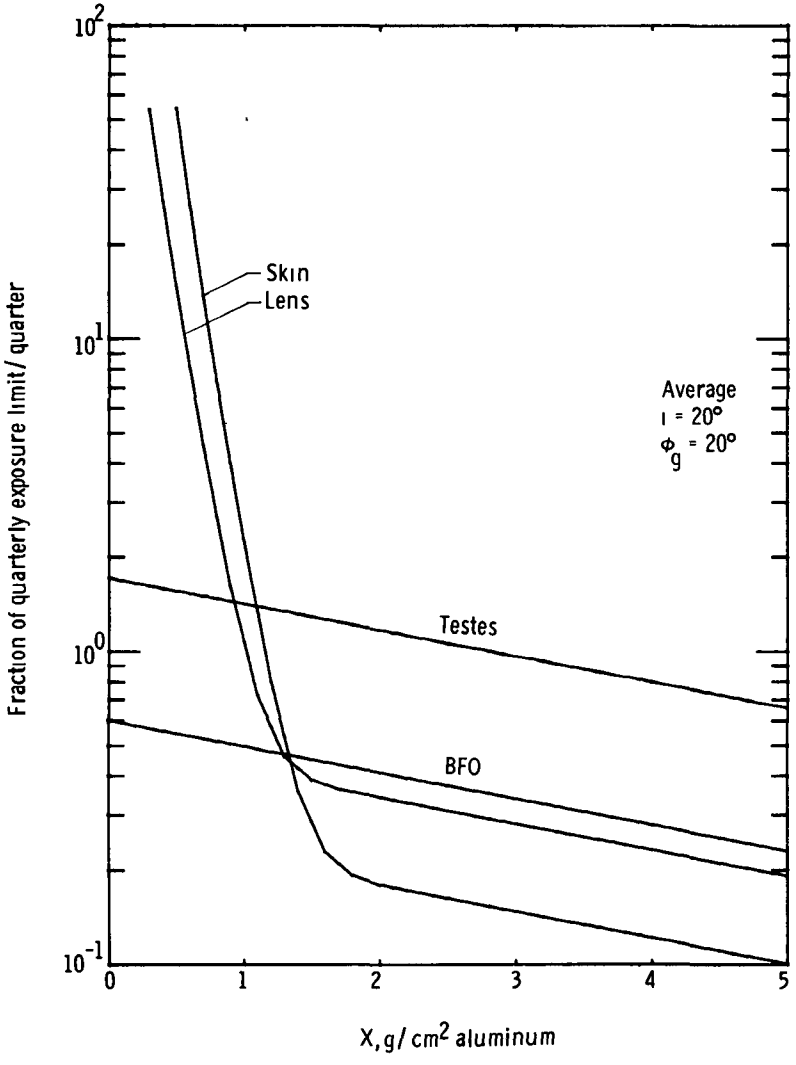

(c) 20° inclination.

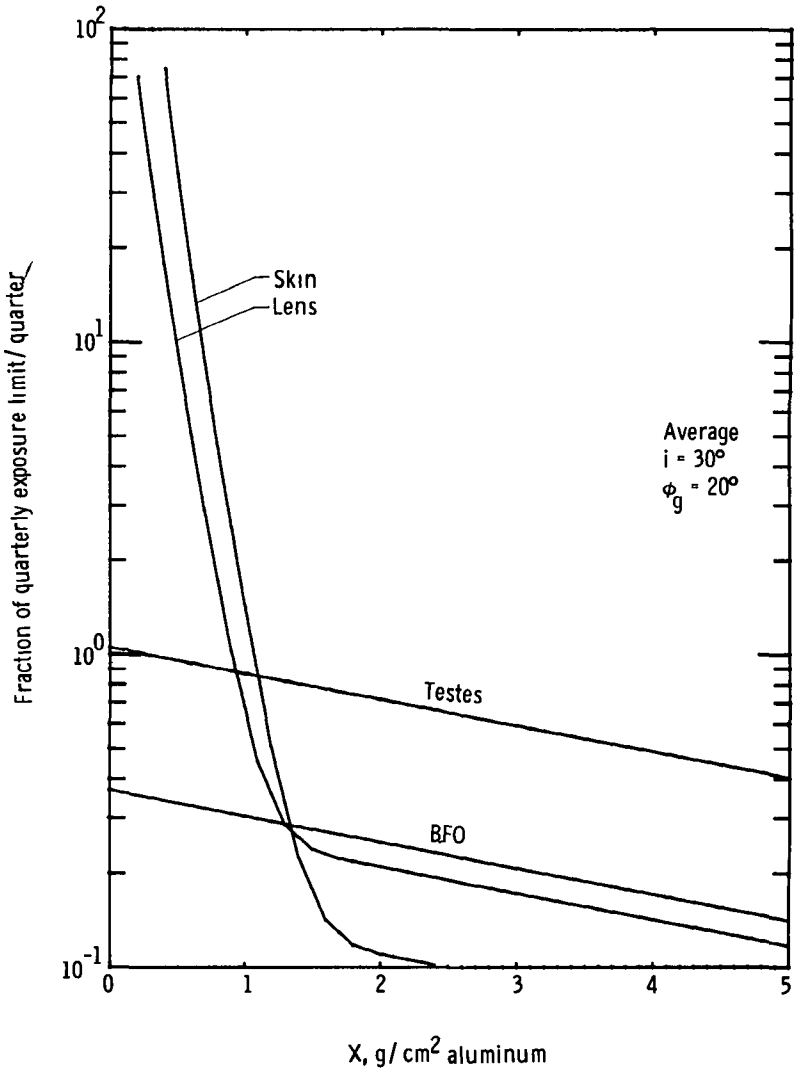

(d) 30° inclination.

Figure 38.- Concluded.

"The aeronautical and space activities of the United States shall be conducted so as to contribute . . to the expansion of human knowledge of phenomena in the atmosphere and space. The Administration shall provide for the widest practicable and appropriate dissemination of information concerning its activities and the results thereof."

—NATIONAL AERONAUTICS AND SPACE ACT OF 1958

NASA SCIENTIFIC AND TECHNICAL PUBLICATIONS

TECHNICAL REPORTS Scientific and technical information considered important, complete, and a lasting contribution to existing knowledge.

TECHNICAL NOTES Information less broad in scope but nevertheless of importance as a contribution to existing knowledge

TECHNICAL MEMORANDUMS Information receiving limited distribution because of preliminary data, security classification, or other reasons Also includes conference proceedings with either limited or unlimited distribution.

CONTRACTOR REPORTS Scientific and technical information generated under a NASA contract or grant and considered an important contribution to existing knowledge

TECHNICAL TRANSLATIONS Information published in a foreign language considered to merit NASA distribution in English

SPECIAL PUBLICATIONS Information derived from or of value to NASA activities. Publications include final reports of major projects, monographs, data compilations, handbooks, sourcebooks, and special bibliographies

TECHNOLOGY UTILIZATION PUBLICATIONS Information on technology used by NASA that may be of particular interest in commercial and other non-aerospace applications Publications include Tech Briefs, Technology Utilization Reports and Technology Surveys.

Details on the availability of these publications may be obtained from:

SCIENTIFIC AND TECHNICAL INFORMATION OFFICE

NATIONAL AERONAUTICS AND SPACE ADMINISTRATION

Washington, D.C. 20546